# TECHNIQUES FOR IMPROVING LANDMINE DETECTION USING GROUND PENETRATING RADAR

---

A Thesis Presented to the Faculty of Graduate School

University of Missouri – Columbia

---

In Partial Fulfillment

Of the Requirements for the Degree

Master of Science

---

By

Udaynag Pisipati

Dr. Dominic K. C. Ho, Thesis Supervisor

MAY 2006

The undersigned, appointed by the Dean of the Graduate School, have examined the thesis entitled

**TECHNIQUES FOR IMPROVING LANDMINE DETECTION USING GROUND PENETRATING RADAR**

Presented by Udaynag Pisipati

a candidate for the degree of Master of Science

and hereby certify that in their opinion it is worthy of acceptance.

_____

Dr. Dominic K. C. Ho

_____

Dr. Justin Legarsky

_____

Dr. Kevin G. Keegan

# ACKNOWLEDGEMENTS

I would like to take this opportunity to gratefully acknowledge everyone who made this research possible. I express my sincere gratitude to my advisor Dr. Dominic K.C.Ho for his constant encouragement, support, inspiration and valuable guidance. I am greatly indebted to his patience to explain the concepts clearly.

I would also like to express my sincere heartfelt thanks to Dr. Justin Legarsky and Dr. Keegan for being on my advisory committee for their valuable time and suggestions to help me improve my work. I greatly appreciate Dr. Kevin G. Keegan for providing me Research Assistantship that supported my education.

I thank University of Missouri, Columbia, for giving me the opportunity to pursue my Master's degree and gain valuable education and experience that made me a better person with a great sense of confidence to face the life ahead.

And finally, I would like to take this opportunity to say that I am forever indebted to my parents and sisters for all their unending love, inspiration, encouragement, and support they gave me when I needed them the most. Thanks for being always there for me. I would also like to thank all my friends for the wonderful times we shared together.

# TECHNIQUES FOR IMPROVING LANDMINE DETECTION USING GROUND PENETRATING RADAR

**UDAYNAG PISIPATI**

**Dr. Dominic K. C. HO, Thesis Supervisor**

## ABSTRACT

Improving the probability of detection of landmines is a challenging task for many scientists all around the world. The goal of this research is to be a part of this challenging work to investigate techniques for landmine detection. Two techniques for detecting the landmines, one in depth domain and the other in frequency domain, have been studied and a few modifications are suggested, along with the results. The data collected from Ground Penetrating Radar (GPR) from various test sites is used to evaluate the performance of these detection techniques. The first technique is proposed for use with Handheld GPR systems, while the second technique is proposed for use with Vehicle mounted GPR systems. The techniques proved to be useful in improving the detection of low metal or plastic mines.

# TABLE OF CONTENTS

**CHAPTER 3**

**CHAPTER 4**

# LIST OF TABLES

# LIST OF FIGURES

Figure

# Chapter 1

# INTRODUCTION

## 1.1 Foreword

According to an estimate from the International Red Cross, around 10 billion mines lie buried in eighty countries, claiming 10,000 deaths annually and at least twice as many seriously injured. Many victims are small children and elderly villagers in poor nations. Land mines can be buried in all types of terrain and environmental conditions. Locating a buried landmine is an important and challenging problem. Mines are very inexpensive to produce at $3 a piece, which makes employing landmines an easy task [1]. However, the difficulty in removing landmines poses a great challenge to researchers around various parts of the world. Signal Processing techniques are currently being developed in both academic and industrial fields and undergo transfer in some form to private companies involved in sensor development. As an effective tool for plastic land mine detection, Ground-penetrating radar has attracted the attention of many researchers and scientists all around the world. This research investigates the methods of improving detection of landmines using signal-processing techniques for Ground penetrating Radar.

## 1.2 Problems and Techniques for Land mine Detection

Land mines are generally embedded in a field cluttered with various materials or encased in metal, plastic, or wood. They come in all shapes and sizes scattered on the surface of earth or buried underground at varying depths, typically at 1 to 6 inches. Simple pressure triggers, trip wires, tilt rods, acoustic and seismic fuses, and magnetic influence fuses are the various fusing mechanisms used. Unpredictable climatic conditions and geographic limitations pose a serious challenge in identification of the mine fields. An efficient land mine detection system should be able to detect various types of explosives like Anti-Tank(AT) land mines, Anti-Personnel(AP) landmines, UXO, TND, RDX, etc., by distinguishing them from background clutter, regardless of size, shape, depth of burial, type of casing, chemical signature of the explosives used or the thermal radiation from these subsurface buried objects. The detection system used should provide a highly precise, cost effective detection with good standoff distance, very low false alarm rate, acceptable operational speed, and imaging capability. The mine detection problem is even more difficult when the target is nonmetallic. It is a highly challenging task to meet such demanding requirements with current detection technology.

Although there are many technologically advanced means of detecting mines in the field, the problem is far from being solved. Generally, man-made objects exhibit the property of being symmetric across a plane. This symmetric nature is absent in clutter objects from nature like rocks, bullet casings etc. Therefore, symmetry in landmines can be used to distinguish them from clutter objects buried beneath the ground.

Infrared Imaging (IR), Electromagnetic Induction (EMI) Array, Ground Penetrating Radar, Thermal Neutron Activation (TNA), Thermography, Photo-Optics, Eddy current and Microwaves, and Sensor fusion are some of the Mine detection technologies used in various applications. Traditional sensors for UXO detection are capable of attaining high detection rates, but pose a risk of increasing the system costs due to high false alarm rates.

The principle of Infrared thermography is based on the principle of difference in the thermal capacitance between soil and mine, which in turn produces difference in their heating and cooling rates and also the infrared emissions of these materials. This technology allows detection of landmines from a remote area by aerial search which is a passive method covering a large area in a short time. This method best suits identification of minefields, rather than the search of individual mines. However, this procedure cannot be applied for detection when the soil and mine are in thermal equilibrium.

Laser detection of land mines can be done by using photo optics. The principle behind this mechanism utilizes the difference in the reflectance and polarization of soil produced when disturbed by laser energy. This system is however difficult to implement because of the large laser power required for this process and complex data interpretation involved in this process.

Generally, Eddy-current can be generated in metals causing complete reflection of microwaves off their surfaces. This principle when applied to metal encased land mines can be used for their detection. The detection process can be done by pulse-induction metallic detectors and microwaves. Microwaves are also scattered by nonmetallic objects,

but to a lesser extent. These reflection signatures are characteristic to material type, and hence can be used to identify explosives. Propagation losses in the soil, low contrast between target and soil, and echoes produced from the rough surface and other shallow contrasts such as rocks, tree roots pose set backs to implement this method for land mine detection. Discrimination of mine from clutter under the wide variety of surface and soil conditions always remains a very difficult issue to solve. Penetrating radiation from neutrons and photons also offers another option for land mine detectors. The technique works on radiation scattering or activation by production of secondary particles unlike the conventional radiographic or tomographic methods. Explosives are usually characterized by high nitrogen content, neutron activation of nitrogen, and the subsequent emission of characteristic gamma rays, can be used for mine detection.
All the techniques discussed above use a signature "finger-print" signal characteristic of mine. Given the wide variety of mine material, casing and shape, as well as the various type of soil and the non-uniformity of clutter, such a characteristic signature varies widely depending on the circumstances; making it difficult to apply any one technique unless the nature of the mine, soil and background clutter is well known. What is needed, therefore, is a technique that is more specific in its identification of the hazardous material in a land mine, i.e. the explosive material itself.

Ground-penetrating radar has attracted the attention of many researchers and institutes all around the world. As an effective tool for plastic land mine detection, Ground Penetrating Radar (GPR) can detect the presence of subsurface targets by distinguishing them as landmines and clutter objects based on the level of symmetry exhibited by the targets. For electromagnetic induction based sensors, detection occurs with respect to their sensitivity

to metals, caused either by targets or clutter. To reduce the false alarm rates, ground penetrating radar (GPR) has been proposed as an efficient detection method for landmines. GPR sensors aim for the detection of dielectric discontinuities below the surface, instead of detecting metallic content of an object. This allows for the detection of low-metal content targets consisting of wood, plastic, or other non-metallic materials. GPR sensor's ability to detect non-metallic materials can be offset by the false alarms generated by any material from tree roots to rocks. However the use of signal detection theory based on symmetry study can help reduce false alarm rates for GPR.

There are certain challenges pertaining to this GPR based land mine detection systems, the major challenge being the visualization of the data. Also, the data collected by the radar has to be presented in a comprehensible format in order to attain a comprehensive conclusion. This data may be a color-mapped image of the energy of a block of data, or a time domain representation of the measured signal. Image processing sometimes becomes equally important to the signal detection. Next, pre-processing the data is also an important factor in order to achieve better detection of the landmines. This can be done in both the time and frequency domains.

## 1.3 Previous work on Landmine Detection

The detection of land mines has been a popular research area over the past few years. Land mines can be categorized into two types. Anti-tank (AT) mines and Anti-Personnel (AP) mines [1]. AT mines are larger, generally 20-30 cm in diameter, whereas AP mines range from approximately 5-15 cm in diameter. In addition, landmines can be categorized as plastic-cased or metal-cased. Plastic cased mines or simply plastic mines have much less metal content than metal cased or metal mines and are very difficult to detect. Because land mines are buried deep under the ground, land mine detection relies mostly on sensors to capture the signal responses from land mines. The standard mine detector has been a metal detector (MD), also known as Electro Magnetic Induction (EMI) sensors. EMI sensors can easily detect metal mines. Unfortunately, most land mines nowadays are either made of plastic or have very low metal content. As a result, metal detectors have problems detecting mines made of plastic or having low metal content. Ground penetrating radar (GPR) is the emerging technique used in mine detection that can detect plastic or low metal content mines [2]. GPR sensors can operate in both the time domain and the frequency domain. They use relatively low frequencies to penetrate deep into the ground. GPR systems are usually of two types: vehicle mounted or handheld. Extensive research has been done which uses handheld GPR system for land mine detection.

Wide varieties of signal processing techniques have been used in the past to process GPR signals. Gader et al. [3]-[4] has suggested a gradient-based method for landmine detection. This method efficiently used the Fuzzy clustering technique by generating

multiple prototypes of training data from a fuzzy clustering of gradient features. In [5]-[8], Hidden Markov Models (HMM) have been used to process GPR signals with some success. Though the technique is still under investigation, it has been proved that HMM can be used to efficiently detect the presence and location of landmines. In [9]-[10], a least squares method has been proposed to remove the ground bounce obtained on a rough surface. However, its performance depends heavily on the reference ground bounce and no method has been given in [9]-[10]. A system identification based clutter removal algorithm is given in [11]-[12], which uses ARMA model to describe clutter and abrupt change detection technique to classify clutter and target signal. The technique focuses on pre-processing the GPR data to reduce the influence of near-surface clutter. Once the clutter is satisfactorily known, this technique easily identifies the target as a small anomaly within the known clutter background. However, the dependency on the reference clutter data is a major drawback of this technique. A linear prediction approach for the detection of land mines has been proposed by Dr. Ho, which uses the prediction model to generate a mine detection alarm if the current and past few signal samples do not fit the linear prediction model. Apart from the above methods, wavelet analysis, principal Component analysis (PCA), Independent component analysis (ICA) has been proposed for clutter suppression in [13]-[14]. Wavelet decomposition and reconstruction will lose some useful target signal component because the ground bounce is usually very strong and would overlap the target signal in the time-frequency plane. Deming [15] proposed Maximum Likelihood Adaptive Neural System (MLANS) for landmine detection, which is a model based neural network, which combines the adaptability of a neural network with the priori knowledge of signal models. The MLANS technique is

designed to adapt to unknown and changing soil conditions, while incorporating signal models based on the physics of electromagnetic scattering for a specific object or clutter type. However, for accurate feature extraction, the technique requires well defined clutter and mine signature models. The Hand-held GPR system has time varying clutter and does not provide clear signature models. Hence, MLANS technique would be more appropriate for vehicle-based systems

## 1.4 Thesis Contribution

In our research, we use two techniques to improve the detection accuracy of land mine. The first technique is the use of Dynamic Template Matching algorithm with the land mine templates in the GPR data, to improve the detection accuracy for a hand-held mine detection unit. The proposed algorithm extracts the mine templates from the data acquired during the first few sweeps, and correlates the templates from the data at subsequent sweeps to enhance the detection of land mines. Thus, the algorithm uses the forward and backward sweeps separately to extract the template and matches them with the subsequent data to find the confidence value. The algorithm is found to be effective to enhance the detection of weak mines, especially the low-metal anti-personnel mines. This research further investigates the use of forward and backward templates together to match with the subsequent data. In this technique, the template from the backward direction (right to left) is flipped and combined with the template in the forward direction (Left to right) to match with the subsequent data. Though this technique does not show apparent improvement over the original template pair approach, it provides some insight into the original algorithm. Further, the original algorithm has been modified to batch processing

where the final mean template from all the sweeps is used to match with the subsequent data. This batch processing technique is found to improve the probability of detection of land mine with less false alarm rate compared to the original algorithm. The effect of scaling on the front and back antenna is verified using the original algorithm and the batch-processing algorithm.

The second technique investigated in the research is to improve the land mine detection using frequency domain features from Ground penetrating radar. For certain specific mine types, the GPR signal return is very weak which presents difficulty in their detection. For these kinds of mines, the GPR signal spectrum sometimes reveals important features, although time domain signature could be weak. This technique is applied to the vehicle mounted GPR system. The GPR return is converted into frequency domain and the normalized frequency domain data is used to generate the spectrum by averaging over a square window. To make use of the energy density spectrum to improve mine detection, the spectral feature vector is generated with spectral energy at different frequency bands. Since the total bandwidth of the radar being studied is 6 G Hz, with the size of each frequency band equal to 600 MHz, there will be 10 frequency bands. The spectral features are generated using windowing in each frequency band. This research investigates the advantage of increasing the number of sub bands to 20, using cosine square window with 50% overlap between two adjacent bands. Further, the effect of using depth estimation routine before converting the data to frequency domain has been studied. This showed some improvement in the probability of detection of weak mines.

## 1.5 Thesis Organization

This thesis is composed of six chapters. The next chapter reviews the existing techniques for land mine detection using GPR. The chapter gives an introduction to the two types of landmine detection systems used and also introduces a few techniques investigated by researchers around the world. Chapter 3 discusses the template matching techniques and evaluates the performance of template matching technique using two different datasets. Chapter 4 discusses the Frequency domain technique of processing GPR signal return and evaluates the effect of varying sub bands on the improvement of mine detection. Chapter 5 includes the investigation of depth estimation routine in the improvement of Probability of detection. Chapters 4 and 5 also include the evaluation of frequency domain technique with data collected from various lanes. Finally, conclusions and possible future works are discussed in Chapter 6.

# Chapter 2

# TECHNIQUES FOR LANDMINE DETECTION

## 2.1 Sensors Used in Landmine Detection

A variety of sensors have been proposed for landmine detection during the past several years. The most widely used sensor for land mine detection is a Metal Detector or Electromagnetic Induction (EMI) sensor. EMI sensors can easily detect landmines. EMI sensors usually contain a pair of coils, one of which is used to transmit either a broadband pulse or a continuous wideband electromagnetic waveform. The other coil is used to receive the decaying secondary field that has been induced in the earth and subsurface objects due to the primary coil. EMI sensors can be of two types, Time domain or Frequency domain. Numerical methods of frequency domain sensors have been developed. The response from a time domain sensor can be modeled mathematically as a sum of decaying exponentials. However, the main disadvantage with the EMI sensors is that they cannot detect plastic or low metal content mines.

GPR sensor, also used for landmine detection, operates by transmitting pulses of ultra high frequency radio waves down into the ground through a transducer or antenna. These GPR sensors [16-18] have the advantage of having the capability to detect plastic cased mines. The transmitted energy is reflected from various buried objects or distinct contacts between different earth materials. The antenna then receives the reflected waves and stores them in the digital control unit. The ground penetrating radar antenna (transducer)

is pulled along the ground by hand or behind a vehicle. When the transmitted signal enters the ground, it contacts objects or subsurface with different electrical conductivities and dielectric constants. Part of the ground penetrating radar waves reflect off of the object or interface; while the rest of waves pass through to the next interface. The control unit present in the antenna system registers the reflections against the ground surface and then amplifies these signals. Recently, considerable efforts have been put into the development of GPR systems for the detection of shallow buried land mines. GPR waves can reach depths up to 100 feet (30 meters) in low conductivity materials. High conductive materials may attenuate or absorb the GPR signals, greatly decreasing the depth of penetration to 30 feet (1 meter) or less. The depth of penetration is also determined by the radar antenna used. Antennas with low frequencies of 25 to 200MHz obtain penetrations of 30-100 feet or more, whereas antennas with high frequencies from 300-1000 MHz obtain reflections from shallow depths and have high resolution. However, the presence of clutter in the mine data hinders the detection accuracy of landmines. The clutter varies with soil and environmental conditions and leads to false alarms in mine detection. Therefore it becomes necessary to overcome the clutter effects when processing the GPR data for detecting small, shallow objects.

Other radar approaches include generating continuous frequencies in a narrow band or bands, either by discrete steps, continuous sweeping or chirping (a short burst of sweep frequencies). Synthetic aperture radar (SAR) utilizes multiple antenna locations to improve resolution of the resulting image, essentially creating a larger antenna from multiple smaller antennas [19]. Bistatic impulse radar emits a short burst of energy which incorporates a broad range of frequencies on a single transmit antenna.

Recently, Energy Focusing Ground Penetrating Radar (EFGPR) has been proposed which incorporates both bistatic impulse radar and synthetic aperture (SAR) principles. EFGPR is designed specifically for the detection of landmines. The system is unique in its ability to focus in hardware and designed by taking a wide variety of environments into consideration.

Though several advances are made in the Sensor industry, Ultra wideband GPR sensors have been accepted as popular radar for the detection of landmines. GPR systems are usually of two types: Vehicle-mounted and Hand-held GPR systems. The vehicle-mounted GPR systems attaches the GPR and EMI sensors in the front of a vehicle and collects the data as the vehicle moves. The vehicle has a constant moving speed and relatively stable sensor to ground distance so that the mine signature is consistent. Hand-held systems have GPR sensors located at the tip of a hand-held unit. The background characteristics in the hand-held GPR sensors are nonstationary and vary with soil conditions and soil types. In addition, sweeping speed and ground to radar distance are not constant due to human factor. The data processing models in hand-held GPR system and vehicle-mounted GPR systems are discussed further in the coming chapters. More about hand-held and vehicle-mounted GPR systems is discussed in Section 2.3 and 2.4

## 2.2 GPR Data Format:

The GPR data is classified as A, B, and C- scans according to the dimension. Each scan can be represented using a set of mathematical equations. Figure 1[20] shows the A, B and C scans obtained from a GPR.

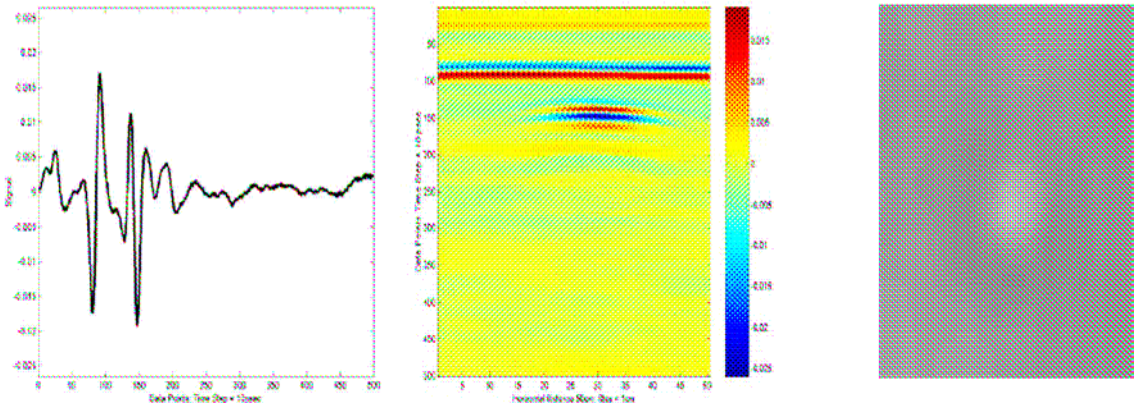

Figure 1(a) Figure 1(b) Figure 1(c)

**Figure 1: A, B, C scans obtained from a GPR**

An A-scan is obtained by a stationary measurement of a signal after placing the antenna above the position of interest. The collected signal is presented as signal strength versus time delay. The positions of the peaks in A-scan correspond to the distance between the antenna and the reflecting surface. The first peak is the air-ground reflection and the second is the mine target. Figure 1(b) is the B-scan of the same object shown in Figure 1(a). The B-scan is a two-dimensional image. Each B-scan has of a number of A-scans. The vertical axis corresponds to the horizontal axis of Figure 1(a) and the horizontal axis represents the scanned width, which is the number of A-scans. The intensity or color of each pixel indicates signal strength, corresponding to the vertical axis of Figure 1(a). The A-scan could detect only the presence of two objects in Figure 1(a) whereas a B-scan can distinguish a mine-like target from the air ground surface and also can give information about the position of object. A C- scan in figure 1(c) is represented as a horizontal slice

for a specific data point, which indicates the depth level. Both horizontal and vertical axes correspond to the horizontal axes of a B-scan, and the depth level corresponds to the vertical axis of B- scan.

## 2.3 Techniques for Hand-held GPR system

The detection accuracy of the GPR system usually depends on the removal of surface clutter present around the landmines. Therefore, the primary goal of any detection system is to reduce the interference from the clutter and to enhance the object reflection. Various techniques have been suggested for the removal of the clutter or ground bounce present near the surface. For shallowly buried plastic landmines, the ground bounce is usually much stronger than the low strength signal returned from landmines, and makes it very difficult to distinguish landmine from the ground bounce. Fuzzy logic method has been proposed by Gader [3], to recognize the hyperbola-like curves in a GPR image from a landmine. Various other methods have been suggested for the background removal from the GPR image. Xu, proposed a background removal technique by subtracting the column-wise average to remove specular reflection [21]. Dr. Ho has suggested a background removal by time gating algorithm in order to reduce specular reflection, which arrives earlier than the landmine reflected signals. These background removal techniques require prior information about the depth of the buried landmines to perform effectively.

Kempen and Sahli together proposed an ARMA model [11] for clutter estimation. The technique models the GPR signal return as given in the equation below

$$\vec{\mathbf{E}}_{\text{rec'd}}(\mathrm{k}) = \vec{\mathbf{E}}_{\text{rad}}(\mathrm{k}) * (\mathbf{h}_{\mathbf{c}}(\mathrm{k}) + \mathbf{h}_{\mathbf{t}}(\mathrm{k})) + \mathrm{n} \qquad (2.3.1)$$

This represents the relationship between the radiated electric field and the received one, where $\mathbf{h_c}$ (k) and $\mathbf{h_t}$ (k) are the impulse response of the clutter and target, respectively and n represents the measurement noise. The removal of $\mathbf{E_{rad}}$ (k) the emitted signal, by deconvolution is the first step in the algorithms. This deconvolution can be performed after the clutter reduction. The technique then estimates a small amount of known clutter samples with the ARMA model. Kalman filtering can also be used to estimate the parameters of the clutter, where the parameters are considered as being constant with some fluctuations. The Kalman filtering method was found to give better results, reducing most of the clutter to zero, while preserving the shape of the original signal.

A few other techniques were proposed which take into account the time varying nature of the background clutter. These techniques are used in the search mode of the handheld detection unit, where the operator sweeps the GPR unit back and forth to detect the presence of a mine. In this approach, as the signal return from the GPR Radar is processed, any difference of observed data from the background is considered to be the presence of mine. Many such anomaly detection techniques are proposed for Handheld GPR sensors, the most popular approaches being Principal Component Analysis (PCA) algorithm proposed by Yu and Mehra [22], and the CorrDet algorithm proposed by Ho [23]. The PCA algorithm [22] generates the principal components from the autocorrelation of background clutter samples collected during the training phase. A GPR signal is then projected onto these principal components. The Corrdet algorithm [23] on the other hand uses a linear prediction model of the background clutter to generate a mine detection algorithm if the linear prediction error is greater than a particular threshold. Section 2.5 explains the linear prediction approach used in the CorrDet algorithm.

## 2.4 Techniques for Vehicle-Mounted GPR systems

The handheld mine detection system is slow, man power intensive and stressful to the operator, who on the other hand can perform the operation only for a short period of time. To increase the sweeping speed and to remove the human factor in mine detection system to reduce the timing errors, vehicle mounted systems are used now a days. Vehicle-mounted GPR is a rapid, continuous data collection system that contains highly accurate and repeatable data as it is moved over a pre-defined path. There are several constraints that need to be taken care before designing any vehicle-mounted system which makes the system expensive. The system has the radar antenna mounted on a vehicle which is remotely controlled from an armour-protected vehicle. The radar vehicle's ground pressure should make it possible to drive over mines without detonating them. The antenna has to be very stable with respect to speed, vibration and other movements. This has a very strong influence in the design of the vehicle.

Various techniques have been developed for vehicle mounted GPR systems recently. Unlike hand held mine detection system, the vehicle-mounted system has a constant moving speed and relatively stable sensor to ground distance. The performance criteria for vehicular based systems is high probability of detection with less probability of false alarm. Hence, feature based techniques are useful in vehicle-mounted GPR systems.

Hidden Markov models have been used in processing data from vehicle-mounted GPR systems [5]-[6]. Another technique for vehicle mounted GPR system is proposed in [24], where signal processing techniques are developed, that automatically extract features from two dimensional as well as three dimensional data, and then utilize these features to

differentiate between a landmine and a clutter. [24] used polynomial fitting techniques to detect the hyperbolic shapes present within a landmine. Another novel technique has been investigated in this research, which uses the frequency domain features from the ground penetrating radar to determine the energy density spectrum present in the mine. This technique is explained in detail in chapters 4 and 5.

## 2.5 Linear Prediction

To start with the linear prediction model, Figures 2(a) and 2(b) [2] show the magnitude plot of the GPR return in various frequencies at a particular position. The nonstationary nature of the background clutter indicates that the removal of background clutter from the landmine signature is a challenging task. Figure 2(a) shows the magnitude plot of GPR data collected over a landmine and Figure 2(b) shows the magnitude plot of GPR data collected over a clutter. The plots show the magnitude plot as the sample number increases. The upper window indicates the position where the mine signatures appear.

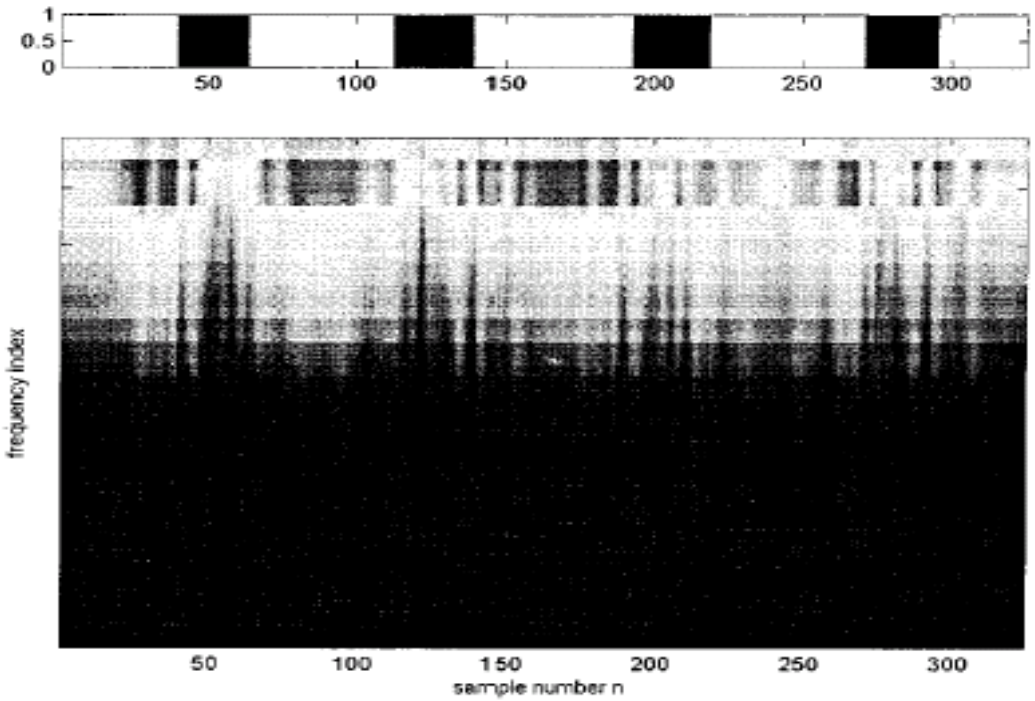


**Figure 2(a) Magnitude plot of GPR data collected over a landmine [2]**

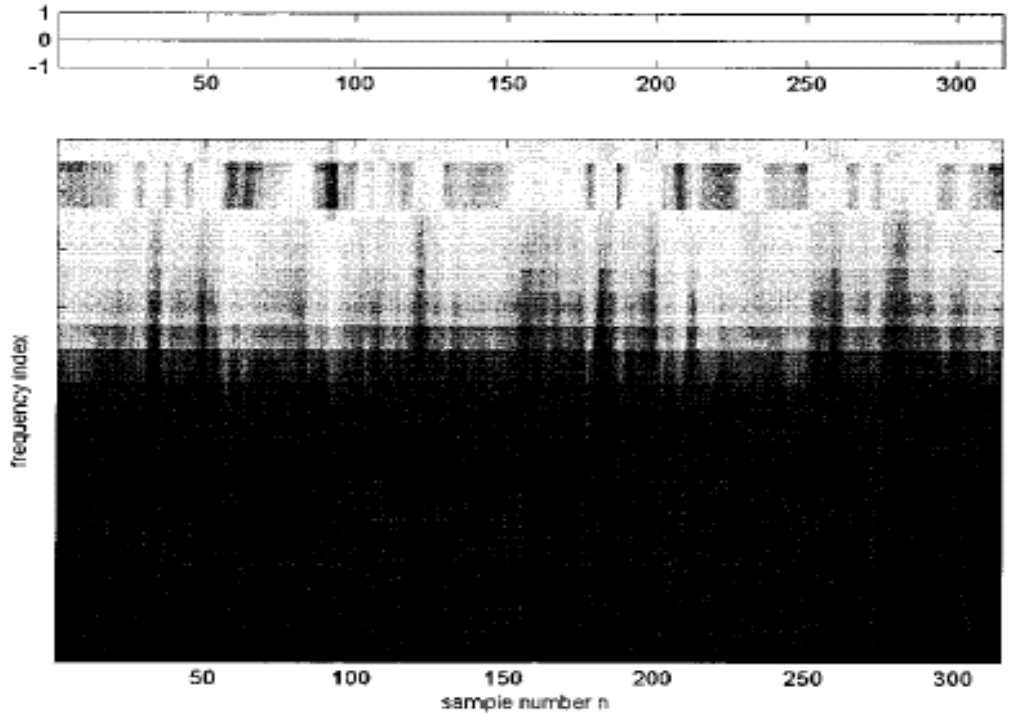


**Figure 2(b) Magnitude plot of GPR data from the clutter [2]**

**Figure 2: Magnitude Plots of GPR data.**

Linear Prediction technique has been proposed by Ho to model the GPR data in the frequency domain. The linear prediction model is given by the following equations:

$$\mathbf{x}(n) = \sum_{k=1}^{P} a_k \, \mathbf{x}(n-k) + \mathbf{e}(n) \;\; = \mathbf{X}(n-1)\mathbf{a}(n) + \mathbf{e}(n) \tag{2.5.1}$$

Where **x** (n) is a vector sample of the GPR data at location n and P is the prediction order, **X** (n-1) = [**x** (n-1), **x** (n-2)… **x** (n-P)] is a collection of P past input vector samples and $\mathbf{a}(n) = [a_1(n), a_2(n) \ldots a_P(n)]^T$ is a vector of the linear prediction coefficients at location n. The linear prediction coefficients are obtained by minimizing $\boldsymbol{\epsilon}^H \boldsymbol{\epsilon}$, giving

$$\mathbf{a}^0(n) = (\mathbf{X}(n-1)^H X(n-1))^{-1} \mathbf{X}(n-1)^H \mathbf{x}(n) \tag{2.5.2}$$

Where the superscript H represents the complex conjugate transpose operation. The resulting error is given by

$$\mathbf{e}(n) = \mathbf{x}(n) - \mathbf{X}(n-1)\mathbf{a}^0(n) \tag{2.5.3}$$

Weighting matrix can be used to find the LP coefficients to improve performance [22].

The advantage of using frequency domain techniques is that sub banding can be used to improve the detection accuracy of the system. Sub banding decomposes each frequency domain vector sample x (n) into M frequency bands that produce test statistic $\xi_i'(n)$ for each sub band. The resulting test statistic is obtained by taking the geometric mean of M test statistics as given by

$$\xi(n) = \prod_{i=1}^{M} \{\xi_i'(n)\}^{1/pi} \tag{2.5.4}$$

Where $\xi_i'(n)$ represents the test statistic for each subband index i and $\xi(n)$ represents the resultant test statistic

Figure 3 shows the steps involved in landmine detection process. The GPR data collected from a hand-held detection unit has two modes of operation. One is the search mode and

the other, locate mode. These modes are discussed in detail in Chapter 3. The operator sweeps the unit back and forth in the search mode and reaches the locate mode when a specific mine location is found. Different algorithms are proposed for the two modes. The search mode algorithm used in this research is CorrDet algorithm proposed by Dr. Ho. This algorithm involves three steps. (a) Weighting matrix is used to improve the performance. Weighting matrix is given by the inverse of the covariance matrix of $\xi(n)$ in clutter. (b) Subbanding is applied in frequency domain to improve performance. (c) After subbanding, linear prediction is applied on each sub band separately. The Error vector from the linear prediction is used in the locate mode to perform template matching based processing. Dynamic template matching along with various modifications to improve detection is explained in the following chapters. Finally, since the prediction error energy is time varying in nature, adaptive threshold is used to decide if the suspected location has a landmine or a clutter. Using a fixed threshold increases the false alarm ratio and hence adaptive threshold is used to take into account the time varying nature of the clutter.

## Flow Chart

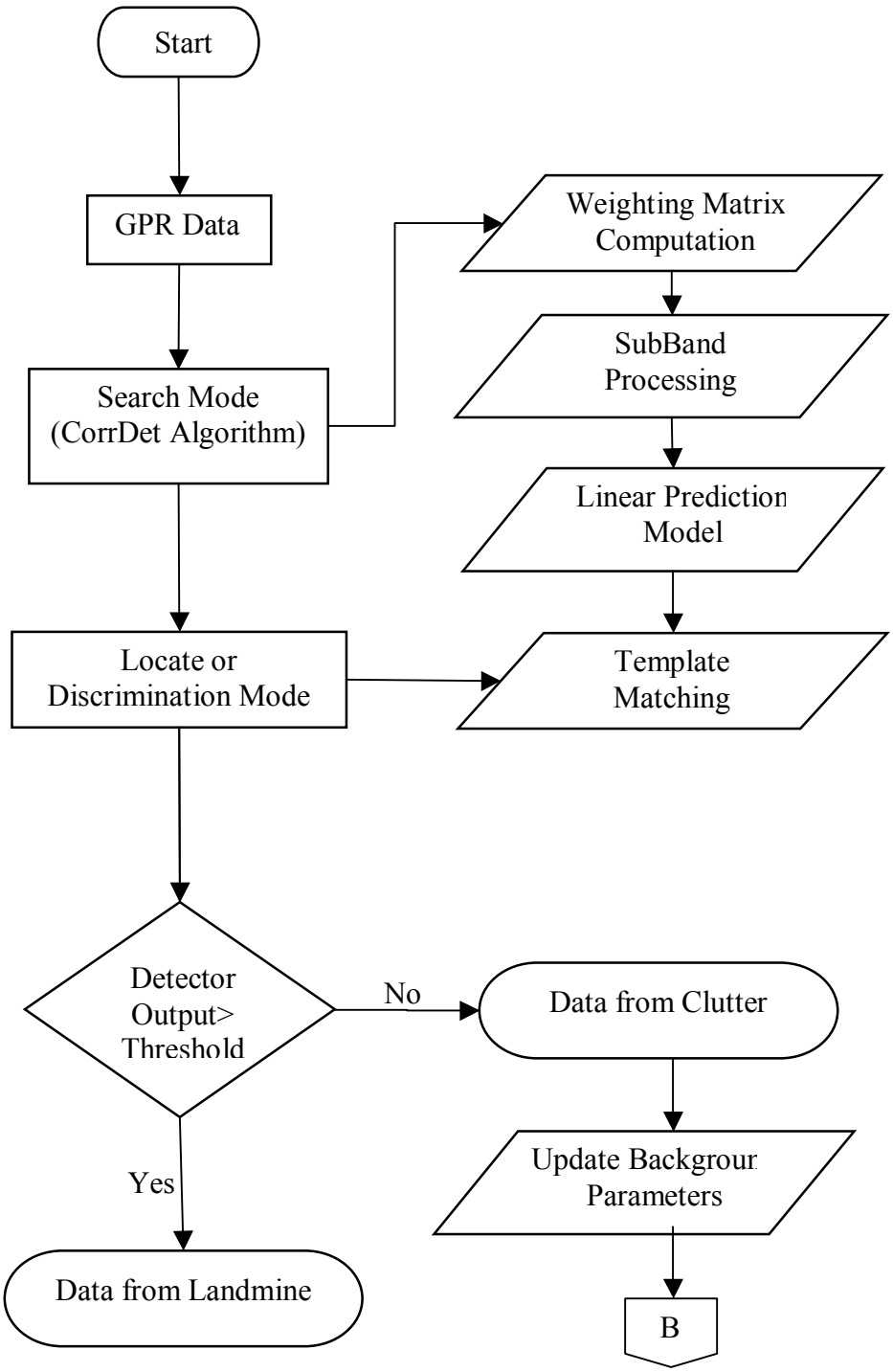


**Figure 3: Flow Chart**

# Chapter 3

# DYNAMIC TEMPLATE MATCHING TECHNIQUE

## 3.1 Introduction to Hand-held GPR system

Detecting minimum metal antipersonnel mines and distinguishing them from the metallic debris of a minefield is difficult with the currently available metal detectors. Previous efforts have attempted to address the requirement for a single system capable of detecting all landmine types and sizes, buried and surface laid, which could be used for all types of terrain. Several promising new technologies are in development to increase the detection rate and to automate these tasks whenever possible to preserve the life of the mine clearing personnel.

The GPR technology is one such widely used system for the detection of buried objects and soil study. Hand-held mine detectors are particularly useful, as they can be employed in areas where access is difficult, and can detect small anti-personnel mines as well as larger anti-vehicle mines. Hand-held system combines metal detection and ground penetrating radar technologies into a single low cost hand-held detector, providing a powerful tool for speeding up mine clearance operations.

The hand-held mine detection system consists of the GPR unit, which the Human operator sweeps across the ground. GPR mine signatures obtained using the hand-held systems may be inconsistent due inconsistency in sweeping speed and variation in sensor to ground distance caused by the human operation factor.

A high detection probability (Pd) is required to avoid casualties and injuries during landmine detection. However, high Pd is often obtained at the price of extremely high false alarm rates. The key challenge lies in the ability to achieve high detection rates along with acceptably low false alarm rates for all types of mines, soil conditions, and false targets.

The hand-held mine detection is generally designed to have two modes of operation: The search mode and the locate mode. Search mode or discrimination mode, generates an initial causal detection on the suspected location and locate mode confirms the existence of a mine. During the search mode, the operator sweeps the detector unit back and forth over the suspected location by walking forward. When an initial detection occurs, the operator works in the locate mode where in the operator stands still near the suspected mine location and interrogates the location using the detector to confirm the landmine location.

The search mode needs to be causal as the position information of the suspected mine location is crucial. Any delay in generating a detection alarm corresponding to the current sample generates a false alarm. This requirement restricts the classes of algorithms used in search mode. However, during the locate mode processing, the causality restriction can be relaxed as the location information is available from search mode and the purpose for locate mode processing is to verify the existence of a buried land mine in the suspected location. This relaxation provides an additional degree-of-freedom to improve the detection performance. Figure 4 illustrates these two modes of operation for the hand-held mine detection unit.

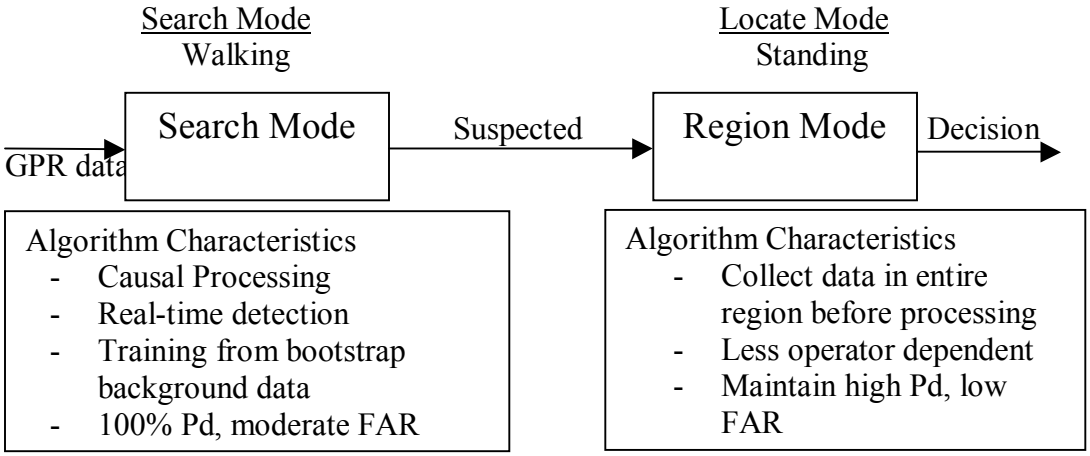


**Figure 4: Comparison of Search Mode and Locate mode Algorithms [25]**

## 3.2 Previous work on Locate Mode Processing

A locate mode processing algorithm has been proposed by Ho and Gader [26] which uses the consistency of detection pattern in several sweeps to improve performance. This algorithm assumes that the Search mode algorithm used is the CorrDet algorithm [23], [27]. The proposed algorithm models the detection pattern mathematically and derives the corresponding Fourier transforms. This Fourier transform is used to find the power spectrum by taking the magnitude square of the FFT. Now, the frequency bin where the first harmonic peak in the spectrum occurs is derived using the following equation

$$I = \frac{1/T}{\text{FFTbinWidth}} = \frac{C/D}{1/L} \qquad (3.2.1)$$

where C is the sweeping speed in m/sec, D is the sweeping distance between two successive crosses on the suspected location in meters, and the total time in collecting the four sweeps is L sec. T is the time duration in which the peak in the detection pattern occurs. The detection confidence is then formed using the peaks in the index range from I-δ to I + δ where δ is the margin for the variation of the peak location.

The locate mode processing algorithm generates a detection value only at the end of the final sweep. Therefore, the operator has to wait until the final sweep to decide the presence of a landmine in that location. A new dynamic template matching based processing [28] is proposed by Ho, which provides a detection confidence value at each sample location, allowing the operator to asses the possibility of mines during the discrimination mode rather than waiting until the final sweep to decide. This technique is further investigated in this research to improve the probability of landmine detection. The algorithm investigated in this research is found to be useful in the detection of weak mines.

## 3.3 Dynamic Template Matching Technique

### 3.3.1 Pre-Processing of GPR data

The GPR data from a hand-held mine detector is dominated by the background and the mine signature is not apparent. Therefore, the GPR data is pre-processed to remove the background. The data for the current research is obtained by pre-processing the GPR data using the Linear Prediction model of the CorrDet Algorithm Proposed by Ho and Gader. The linear prediction algorithm is explained in Chapter 2.4. Therefore the pre-processed data is then equal to the resulting LP error given by

$$\mathbf{Z}(n) = \mathbf{x}(n) - \mathbf{X}(n-1)\mathbf{a}^{\mathbf{0}}(n) \qquad (3.3.1.1)$$

Where x (n) are the input samples, $a^0$ (n) are the linear prediction coefficients obtained by minimizing the mean square error and **X** (n-1) = [**x** (n-1), **x** (n-2)…**x** (n-P)] is a collection of P past input samples. The steps involved in the template-matching algorithm are explained sequentially in sections 3.3.2 through 3.3.3.

### 3.3.2. Data size Reduction

The data samples from the linear prediction step contain 64 data points in frequency domain. The inverse fast flourier transform is applied to convert the pre-processed data to the depth domain. Only the real part of the inverse FFT is used initially in further processing, though the results are also verified using the complex part at later stages in this thesis. Using only the real part reduces the data size and saves the computation required, sometimes at the expense of a little probability of detection.

Considering the fact that the mine signatures appear only the ground level region, the ground level is estimated using the clutter data and only that portion around the ground level is used for further processing. The ground level is estimated taking the depth bin where the maximum of average of GPR data in the depth domain occurs. Figure 5(a) gives the example of depth domain data after data reduction. Only 19 depth data points around the ground level were kept in each sample. Experiments on varying the number of depth bins to be taken proved that using 19 depth bins decreases the probability of false alarms at a given probability of detection.

### 3.3.3 Extraction of template pair

The CorrDet output is then used to identify the template location. Figure 5(b) shows the Linear Prediction Error from the CorrDet algorithm, which is used to identify the template location. In particular, the Corrdet output is threshold by an adaptive threshold value and low pass filtered for smoothing. The smoothed CorrDet output is then scanned starting from the beginning until the final maximum occurs. The location of maximum gives the center of the first possible template. In order to take the dimension of the template into account, the smoothed CorrDet output whose values are bigger than, say 30% is defined to be the start of the template. This 30% or 0.3 is defined as the peak width fraction. This criteria provides a larger template for a larger mine. It is verified that the peak width fraction of 0.3 gives less false alarm at higher probabilities, compared to using a value less than or greater than 0.3.

### 3.3.4 Identification of template pair

Since the GPR data is collected by sweeping the unit back and forth, consecutive sweeps are in the opposite direction. Therefore, the second template should match with the first template flipped in left to right direction. Figure 6 shows the two templates in different sweeping directions. The two templates appear as mirror images to each other. The Template extraction described above is continued further to extract another possible template. After matching the first two templates, if the matching score is high, then the two templates represent a pair that is high likely to represent a signature from a mine target. If the matching score is low, the search for the template continues, which is then

matched with flipped version of the first, and second templates separately. This process continues until a pair is found or the maximum number of samples is reached.

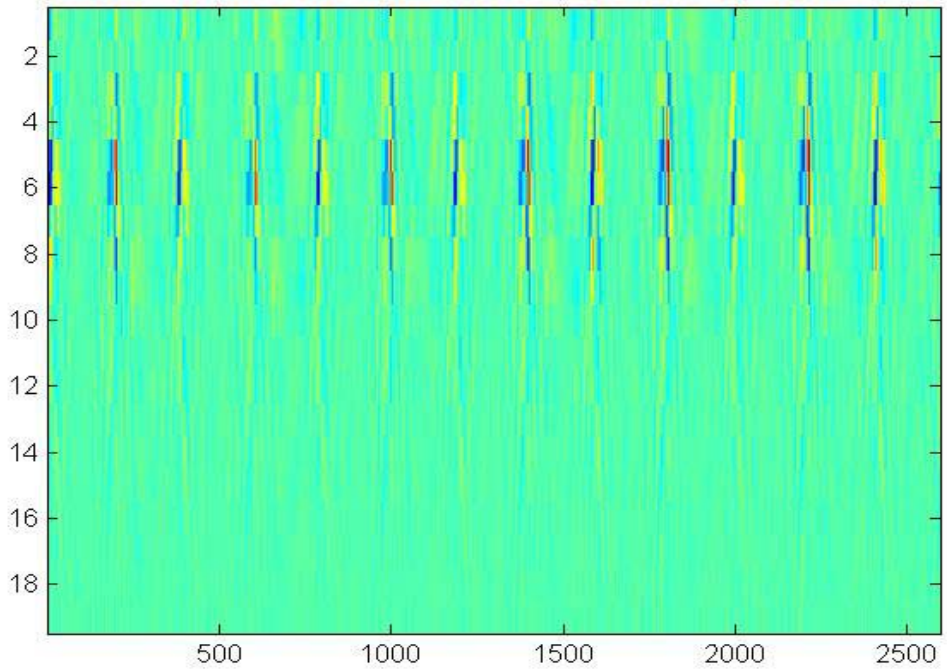


**Figure 5(a): 19 Depth bins used in Template Matching, after removing Ground level**

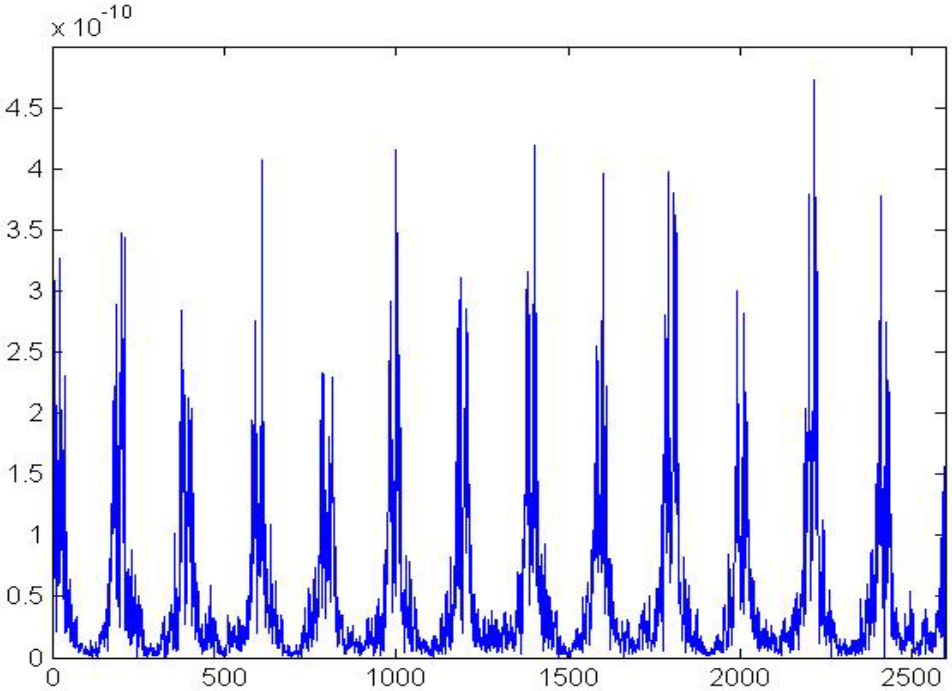


**Figure 5(b): LP Error from CorrDet Algorithm used to identify the template location**

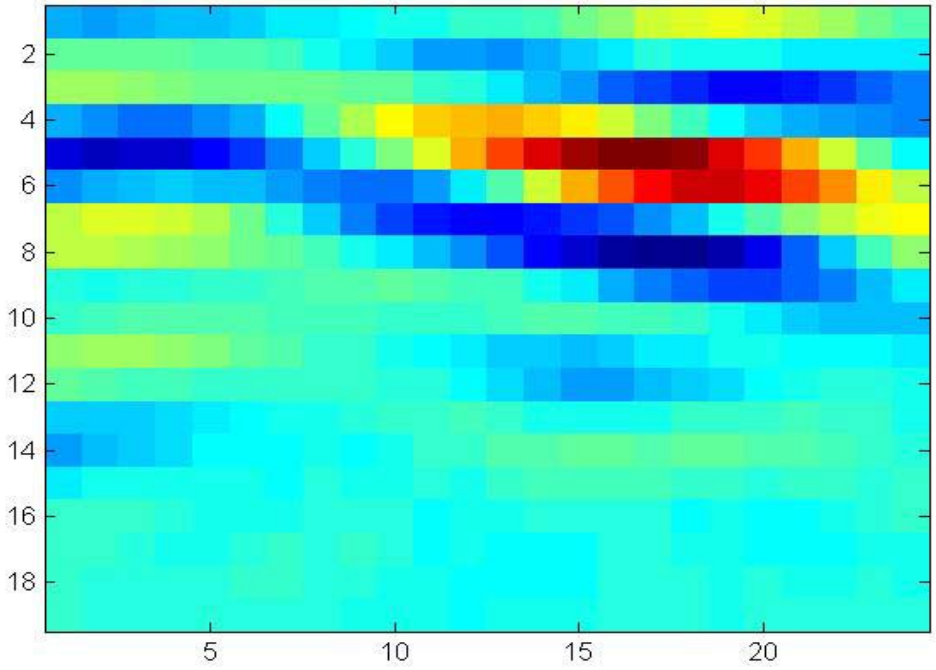


**Figure 6(a) Template from Left to Right Sweep**

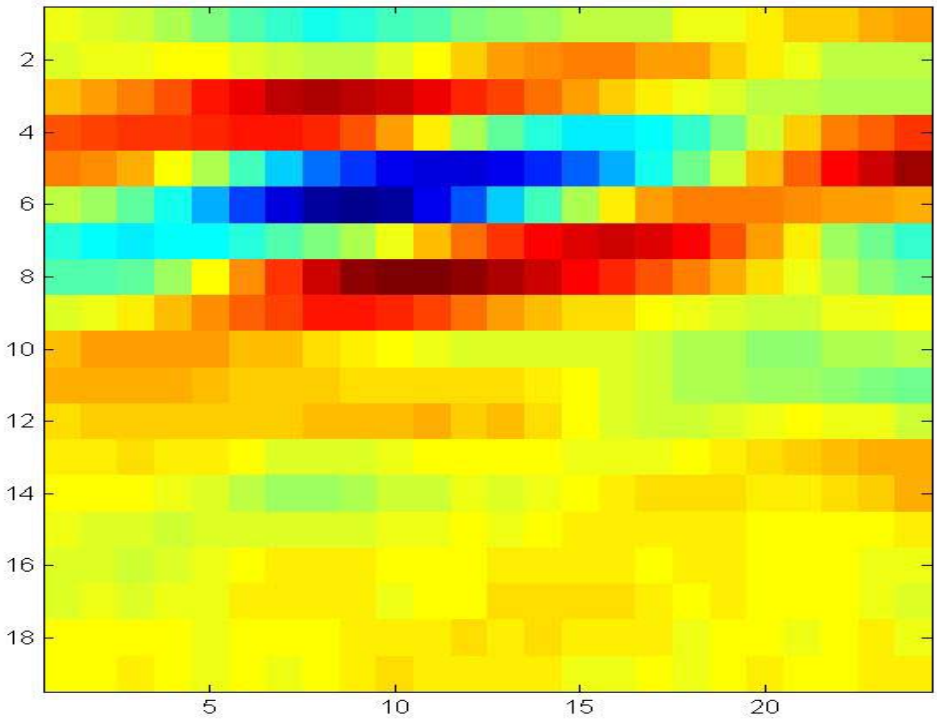


**Figure 6(b): Template from Right to Left sweep**

**Figure 6: Templates in different sweeping directions.**

### 3.3.5 Template Reduction

In order to reduce the delay for the detector to go past the mine and collect the entire mine segment for matching; only the first half of two templates is kept. The resulting two templates $tp_1$ and $tp_2$ are normalized to have unit energy. When applying template matching, the largest score will occur at the center of the mine. This is the major advantage of Template Matching technique compared to other algorithms. The template matching provides a peak detection confidence at the center of the template, clearly distinguishing the strong peak.

### 3.3.6 Template Alignment and Mean Template

After finding the template boundaries, the current template from the forward or reverse sweep is aligned with the previous template in the corresponding direction in order to avoid any relative shift with respect to each other. This step avoids any misalignment in the templates when taking the average of the templates. The mean templates are then obtained in the forward and reverse direction, which are used to find a matching score with the subsequent data.

### 3.3.7 Template Matching

The two templates $tp_1$ and $tp_2$ are used to perform template matching of a segment of preprocessed data in sequential manner. Let y (i, j) be the pre processed data in depth domain; the matching score between the data segment at instant n and $tp_1$ is given by

$$C_1(n) = \sum_{i=1}^{M} \sum_{j=1}^{N} tp_1(i,j) y(i, n - N + j) \quad (3.3.7.1)$$

and that with $tp_2$ is given by

$$C_2(n) = \sum_{i=1}^{M} \sum_{j=1}^{N} tp_2(i,j) y(i, n - N + j) \quad (3.3.7.2)$$

Where the size of two templates is given by M depth bins times N samples

The detection confidence at location n is taken to be the maximum of c1 (n) and c2 (n) as given by the equation below:

$$Conf(n) = \max\{C_1(n), C_2(n)\} \quad (3.3.7.3)$$

The CorrDet algorithm processed data in two sub bands and produces the LP Error in two sub bands, the upper and the lower band. A confidence value from the template matching is obtained from the lower and upper band separately and the geometric mean is used to combine the confidence values from the two bands. Figure 7 shows the Confidence values for a plastic anti-tank mine in standing mode, before and after applying the template matching technique. It is clearly evident from the figure that the template matching technique generates peak detection value at the centre of the mine.

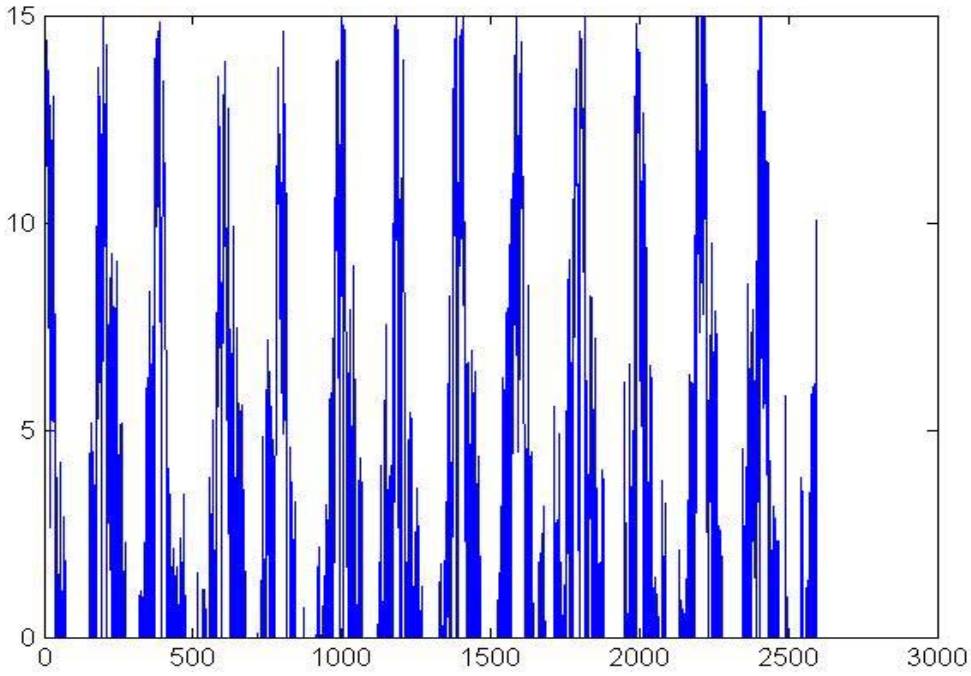


**Figure 7(a): Detection values from Original CorrDet Algorithm**

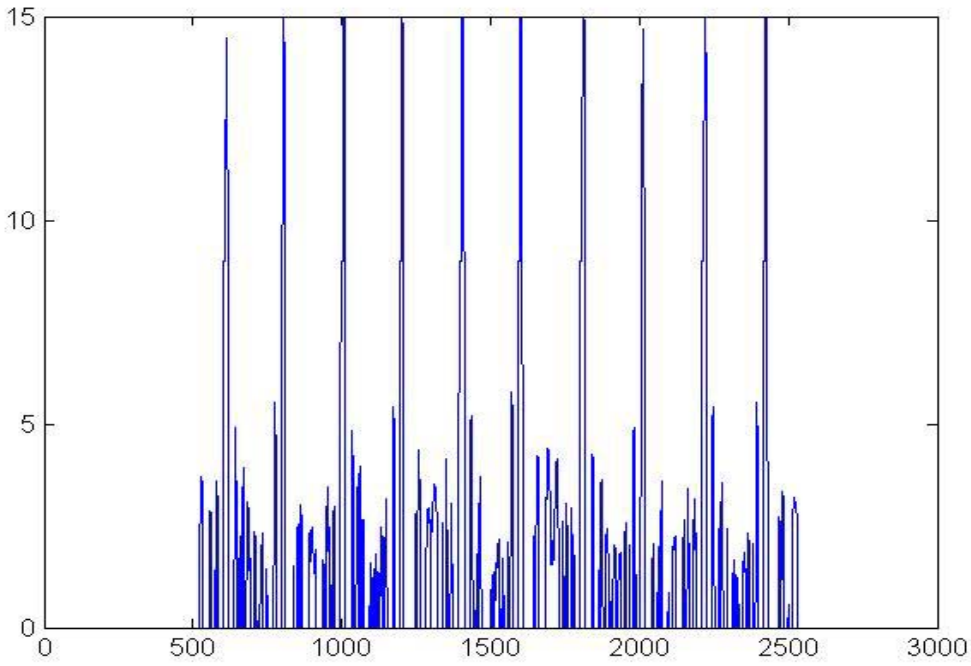


**Figure 7(b): Detection values from Template Matching Technique**

**Figure 7: Confidence values of mine in standing mode.**

### 3.3.8 Receiver Operating Characteristics (ROC) Curve

To evaluate the performance of the algorithm, a ROC curve is generated for 461 mine targets collected at a test site. The data set contains anti-tank metal, anti-tank low-metal and anti-personnel low-metal mines. The data set has walking and standing mode data, where standing mode data is used to apply template matching. To evaluate the performance of Template Matching technique on all the targets in the dataset, the confidence values obtained from different files are scored together. The ROC curves are used to plot the probability of detection of a mine with the probability of false alarm. The Probability of detection (Pd) is calculated as the total number of detected land mines to the total number of mines. The false alarms are computed using the clutter files only. The Probability of false alarm (Pfa) is the number of false alarms divided by the time in collecting data. The number of false alarms is equal to the ratio of the ceiling of the number of clutter samples above the threshold to the alarm size, taken as five here. Each point on the ROC curve corresponds to a particular threshold, and represents a mine region that is above the threshold. Before using the scoring algorithm for the ROC curve, the dynamic range of the confidence values was reduced using natural logarithm. Figure 8 shows the ROC curve generated for the CorrDet algorithm with and without the template matching technique. The solid curve corresponds to the ROC obtained from the CorrDet algorithm and the dashed curve represents ROC obtained after applying the template matching technique. To interpret the ROC curve, consider a point on figure 8 at which the probability of detection (Pd) is 0.9. Before template matching is applied, the Pd reaches 0.9 at a false alarm probability (Pfa) of 0.019. After template matching is applied the Pd is 0.9 at a Pfa of 0.01. Therefore, at 90% probability, the Pfa decreased by 9%.

Similarly, at a Pfa of 0.01, the Pd is only 0.7 without template matching, whereas the Pd increased to 0.9 at a Pfa of 0.01 with Template matching, thereby increasing the Pd by 20%. Hence, it can be concluded that the template matching technique is useful to reduce the probability of false alarms.

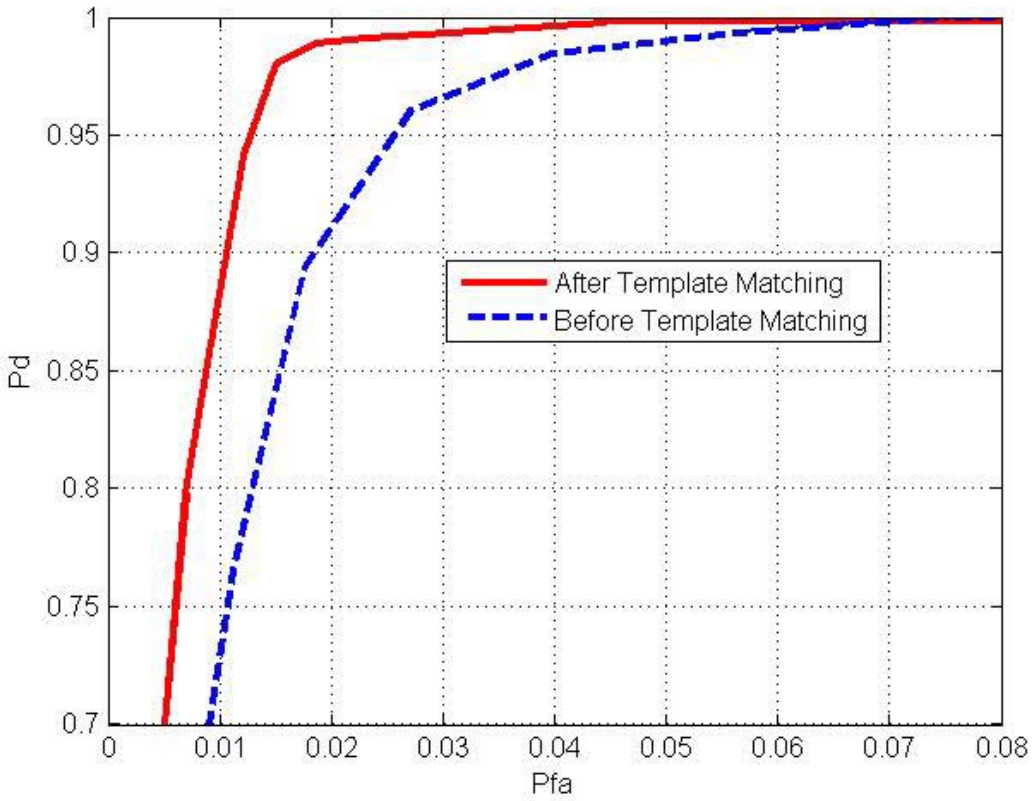


**Figure 8: ROC curve before and after Template Matching, on a dataset with 461 Mine targets**

## 3.4 Modified Template Matching Techniques

### 3.4.1 Flip and Combine approach

The original template matching technique uses the feature templates from the left to right sweeps separately to match with the subsequent data in left to right direction and generates a confidence value at each sample location. Similarly, the templates from the right to left sweep are used to match with the subsequent data in the right to left direction.

The modified technique proposed in this research investigates the use of the templates obtained by combining the left to right sweep with the templates from the right to left sweep to obtain a confidence value at each sample location. Since, the two templates are mirror images of each other, the templates obtained from right to left direction are flipped and combined with the templates obtained from left to right direction to obtain a matching score. The templates from the forward and backward sweeps have to be aligned, so that there is no relative shift with respect to each other.

**Results from Flip and Combine approach**

Figure 9(a) and 9(b) show the detection values obtained from a plastic anti-tank mine, by using the original Template matching technique and the modified template matching technique using the flip and combine approach.

The odd peaks in the figure 9(a) correspond to the detection peaks from the mean of forward templates and the even peaks correspond to the mean of backward templates. In figure 9(b), the peaks represent the maximum confidence value obtained by combining the flipped templates in backward direction with templates in forward direction. Figure 10 is the ROC curve obtained for the modified technique compared with the ROC from Original technique

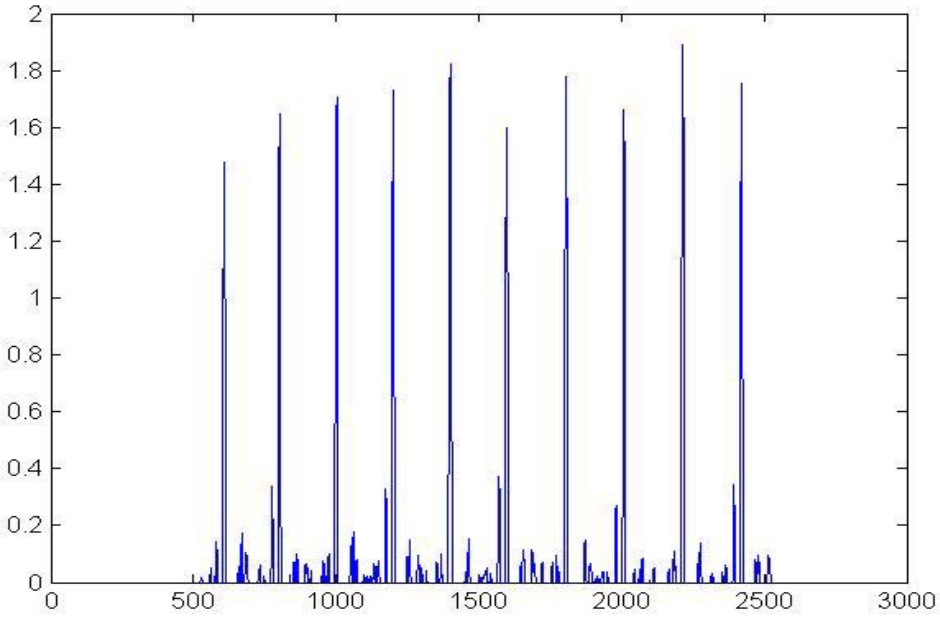


**Figure 9(a): Confidence values for a plastic anti-tank after fusion of results from Lower and Upper bands of front antenna, with Original Template Matching Technique**

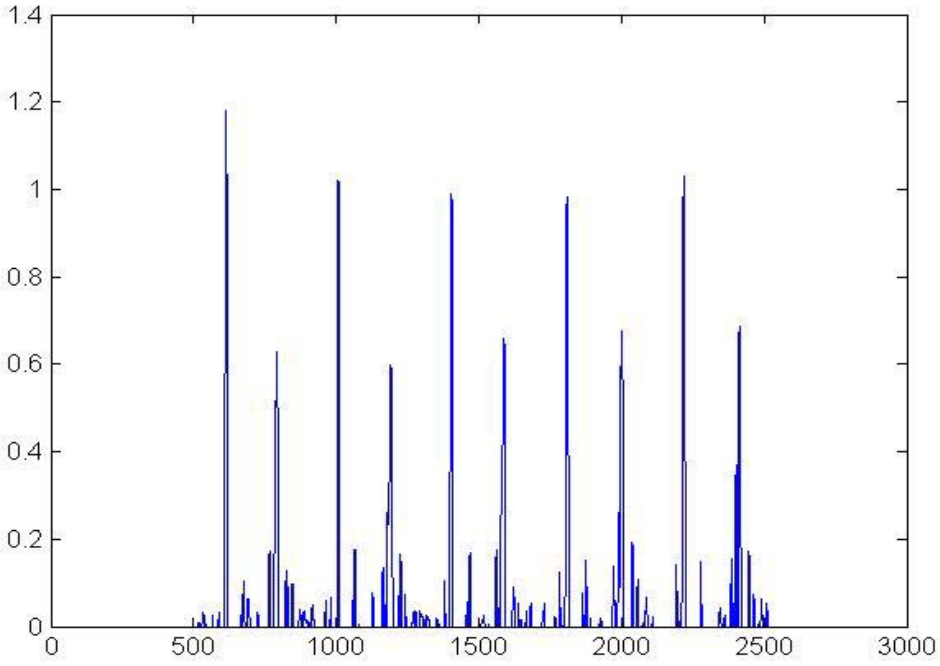


**Figure 9(b): Confidence values for a plastic anti-tank mine after fusion of results from Lower and Upper bands of front antenna, with Modified Template Matching Technique**

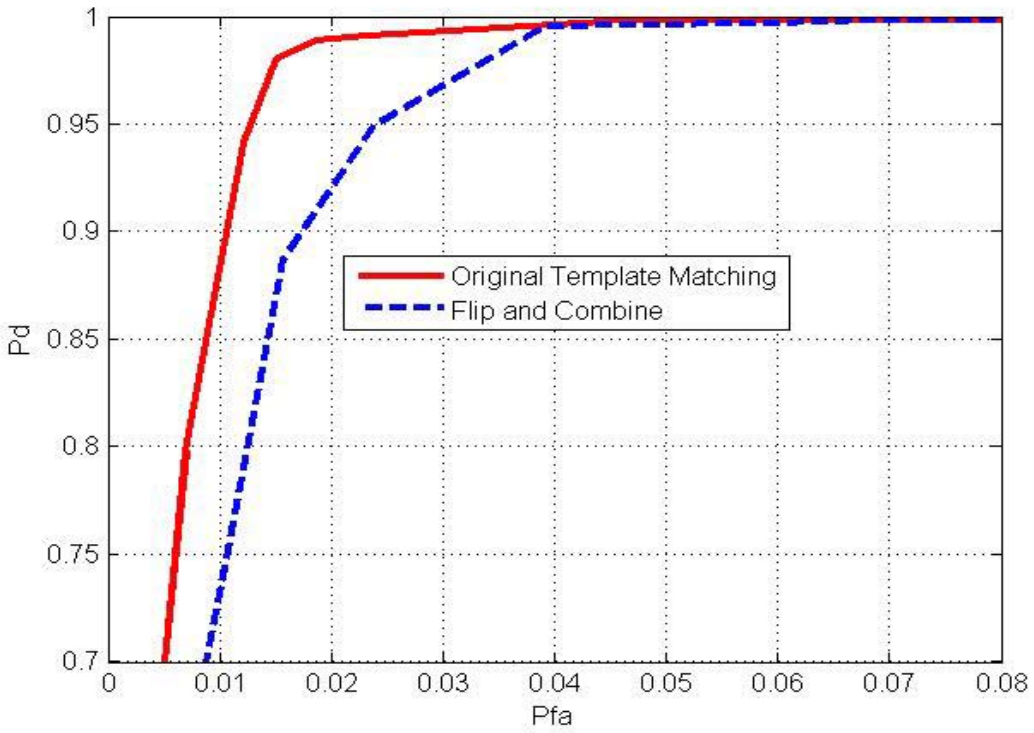


**Figure 10: ROC comparison of Original Template Matching with Modified Template Matching**

At a probability of 0.9 for detection, the false alarm associated for the original technique is 0.01, whereas that associated with modified technique is 0.18, which is a degradation of 8%. Similarly, as we compare the probability of detection at a fixed false alarm, at a Pfa of 0.02, the Pd with the original technique is 0.99 , whereas with the modified technique the Pd is only 0.92, which means that the original technique gave higher Pd compared to the modified technique. Thus, from the figures, it can be seen that combining the templates in opposite directions reduced the peak confidence value, which further reduce the probability of detection (Pd) wit a fixed Probability of False Alarm (Pfa) as observed from the ROC in Figure 10.

### 3.4.2 Batch Processing Approach

The original Template Matching technique correlates the mean template obtained from each sweep with the subsequent data to find the final confidence value. The batch processing, on the other hand, uses the final mean template obtained from all the sweeps together, to perform correlation with the subsequent data. This technique uses the fact that the mean template obtained at the end of all sweeps has strong detection peaks compared to the detection peaks obtained with individual sweeps.

**Results with Batch Processing**

Figures 11(a) and 11(b) show the confidence values obtained for a mine file buried at a depth of 1inch under the ground. The correlation values correspond to the front antenna with and without batch processing. There is an improvement in the detection confidence when batch processing is used. This is because we use the mean template obtained at the end of all sweeps, which is better than the individual template. Figure 12 shows the ROC comparison for Original Template Matching technique with and without Batch processing. Probability of detection increased with the batch processing along the lower part of the curve. The ROC showed improvement before reaching 95% probability of detection, after which the curve is same for both the techniques.

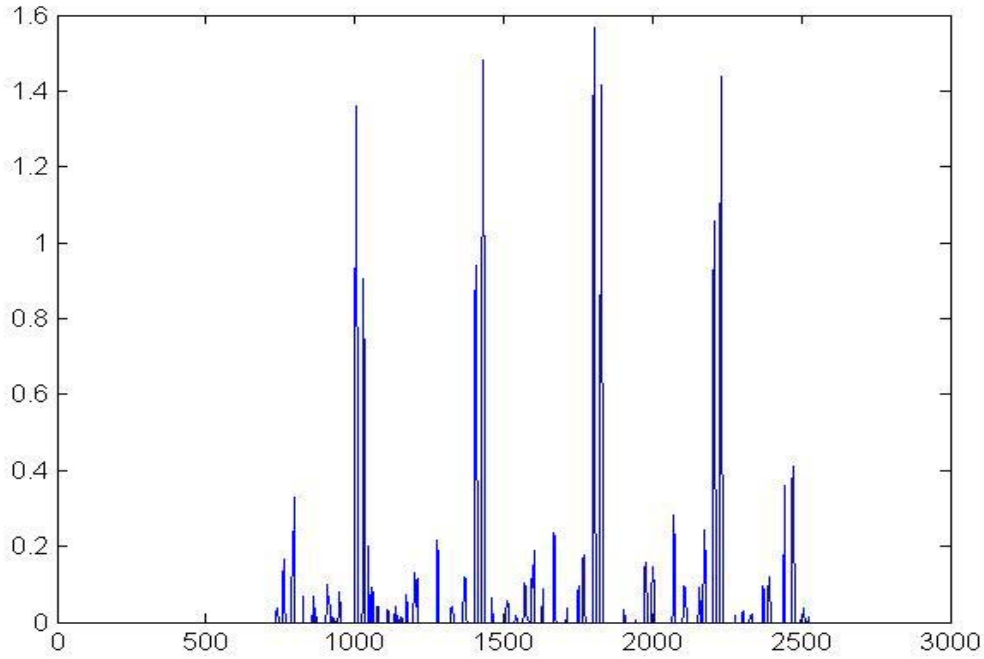


**Figure 11(a): Detection values for a plastic anti-tank mine, 1 inch deep, with the front antenna using the Original Template Matching Technique**

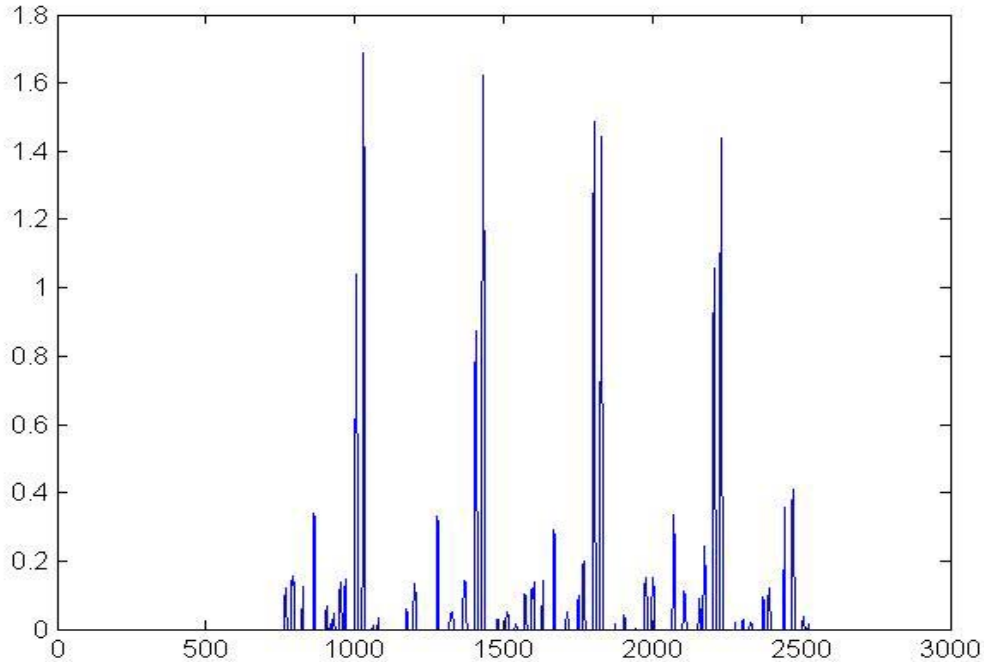


**Figure 11(b): Detection values for a plastic anti-tank mine, 1 inch deep, with the front antenna using the Batch Processing**

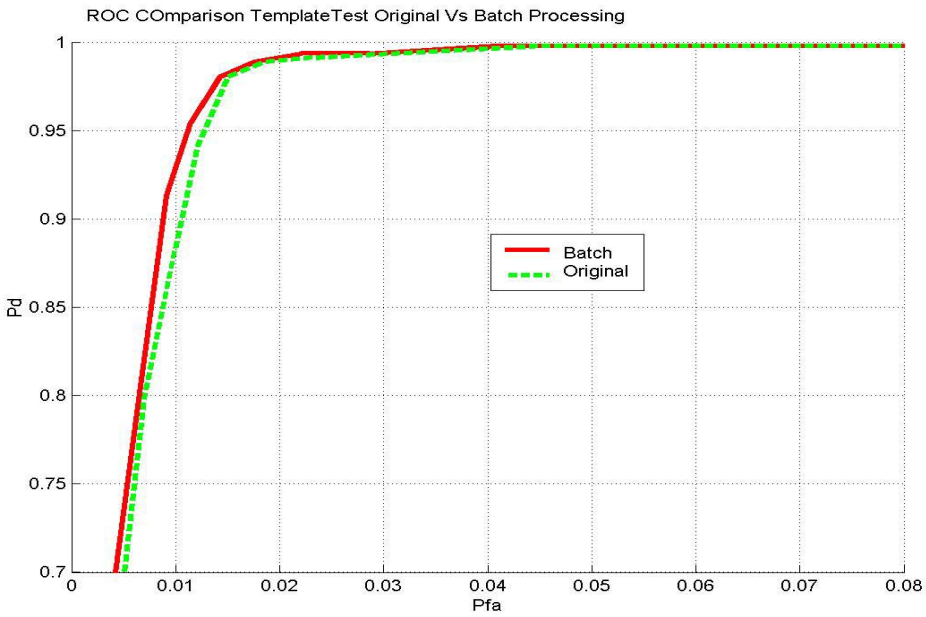


**Figure 12: ROC Comparison for Original Template Matching vs. Batch Processing**

It is evident from the figure 12 above that the batch processing technique has reduced the probability of false alarm at a given detection probability.

### 3.4.3 Effect of Scaling on Front and Back antennas

In the original template matching technique, the dynamic range of the detection values is adjusted to be in the range 0 to 1.5 before scoring. Originally, the forward and backward antennas are set to be in the dynamic range of 0 to 1.5. Figure 13 (a) and 13(b) show the confidence values obtained by using the original template matching technique on the front and back antenna. The maximum of the detection value for the two antennas differs by a large value, which forced this research to investigate the effect of scaling on the two antennas.

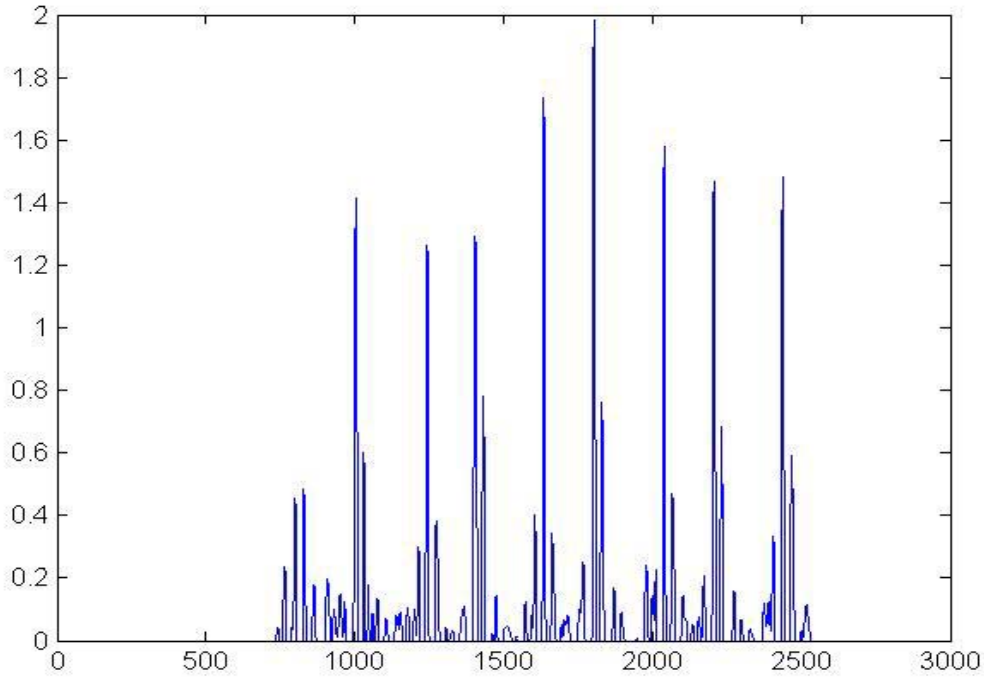


**Figure 13(a): Lower Band Correlation values for the front antenna for a mine file**

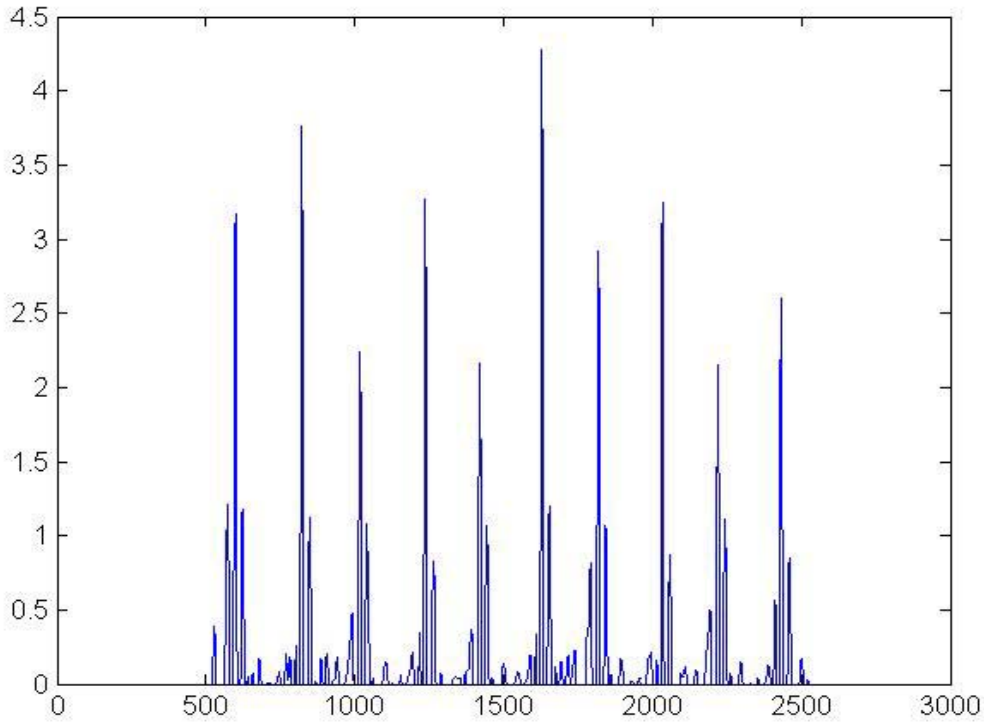


**Figure 13(b): Lower Band Correlation values for the back antenna for a mine file**

The Scaling factor for one of the antennas is obtained by taking the average of the ratio of maximum peak values obtained for the two antennas, keeping the scaling factor for the other antenna as reference. The scaling factor for the back antenna is kept as 1.5 and the scaling factor for front antenna is found to be 0.9. These Scales are also used with the batch processing technique to interpret the effect of scaling on the two antennas. Figure 14 shows the ROC comparison for the Original Template Matching technique with scaling factor of 1.5 on both antennas, scaling factor of 0.9 for front antenna and 1.5 for back antenna using Original Template matching and Batch processing. The ROC improved when different scales are used for the front and back antennas. At a Pd of 90%, the false alarm reduced by 10% with different scales for the two antennas.

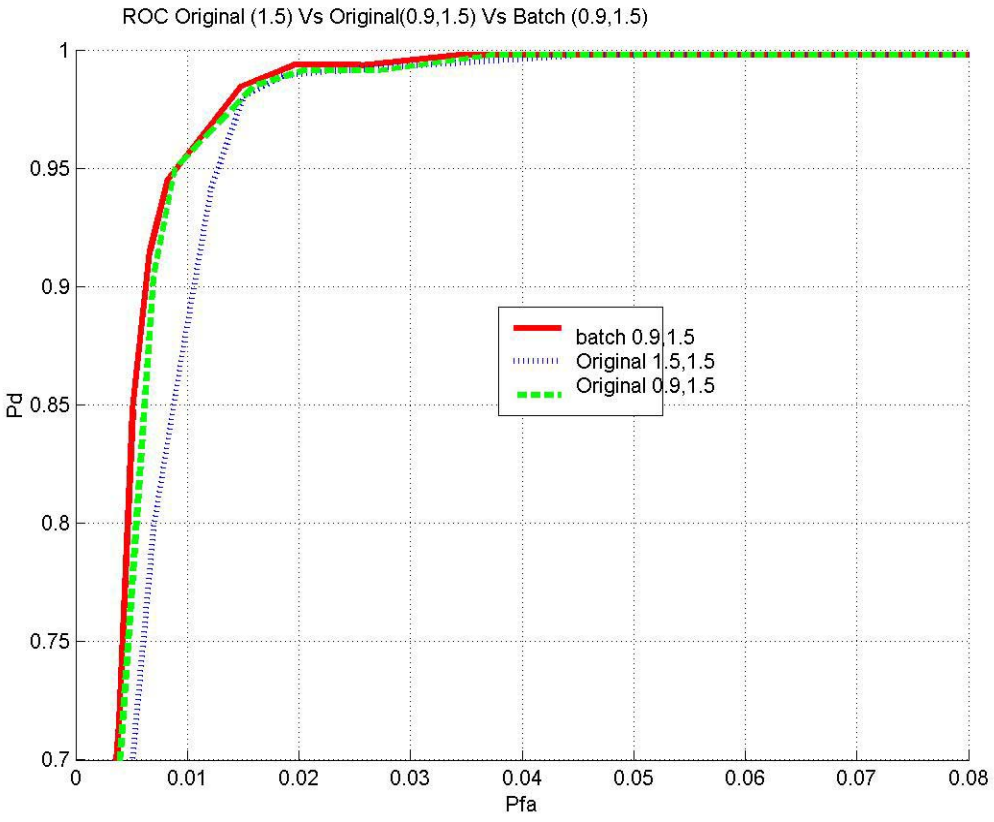


**Figure 14: ROC for Original Technique vs. Batch Processing with different scales**

### 3.4.4 Effect of Using Complex data with different scales for front and back antenna

The depth domain data used in the Template matching technique is originally complex data, of which only the real part was used for Template matching. In this section, the ROC analysis is performed using Complex data to verify for better results. Figure 15 shows the ROC curve generated using the complex data with and without batch processing. Scaling factors of 1.1 and 1.41 are used with the complex data for the front and back antennas respectively. The curve also compares the ROC from the original algorithm with the ROC from real data and complex data. For a given probability of detection, the false alarm is reduced using the complex data compared to the real data. Further, as expected, the Batch processing performed better than the original template matching technique using the real data and the complex data. At a Pd of 90%, the original algorithm with scale 1.5 on both antennas has a false alarm of 0.01, whereas with the batch processing on real data has a false alarm of 0.009, which is a 1% reduction. With batch processing on complex data with scales 1.1 and 1.41, the false alarm further reduced to 0.007, which is a reduction of 3% compared to the original algorithm with real data. Above the Pd of 97%, all the techniques showed the same performance. Below the Pd of 97%, the batch processing with the complex data and different scaling factors for both antennas, performed better than any other technique. Therefore, using complex data resulted in better performance of the ROC curve.

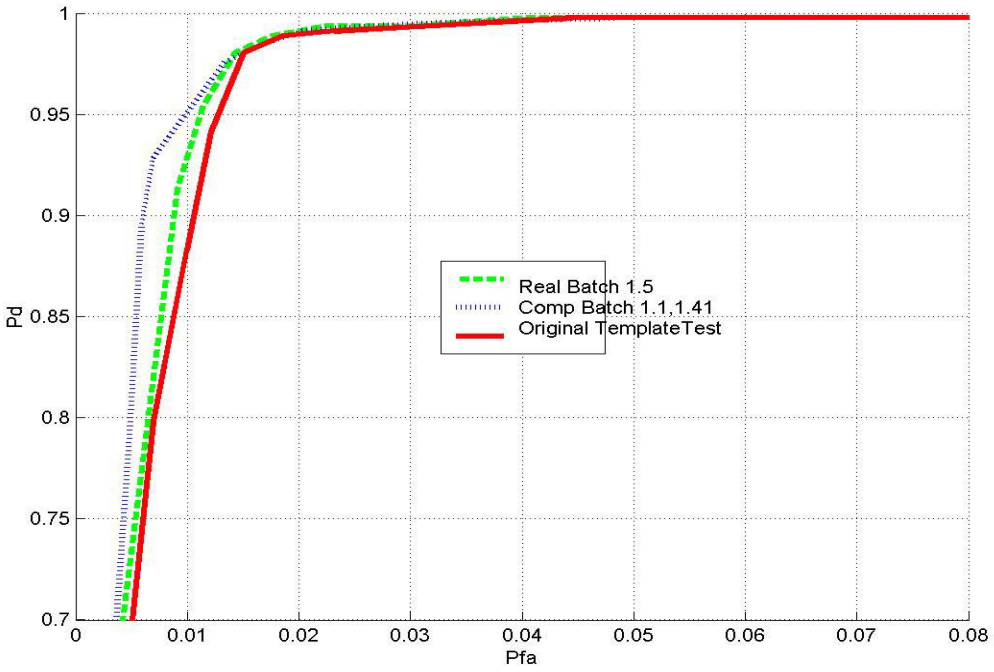


**Figure 15: ROC Using Complex data with different scales for front and back antennas**

### 3.4.5 Results from Template Matching Using a different Dataset

The above techniques are also applied on a different data set from a different test site. The data set consisted of 225 target locations at various depths. For comparison, the Confidence values obtained from a different technique provided with the dataset are used. The dataset has 8 sweeps of data collected for the front and the back antenna, of which the first 6 sweeps contain data collected by sweeping the GPR unit from left to right and right to left. The remaining 2 sweeps are collected by sweeping the GPR unit in the horizontal direction. The above techniques are applied to the data set using 6 sweeps as well as all the 8 sweeps.

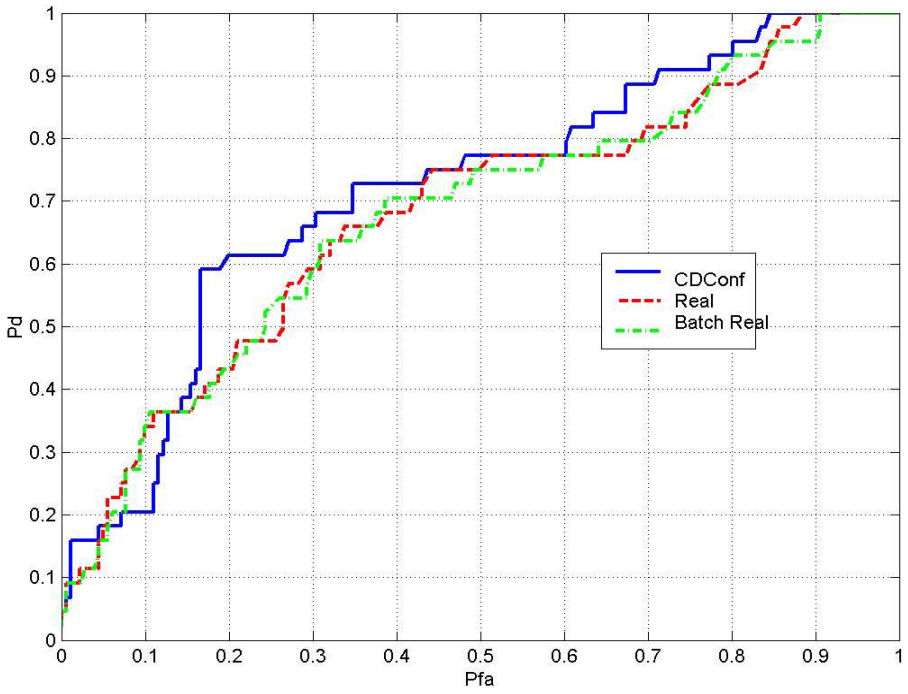


**Figure 16: ROC comparison with Confidence values from the data set vs. Template Matching**

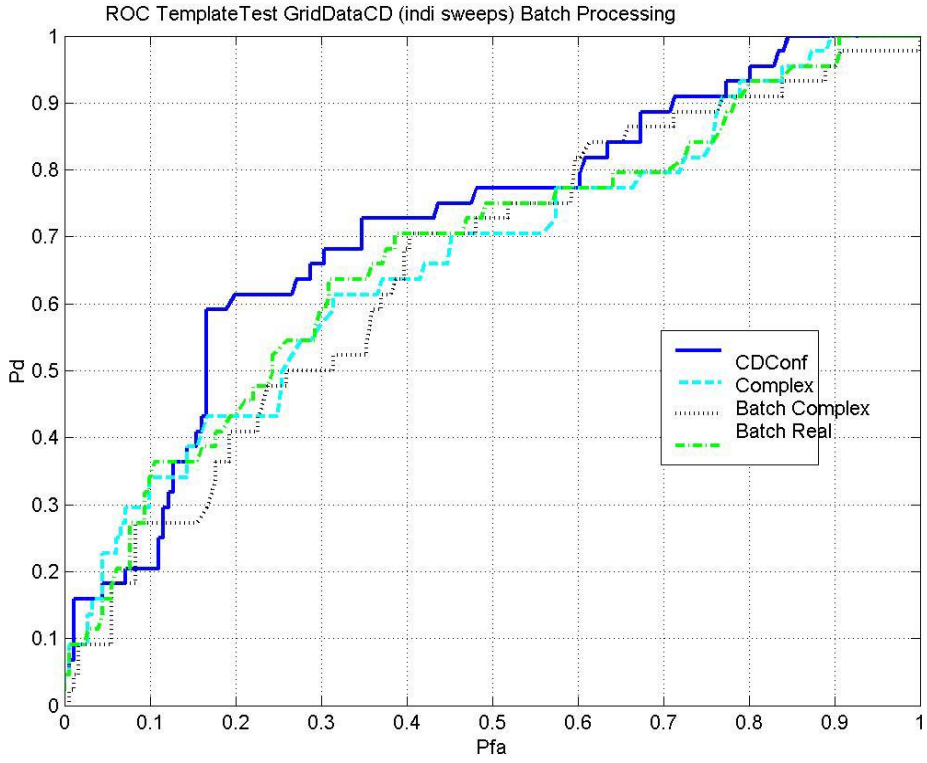


**Figure 17: ROC comparison of Original structure with Template Matching using Complex data with and without batch processing**

Figure 16 shows the ROC curve generated using the confidence values from the data set and also using the template matching technique with and without batch processing for real data. Unfortunately, the technique did not generate better results than the original ROC. Using Batch processing could not even improve the performance of the ROC curve.

Figure 17 shows the ROC for the Template Matching technique using the real and complex data. The figure also compares the performance of batch processing with this data set. The ROC using real data is better than the ROC using complex data, though the ROC performance did not improve compared to the original ROC obtained from confidence values within the structure. Figure 18 shows the ROC curve using the first 6 sweeps and also using all the 8 sweeps. The ROC still did not show any improvement in its performance.

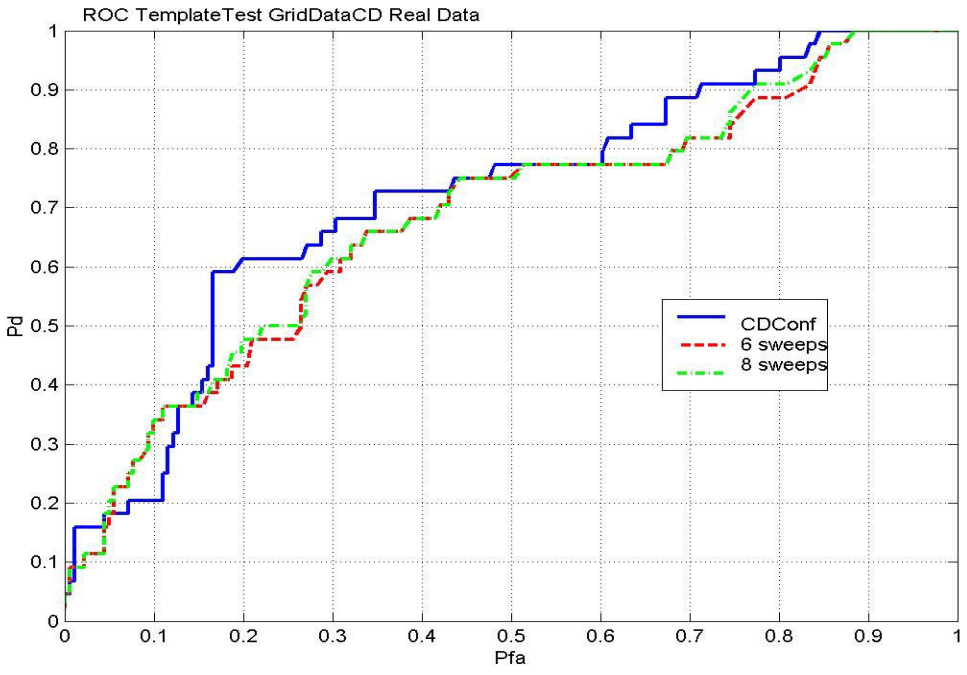


**Figure 18: ROC comparison using first 6 sweeps and all the 8 sweeps**

## 3.5 Conclusions

The template matching technique and some of its modifications developed in this research improved the probability of detection of landmines, reducing the probability of false alarms. Though a few of the modifications failed to improve the probability of detection, they certainly proved that further research using data collected from various other test sites is necessary before discussing any disadvantages of these modified template matching techniques. Further, this research does not use the depth information present in the data to investigate its effect on Template Matching. Therefore, Future work on template matching should also concentrate on considering the depth of the landmine into account. More research also needs to be done on the batch processing, in order to evaluate its performance on various datasets collected from different soil conditions.

# Chapter 4

# LANDMINE DETECTION USING FREQUENCY DOMAIN FEATURES FROM GROUND PENETRATING RADAR

## 4.1 Introduction

Handheld mine detection systems have the capability of detecting small low-metal antipersonnel mines. The GPR signatures from Hand held GPR radar are very unstable and require a feedback to be provided to the operator as soon as a part of mine has been detected. Hence, anomaly detection algorithms are used in this case. In the case of vehicle mounted GPR systems, the signal returns are usually corrupted by background noise and clutter and the pattern of signal return from a mine could be distinctive, even if the energy of the signal return from a mine was relatively low. Hence, feature based processing techniques are usually employed in this case.

## 4.2 Vehicle Mounted GPR Systems

The Landmine detection equipment should be able to sweep large surfaces such as roads at a reasonable speed with a reduced hazard level. Variety of Vehicle mounted GPR systems have been developed so far with this strategy in mind to improve the probability of detection of landmines made of plastic or low metal content. Conventional vehicle mounted mine detector systems employ an array of sensor elements, sometimes more than one sensor technology. For example, Improved Landmine Detection System (ILDS) [23] is a multisensor, teleported system which uses 24 metal detector coils to cover a 3 m

swath. It also uses 3 GPR modules, each consisting of a number of transmit/receive antenna pairs, to achieve the required coverage. The other end of the system has an operator with hand-held metal detector. The output of these detectors would then be combined using data fusion to reduce individual detector false alarm rates. Another such vehicle mounted system is the articulated robotic sensor system [30] which uses a generic robotic device which moves a mine detection sensor over rough surfaces, similar to human operator. This device is operated remotely to increase the safety of the personnel performing mine detection. The system replaces an array of sensors with a single sensor, but provides similar coverage. Thus, the system reduces the cost, size and overall complexity, with minor increase in mechanical complexity. Another system which is being used recently to collect data in the field in the government test lanes against antitank landmines is the Wichmann/NIITEK system. In this system, the Wichmann/NIITEK radar mounted on a vehicle with anti-tank mine overpass abilities. The system is also equipped with global positioning system (GPS) sensors to track the system's location. At the rear of the vehicular system will be a marking system to mark the locations at which the targets are determined. The Wichmann/NIITEK radar is very wideband (200 MHz – 7 GHz) radar with extremely low radar cross section. Due to the high bandwidth, even the inner structure of the buried object could also be easily determined. Thus, subsurface target identification and discrimination is possible using the signals measured with this system. The application of feature based detection technique [31] to data collected from NIITEK radar is the topic covered in this chapter.

## 4.3 Wichmann/NIITEK GPR Data

The NIITEK data is collected using 1.2 m wide array with 24 antennas, or channels, spread approximately 5 cm apart on a vehicular system. Therefore, the data consists of 24 cross-track channels for each scan. The data in the 24 channels is sampled every 5cm down-track as the vehicle moves in down track direction. Because of the antenna's hardware and sampling aperture, each channel records 415 point vector of time samples and hence gives 24, 415 point time-domain vectors for every 5 cm down track. To avoid computational complexity in locating the position of interest, pre processing is required on the collected data. The data after Preprocessing is as shown in figure 19 below.

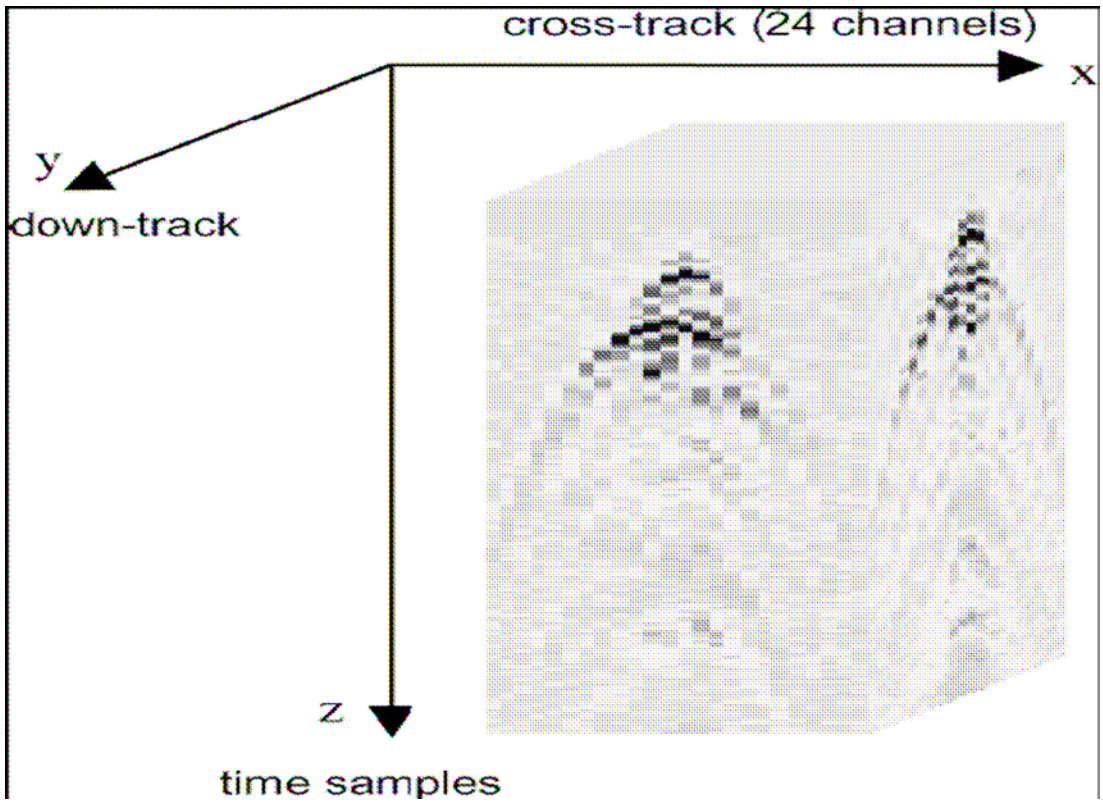


**Figure 19: Three-dimensional Wichmann/NIITEK GPR data after pre-processing [29]**

## 4.4 Introduction to Frequency Domain Feature Extraction Techniques

The GPR data from the radar contains undesired signal generated due to high dielectric discontinuity present between the soil and air, known as ground bounce. Hence signal processing is necessary to improve the detection of landmines and reduce false alarms. The signal processing algorithms presented earlier were performed in depth domain [32-35]. In cases where the GPR signal return is very weak, the GPR signal spectrum may contain important features for detection. The remaining part of this chapter investigates such a novel frequency domain technique to improve the detection of low metal or plastic mines. The next section summarizes the procedure to generate the energy density spectrum of a suspected mine location. The energy density spectrum is then used to extract the feature vectors and generate confidence values to detect the presence of mine, as explained in the subsequent chapters.

## 4.5 Energy Density Spectrum Generation

Dr. Ho and Dr. Gader proposed a frequency domain technique [31] that explores the spectral characteristics of landmines in order to improve their probability of detection. The technique uses the energy density spectrum obtained from the mine targets to improve the detection. The initial algorithm proposed by Dr. Ho is used as a reference to improve the probability of detection in this chapter.

The Bandwidth of the radar used in this study is upto 6 GHz and the sampling rate is 62 GHz. Hence, due to the large bandwidth, this radar provides very high resolution in

depth, and due to high sampling frequency, the frequency resolution is low and has a value of

$$\text{Resolution} = \frac{62*10^9}{415} \tag{4.5.1}$$

Where, each scan has 415 data points in it.

If the GPR data at cross track x and the down track y, is denoted as g(x, y, z) where z is the depth, the data measurement is modeled as

$$d(x,y,z) = g(x,y,z) + v(x,y,z) + w(x,y,z) \tag{4.5.2}$$

where v(x, y, z) denotes the clutter response and w(x, y, z) represents the noise. The steps in the generation of energy density spectrum are discussed in the following subsections.

### 4.5.1 Pre-processing

This step removes the data above and below the ground level. The ground level is estimated to be the mean of the position where the maximum and minimum value occur in each vector sample, and averaging across down track and cross track. The data above the ground level is only used for further processing. From the resultant data, the first 25 depth bins are also removed and only the data above the first 25 depth bins are used in the subsequent steps.

### 4.5.2 Non-linear Smoothing and Whitening

To remove the noise present in the depth domain data, median filtering is applied on each depth bin separately. The length of the median filter taken is 5. After median filtering, each vector sample is zero padded to make the length to 512, which is the FFT size used to convert the depth domain data to frequency domain. The FFT data before and after the

current location of interest, are used to compute the mean and standard deviation of the background for normalization.

Let $(x_0,y_0)$ be the current location of interest, and $D(x,y,k_z)$ represent the FFT data along depth( z dimension) at position (x,y) and $k_z$ is the frequency domain index for depth dimension, the mean (m) and standard deviation ($\sigma^2$) of the background for normalization is calculated using the following equations 4.3 and 4.4

$$m(x_0,k_z)=1/2L\left[\sum_{i=y0-G-L}^{y0-G-1} D(x_0,i,k_z)+\sum_{i=y0+G+1}^{y0+G+L} D(x_0,i,k_z)\right] \qquad (4.5.2.1)$$

G is the number of guard samples that is set to 6 and L is the number of scans before or after the current location to perform averaging, which is also set to 6.

$$\sigma^2(x_0,k_z)=1/2L\left[\sum_{i=y0-G-L}^{y0-G-1} D(x_0,i,k_z)^2+\sum_{i=y0+G+1}^{y0+G+L} D(x_0,i,k_z)^2\right] \qquad (4.5.2.2)$$

The normalization is then applied to the scans from $y_0$-G to $y_0$+G at each frequency bin index $k_z$, given by equation

$$\tilde{D}(x_0,y,k_z)=\left[\frac{D(x_0,y,k_z)-m(x_0,k_z)}{\sigma(x_0,k_z)}\right] \qquad (4.5.2.3)$$

The resulting normalized data is then subtracted out the mean and clipped at root mean square value, computed at each frequency bin over $y_0$-G: $y_0$+G. The data is finally magnitude squared, and denoted by $U(x_0, y, k_z)$.

### 4.5.3 Spectrum Generation

The spectrum is generated by averaging $U(x_0, y, k_z)$ over a square window of N samples cross track times N samples down-track. N is set to 5 for this study

$$P(x_0, y_0, k_z) = \frac{1}{N^2} \sum_{x=x0-(N-1)/2}^{x0+(N-1)/2} \sum_{y=y0-(N-1)/2}^{y0+(N-1)/2} P(x, y, k_z) \qquad (4.5.3.1)$$

Figure 20 shows the energy density spectra of plastic anti-tank mines. From the figure, it can be seen that the spectra has strong spectral peaks. Similarly Figure 21 shows the spectral peaks for clutter file. Both of them have high GPR signal return. But, the spectra do not seem to show any strong harmonic peaks.

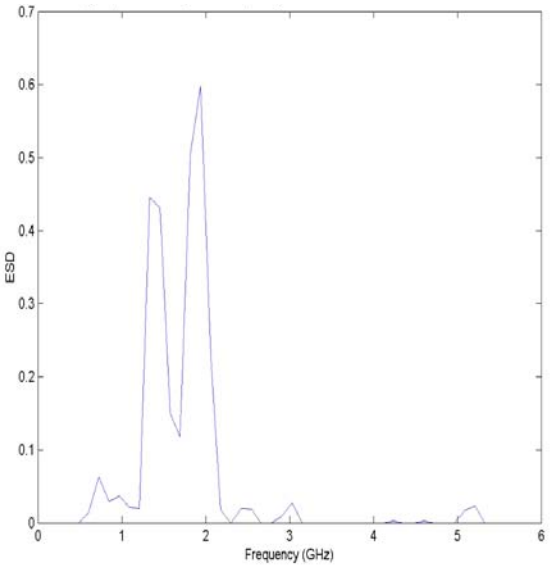


Figure 20(a)

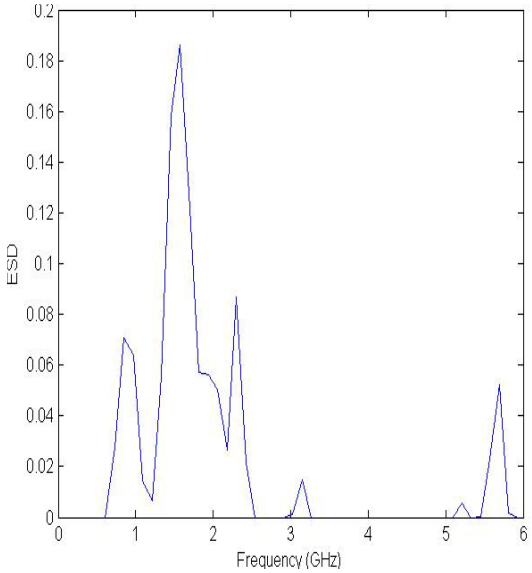


Figure 20(b)

**Figure 20: Energy Spectral Density for Mine Files**

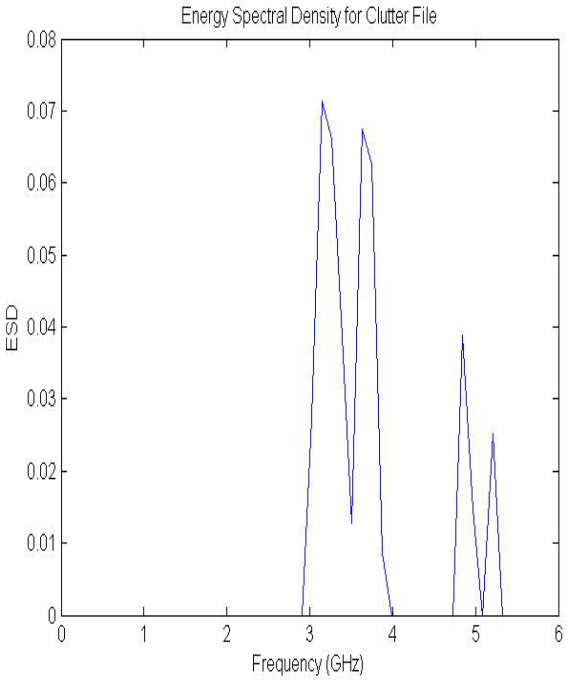


**Figure 21(a)**

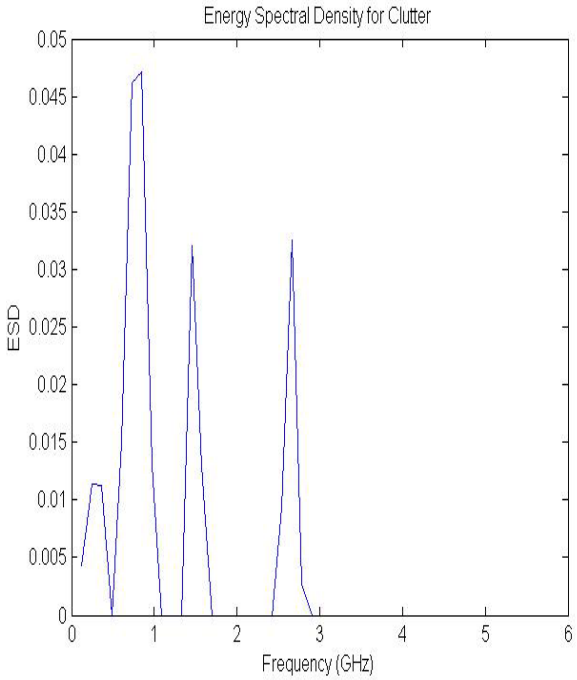


**Figure 21(b)**

**Figure 21: Energy Spectral Density for Clutter Files**

### 4.5.4 Spectral Feature Generation

Now that we have the energy density spectrum, there should be some measure to detect the confidence value. Since, the GPR radar is wideband, sub-banding is used in frequency domain to reduce computational complexity. A cosine window is used in separating frequency band energies. 50% overlap is used in windowing each frequency band. The spectral energy in each frequency band is used a feature vector in this study. Therefore, a spectral feature vector is generated with the spectral energy in it. The size of each frequency band is 600 MHz. Hence over the total bandwidth of 6 GHz, there will be 10 spectral features. Initially, 600 MHz is used as the frequency band size for the study. After examining the probability of detection using 600 MHz as the band size, the band size is reduced to see if there is any further improvement in the estimation. With 600 MHz as the band size, FFT size as 512 and sampling frequency 62 GHz , the frequency

bin size is found to be 62/512 = 120 MHz. Therefore, each frequency band covers 600/120 which is equal to 5 samples. The frequency bands are decomposed using a cosine square window, using the equation below

$$Q(x_0, y_0, j) = \sum_{i=(M-1)/2}^{(M-1)/2} P(x_0, y_0, Bj - \frac{B}{2} + i) \cos^2(\frac{\pi}{M} i) \qquad (4.5.4.1)$$

Where B is the frequency band size equal to 5. M = 2B-1 is the window size. J takes values from 1 to 10 for 10 subbands and there is 50% overlap between two adjacent bands. To investigate the effectiveness of the spectral features, a confidence value is generated based on the spectral feature vector, given by

$$Conf = \log(W^T Q + 1) \qquad (4.5.4.2)$$

**Q** is the feature vector, W is the weight vector which indicates the strength of the mine. The weight vector taken for this study is

$$W = [0.2,0.4,1,0.4,0.2,0,0,0,0,0]^T \qquad (4.5.4.3)$$

Figure 22 shows the feature vectors obtained for 10 subbands. It can be seen from the figure, that the maximum occurs at 1.5 GHz and has non-zero values upto 3 GHz

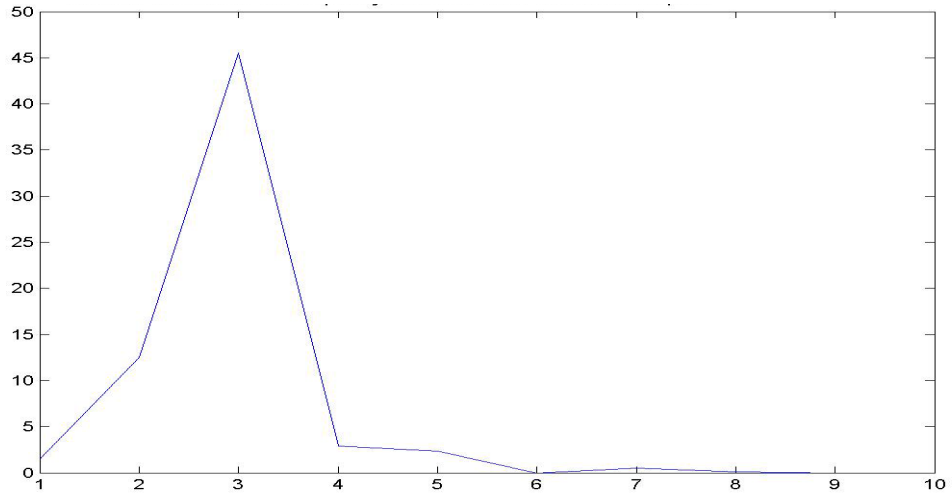


**Figure 22: Spectral Features for 10 Subbands for Plastic Anti Tank**

In order to take the spectral sharpness into account, another factor Idtrc is introduced into the confidence value. Idtrc is obtained by correlating the feature vectors obtained. Finally, the spectral confidence value is fused with the Idtrc coefficient. In the later sections of the chapter, ROC characteristics are verified for Idtrc = 0 and Idtrc obtained from correlation.

## 4.6 Effect of Varying Subbands

The effect of increasing the number of subbands from 10 to 20 has been studied in this research. Since the frequency of the radar is 6 GHz, for 20 subbands, the size of each frequency band is going to 6 GHz / 20 = 300 MHz. With the frequency bin size equal to 120 MHz, there will be 300 / 120 = 2.5 (~ 3) samples in each frequency band. With 50 % overlap present between 2 subbands, the size of the cosine window is going to be 5 samples. In the initial case of 10 Subbands, 50% overlap between two adjacent subbands corresponds to 2 sample overlap, since there are 5 samples in each frequency band. But, in the case of 20 Subbands, 50% overlap corresponds to 1 sample overlap, which means a narrow spectrum, than in the case of 10 subbands. Therefore, the overlap samples are increased from 1 sample to 2 samples to check if it gives any better results. Using the cosine window, the spectral features are generated for each frequency band. To detect the confidence value as a weighed sum of the 20 spectral features, a weighting matrix is computed as explained in next section.

## 4.7 Design of Weighting Mask

For the case of 10 subbands, the weighting mask is found by experimentation to be [0.2, 0.4, 1, 0.4, 0.2, 0, 0, 0, 0, 0]. For the case of 20 subbands, to take the strength of the mines into account, the feature vectors obtained from various datasets are used to perform averaging and the resultant matrix is used as the mask. Since different datasets have different pattern of spectral features, three masks are obtained for frequently occurring patterns. Using the datasets we have, feature vectors were generated with the proposed algorithm using 20 subbands. Averaging is performed on these feature vectors to consider all the vectors that were close to each other and follow a similar pattern. With the four datasets we had initially, three different masks were generated with three different patterns, and the maximum confidence value obtained from the three masks is used as the final confidence value, given below

w1= [0.02 0.1 0.177 0.558 1 0.243 0.03 0.01 0.002 0 0 0 0 0 0 0 0 0 0 0]

w2= [0.014 0.155 0.638 1 0.042 0.13 0.539 0.25118 0.0137 0 0 0 0 0 0 0 0 0 0 0]

w3= [0.03 0.1 0.25 0.57 0.83 1 0.83 0.57 0.25 0 0 0 0 0 0 0 0 0 0 0]

To test if the feature vectors really had effect on the datasets, another 4 datasets were taken and confidence values are obtained using these three weighting masks. The ROC characteristics obtained from these datasets showed some improvement in the probability of detection.

## 4.8 ROC Characteristics

The above algorithm is implemented on the data collected from various test sites and the spectral confidence values obtained are used to estimate the probability of detection of a mine. Special software developed by NIITEK, namely Counter Mine Test Measurement system (CMTS) is used to score the confidence values and plot the ROC characteristics. The ROC obtained from the feature based detection technique is compared with the FROSAW algorithm [35] where, feature vectors are generated using feature based rules, Order statistics and Adaptive Weightening. It can be seen from Figure 23 that, the spectral features method improved the probability of detection of weak mines while reducing the false alarms

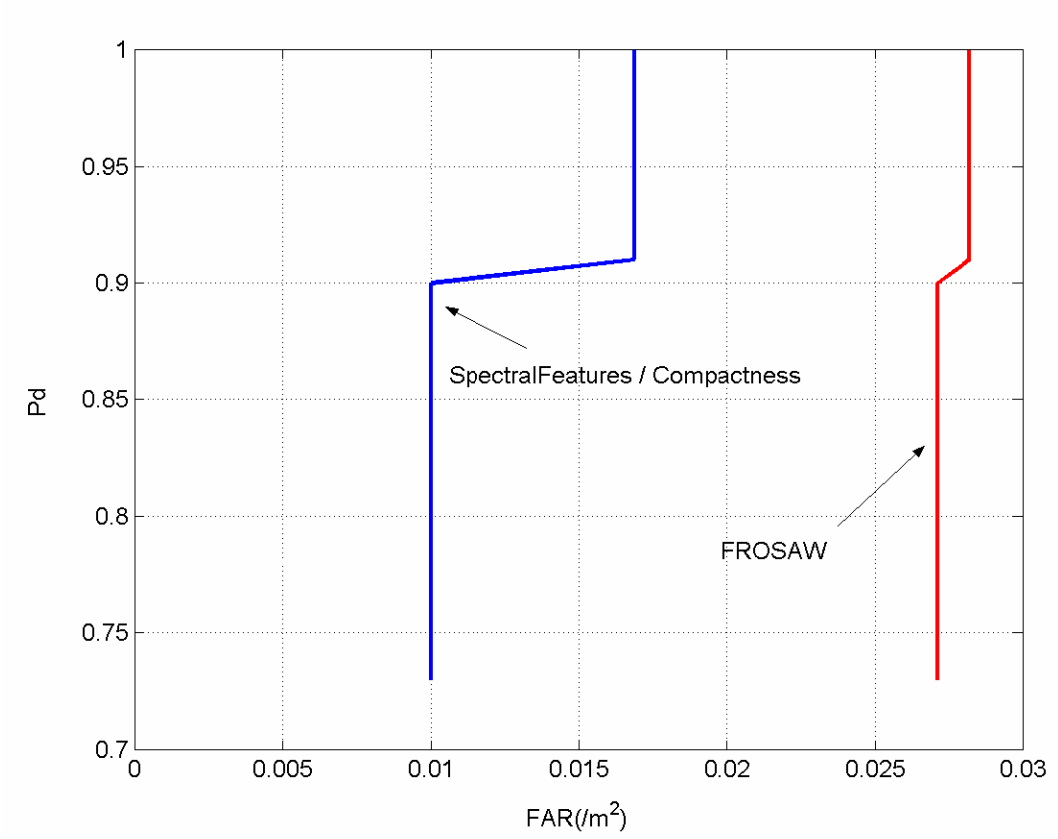


**Figure 23: Comparison of Spectral Features Method with FROSAW algorithm [35]**

## 4.9 Effect of Increasing Number of Subbands

The effect of increasing the number of subbands from 10 to 20 is studied for 8 datasets collected from different test sites. Counter Mine Test Management Systems (CTMS) is used to score the data and obtain the ROC curves. CTMS is software used to streamline countermine test systems. It can be used to collect, mark and analyze the collected test data. It also generates reports and statistics which can be saved in various formats. Our present study used the software to score the test data and obtain ROC characteristics. Figures 6-13 show the ROC curves generated for the 8 datasets. For datasets 1 and 2 the probability of detection decreased with 20 subbands when compared to 10 subbands. For datasets 3 to 6, 20 subbands seem to improve the probability of detection, while reducing the false alarm. For datasets 7 and 8, though the ROC does not seem to improve, it did not even get worse. Similarly, if we compare the ROC curves obtained with 1 sample and 2 sample overlap in 20 subbands case, the results seem to be a litter better with 2 sample overlap between adjacent subbands almost for all the subsets. Hence, 2 sample overlap is used in further study in this research.

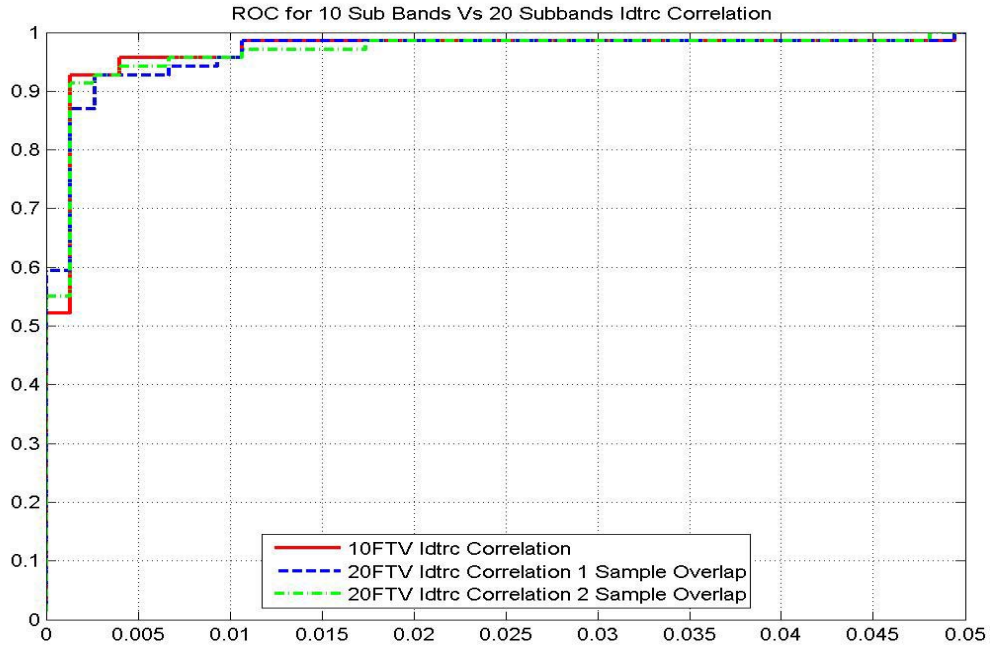


**Figure 24: ROC for Dataset 1 with Idtrc obtained from correlation for 1 Sample and 2 Sample overlap**

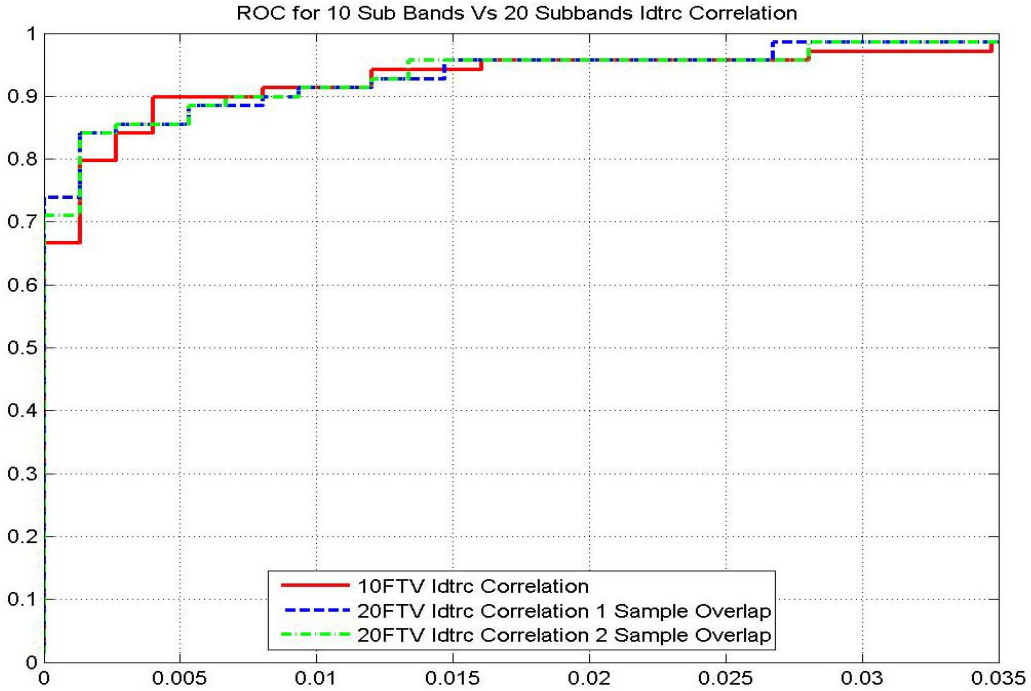


**Figure 25: ROC for Dataset 2 with Idtrc obtained from correlation for 1 Sample and 2 Sample overlap**

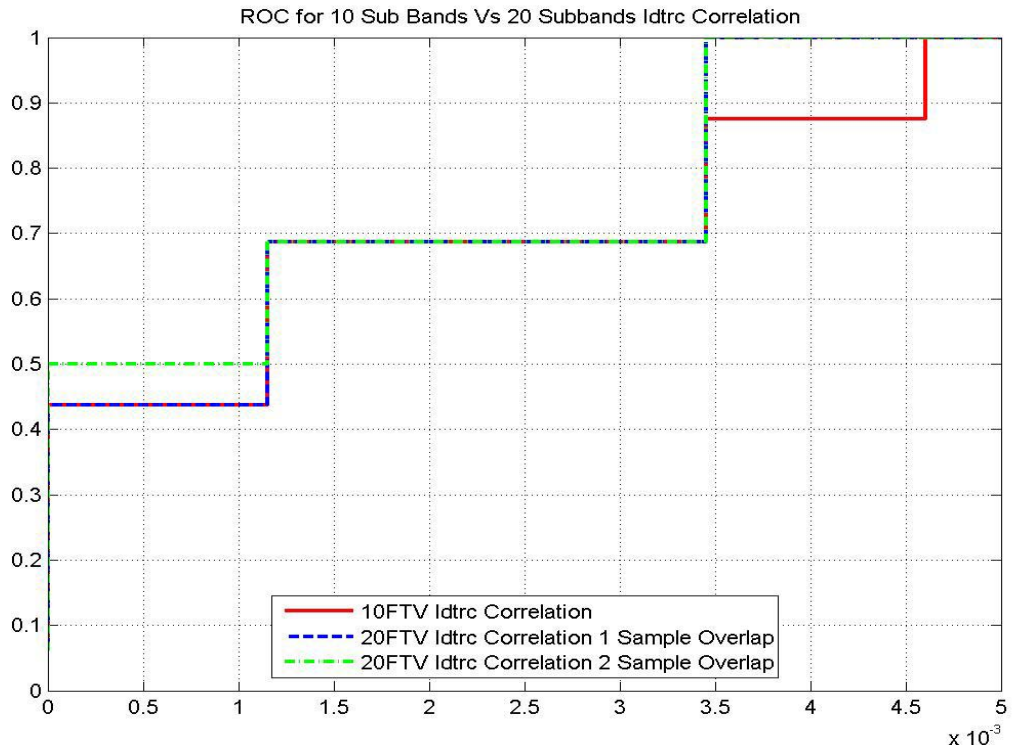


**Figure 26: ROC for Dataset 3 with Idtrc obtained from correlation for 1 Sample and 2 Sample overlap**

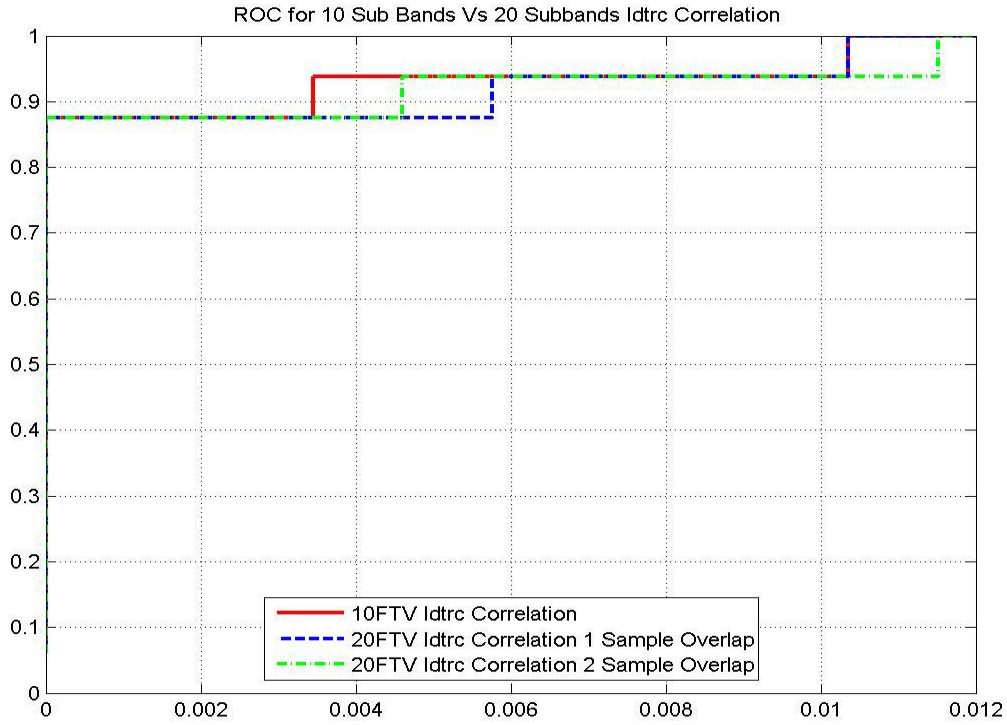


**Figure 27: ROC for Dataset 4 with Idtrc obtained from correlation for 1 Sample and 2 Sample overlap**

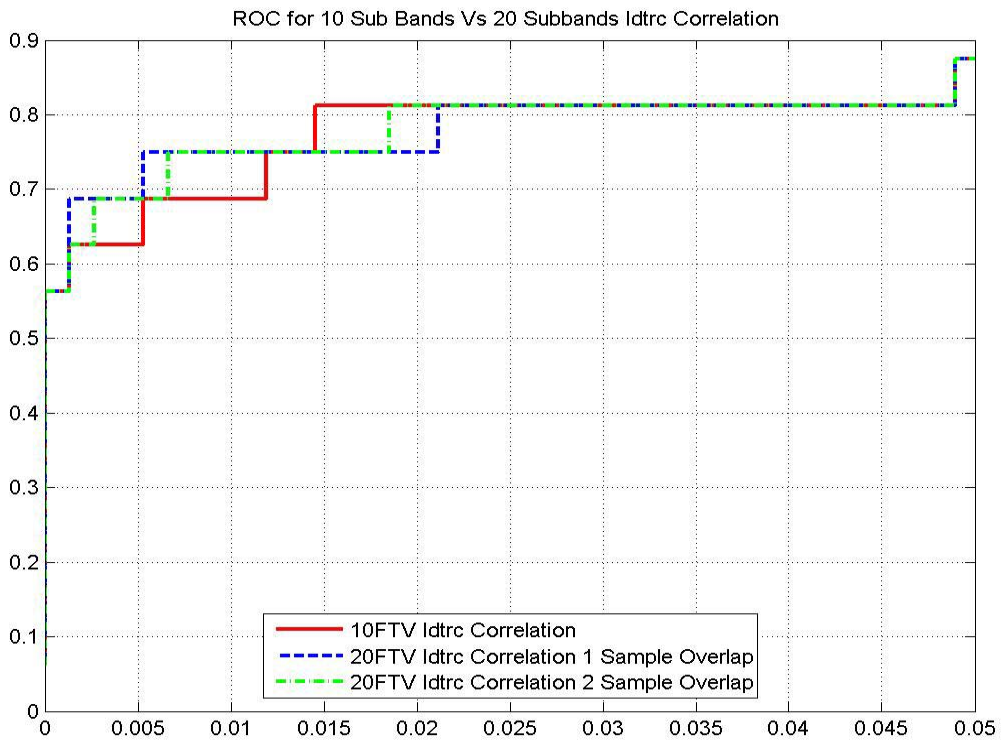


**Figure 28: ROC for Dataset 5 with Idtrc obtained from correlation for 1 Sample and 2 Sample overlap**

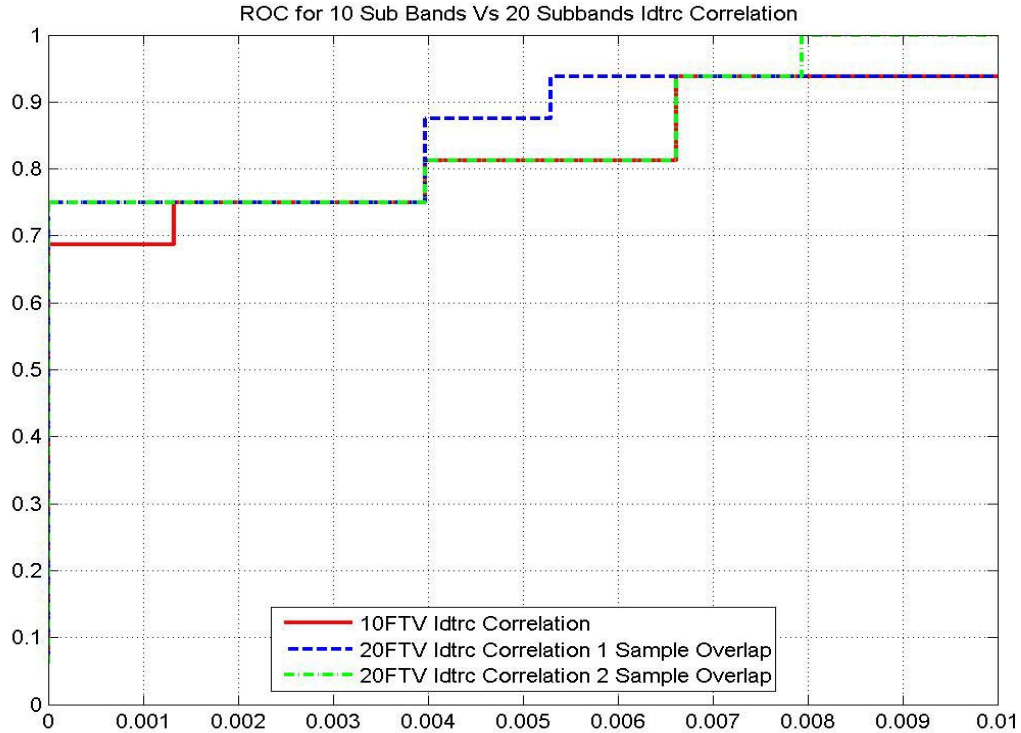


**Figure 29: ROC for Dataset 6 with Idtrc obtained from correlation for 1 Sample and 2 Sample overlap**

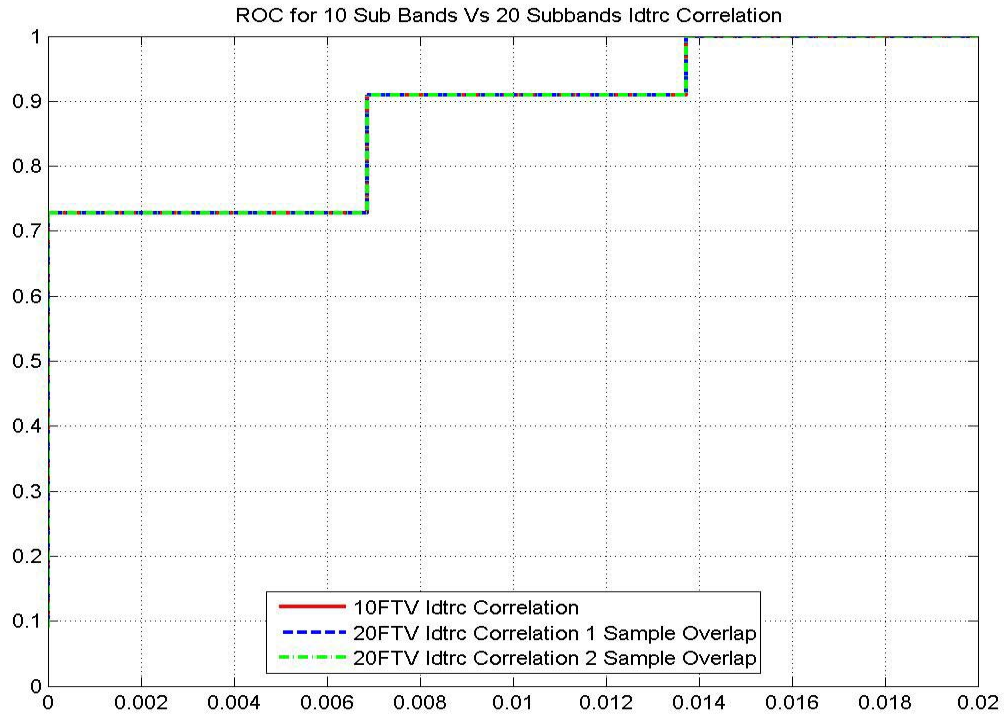


**Figure 30: ROC for Dataset 7 with Idtrc obtained from correlation for 1 Sample and 2 Sample overlap**

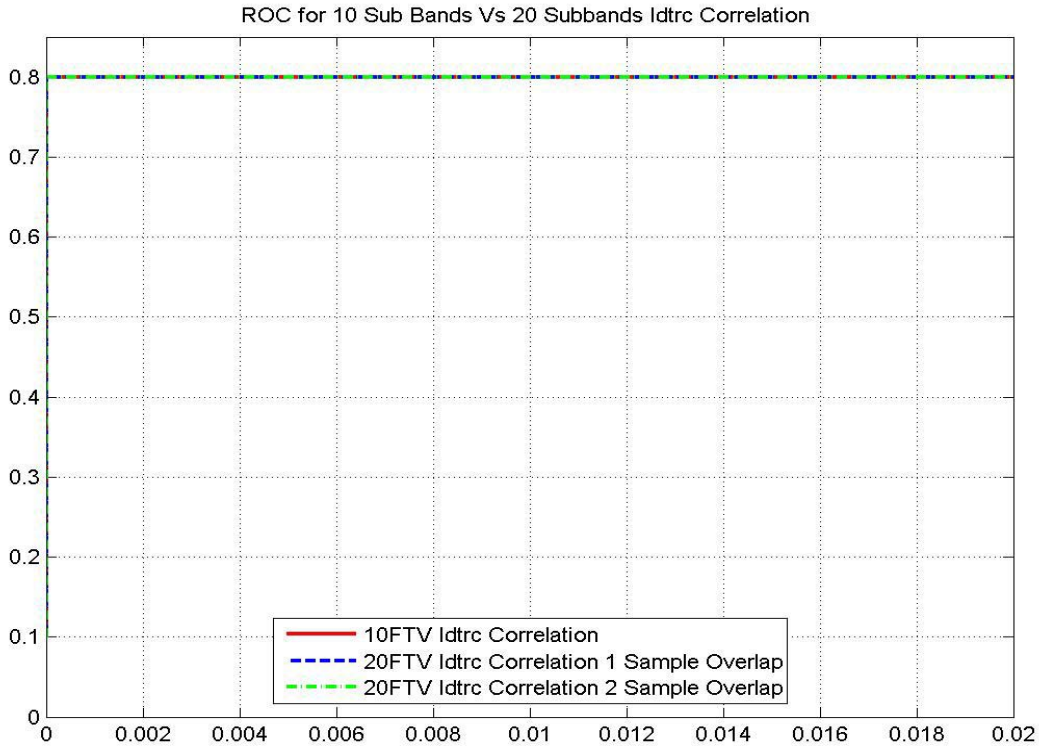


**Figure 31: ROC for Dataset 8 with Idtrc obtained from correlation for 1 Sample and 2 Sample overlap**

Table 1(a) and 1(b) show the False Alarm Rate (FAR) at Probability of detection of 90% and 95% respectively. NA represents that 90% probability of detection is not achieved with the datasets 5 and 8. From the values of FAR, it can be seen that for datasets 3, 6 and 7, increasing number of subbands to 20 has reduced the FAR. Dataset 2 showed partial improvement with reduction in FAR at 95% Pd, but for 90% Pd the FAR has increased a little. Dataset 4 has shown a little worse performance with 20 subbands. The remaining datasets 1, 5 and 8 showed no improvement for 20 subbands.

| | Dataset 1 | | Dataset 2 | | Dataset 3 | | Dataset 4 | |
|---|---|---|---|---|---|---|---|---|
| | 10 Subbands | 20 subbands | 10 subbands | 20 subbands | 10 subbands | 20 subbands | 10 subbands | 20 subbands |
| FAR at 90% Pd | 0.001336 | 0.001336 | 0.008017 | 0.009353 | 0.005292 | 0.003453 | 0.003453 | 0.004604 |
| FAR at 95% Pd | 0.004008 | 0.006681 | 0.028058 | 0.013361 | 0.005292 | 0.003453 | 0.010359 | 0.011510 |

**Table 1(a): FAR at 90% and 95% Pd for 10 vs. 20 Subbands with datasets 1 to 4**

| | Dataset 5 | | Dataset 6 | | Dataset 7 | | Dataset 8 | |
|---|---|---|---|---|---|---|---|---|
| | 10 Subbands | 20 subbands | 10 subbands | 20 subbands | 10 subbands | 20 subbands | 10 subbands | 20 subbands |
| FAR at 90% Pd | NA | NA | 0.006616 | 0.006616 | 0.013736 | 0.006868 | NA | NA |
| FAR at 95% Pd | NA | NA | 0.010585 | 0.007939 | 0.013736 | 0.013736 | NA | NA |

**Table 1(b): FAR at 90% and 95% Pd for 10 vs. 20 Subbands with datasets 5 to 8**

## 4.10 Effect of Idtrc

Idtrc is a measure of sharpness of the spectrum. If the value of Idtrc is close to zero, the spectrum has sharp peaks, and generates a good confidence value. Higher Idtrc factor corresponds to less sharp spectrum. Idtrc is obtained by cross correlating the time shifted versions of the feature vectors from all the subbands. The results obtained above are further compared by changing the Idtrc value obtained from correlation to zero. Figures 32 to 39 show the ROC characteristics with Idtrc from correlation and Idtrc equal to zero. With Idtrc equal to zero, the probability of detection is improved for all the datasets, with reduction in false alarms. For each figure, Part (a) shows the ROC characteristics obtained using 10 frequency bands with Idtrc from Correlation and Idtrc equal to zero. Part (b) shows the ROC characteristics obtained using 20 frequency bands with Idtrc from Correlation and Idtrc equal to zero, for 2 sample overlap between adjacent frequency bands.

Tables 2(a) and 2(b) show the effect of Idtrc on the Probability of detection and False Alarm Rate. A small value of Idtrc indicates a sharp spectrum and hence good ROC characteristics. From the Values of FAR at 90% Pd, for datasets 2,3,6 and 7, the FAR at 90% Pd decreased with Idtrc equal to zero , when compared to FAR at 90% Pd for Idtrc obtained from correlation. For datasets 1 and 4, the FAR increased with Idtrc set to zero. For datasets 5 and 8, though a Pd of 90% is not reached, the ROC characteristics still remain the same with Idtrc from Correlation and Idtrc equal to zero.

| | Dataset 1 | | Dataset 2 | | Dataset 3 | | Dataset 4 | |
|---|---|---|---|---|---|---|---|---|
| | Idtrc Correlation | Idtrc Zero | Idtrc Correlation | Idtrc Zero | Idtrc Correlation | Idtrc Zero | Idtrc Correlation | Idtrc Zero |
| FAR at 90% Pd | 0.001336 | 0.001634 | 0.008017 | 0.004902 | 0.005292 | 0.003453 | 0.003453 | 0.004604 |
| FAR at 95% Pd | 0.004008 | 0.006537 | 0.028058 | 0.013073 | 0.005292 | 0.003453 | 0.010359 | 0.011510 |

**Table 2(a): FAR at 90% and 95% Pd for 10 Subbands with Idtrc from Correlation and Idtrc = 0 for datasets 1 to 4**

| | Dataset 5 | | Dataset 6 | | Dataset 7 | | Dataset 8 | |
|---|---|---|---|---|---|---|---|---|
| | Idtrc Correlation | Idtrc Zero | Idtrc Correlation | Idtrc Zero | Idtrc Correlation | Idtrc Zero | Idtrc Correlation | Idtrc Zero |
| FAR at 90% Pd | NA | NA | 0.006616 | 0.00396 | 0.013736 | 0.006868 | NA | NA |
| FAR at 95% Pd | NA | NA | 0.010585 | 0.006616 | 0.013736 | 0.013736 | NA | NA |

**Table 2(b): FAR at 90% and 95% Pd for 10 Subbands with Idtrc from Correlation and Idtrc = 0 for datasets 5 to 8**

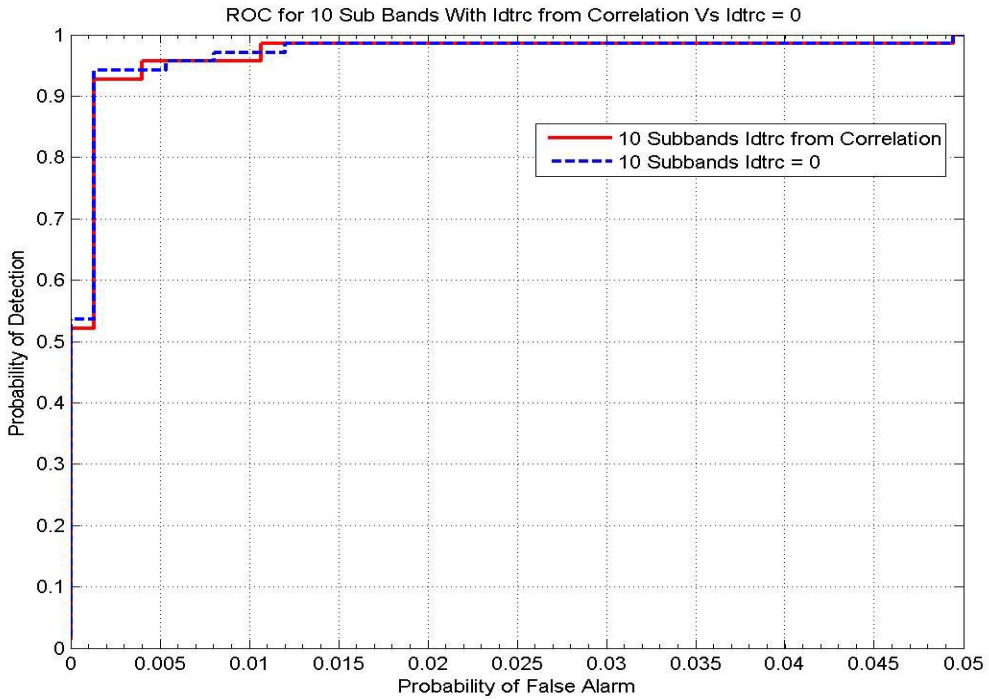


**Figure 32(a): Dataset 1 ROC for 10 Subbands with Idtrc from Correlation and Idtrc = 0**

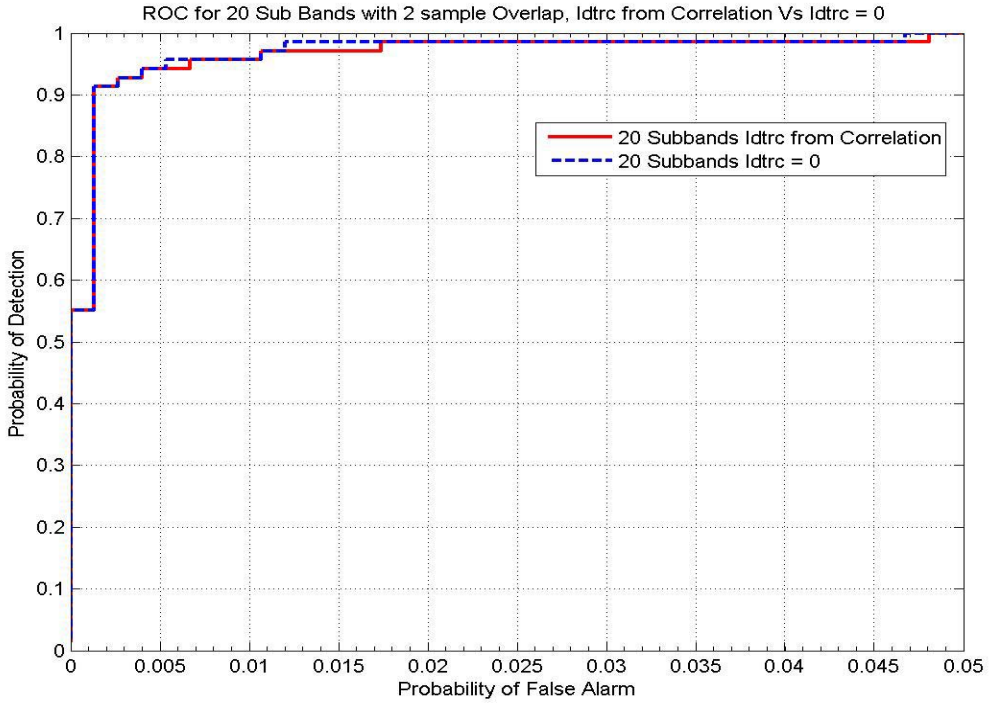


**Figure 32(b): Dataset 1 ROC for 20 Subbands with Idtrc from Correlation Vs Idtrc= 0 for 2 sample overlap in subbands**

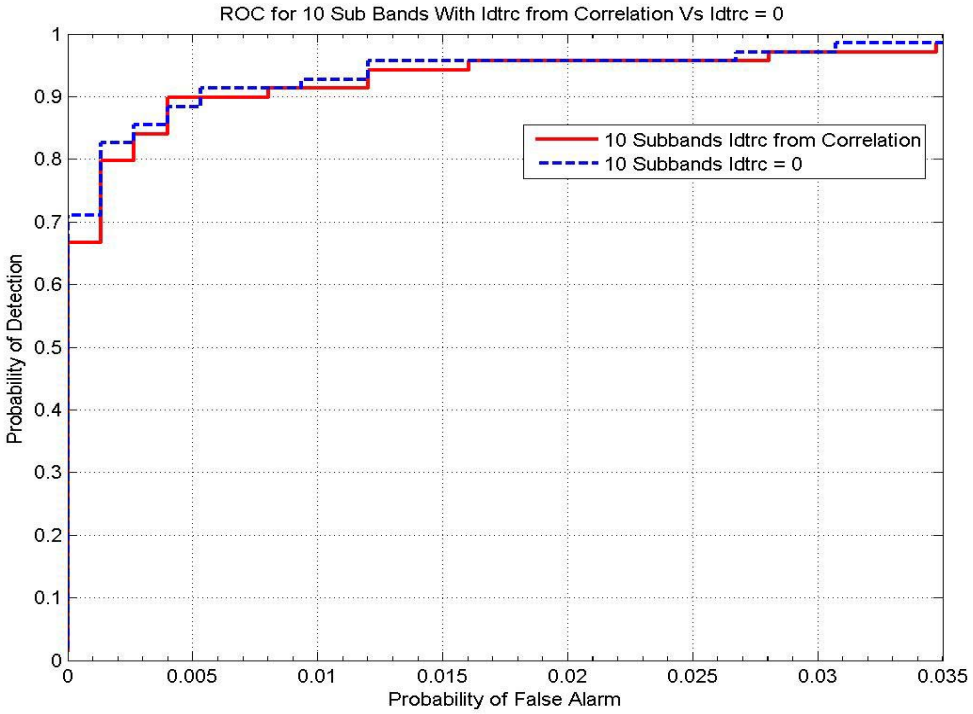


**Figure 33(a): Dataset 2 ROC for 10 Subbands with Idtrc from Correlation and Idtrc = 0**

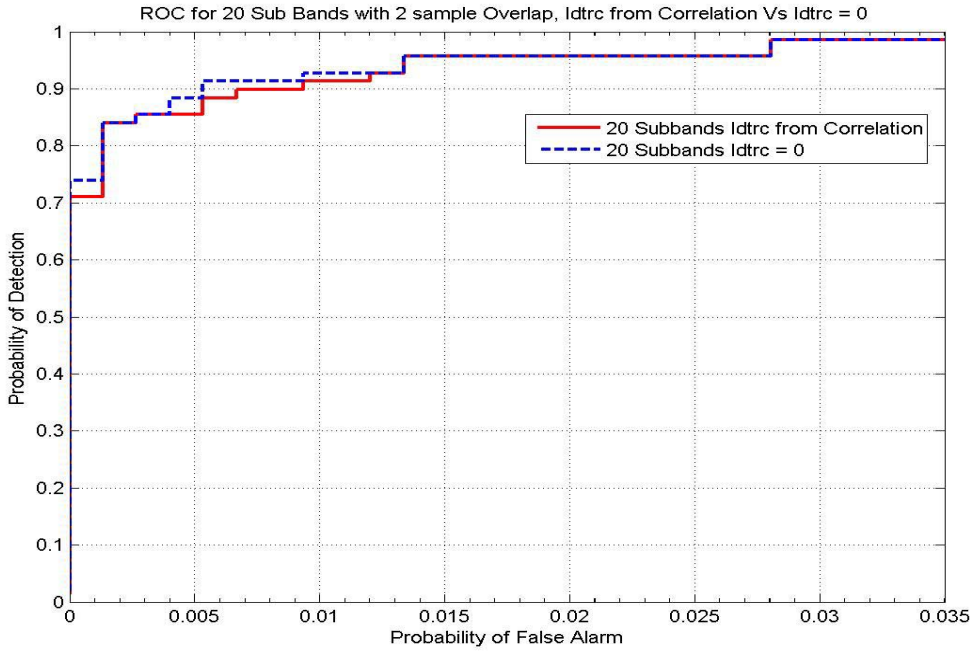


**Figure 33(b): Dataset 2 ROC for 20 Subbands with Idtrc from Correlation and Idtrc = 0 for 2 sample overlap in subbands**

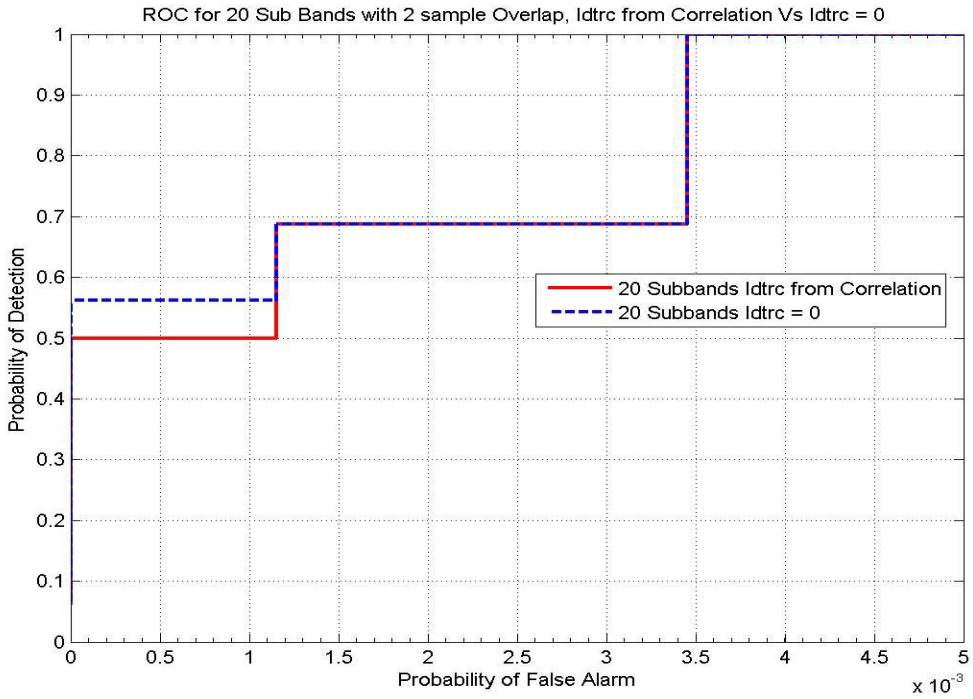


**Figure 34(a): Dataset 3 ROC for 10 Subbands with Idtrc from Correlation and Idtrc = 0**

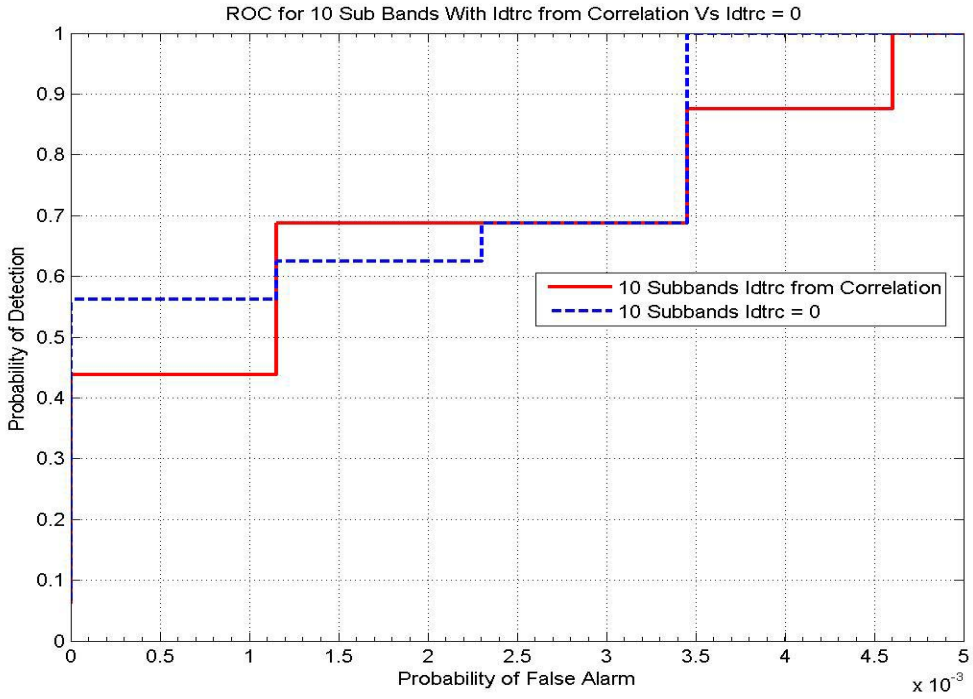


**Figure 34(b): Dataset 3 ROC for 20 Subbands with Idtrc from Correlation and Idtrc = 0 for 2 sample overlap in subbands**

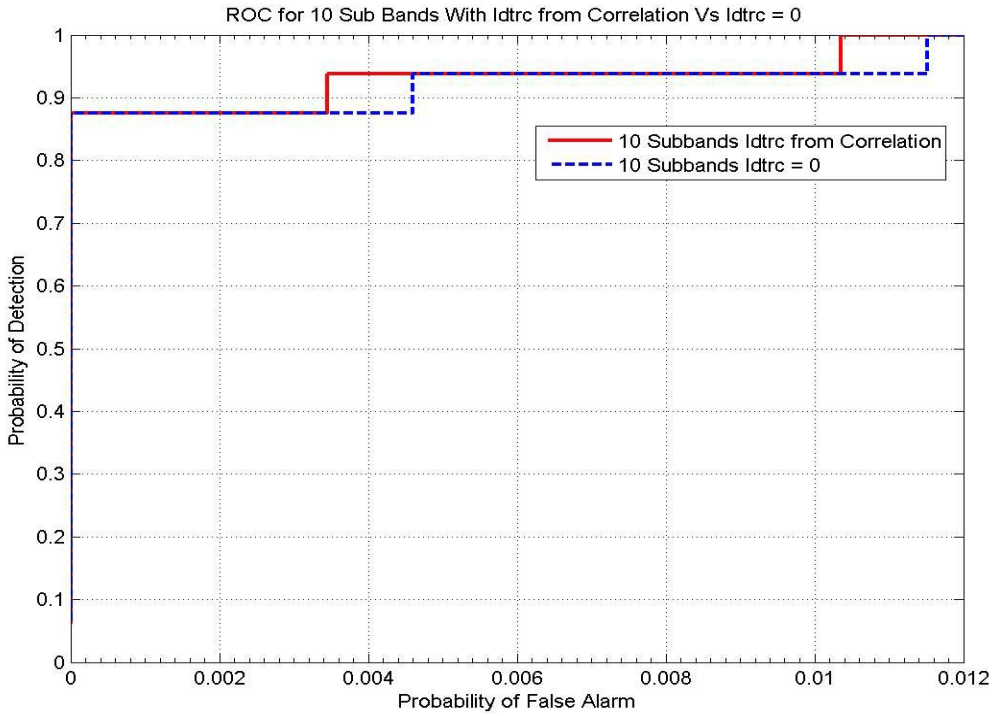


**Figure 35(a): Dataset 4 ROC for 10 Subbands with Idtrc from Correlation and Idtrc = 0**

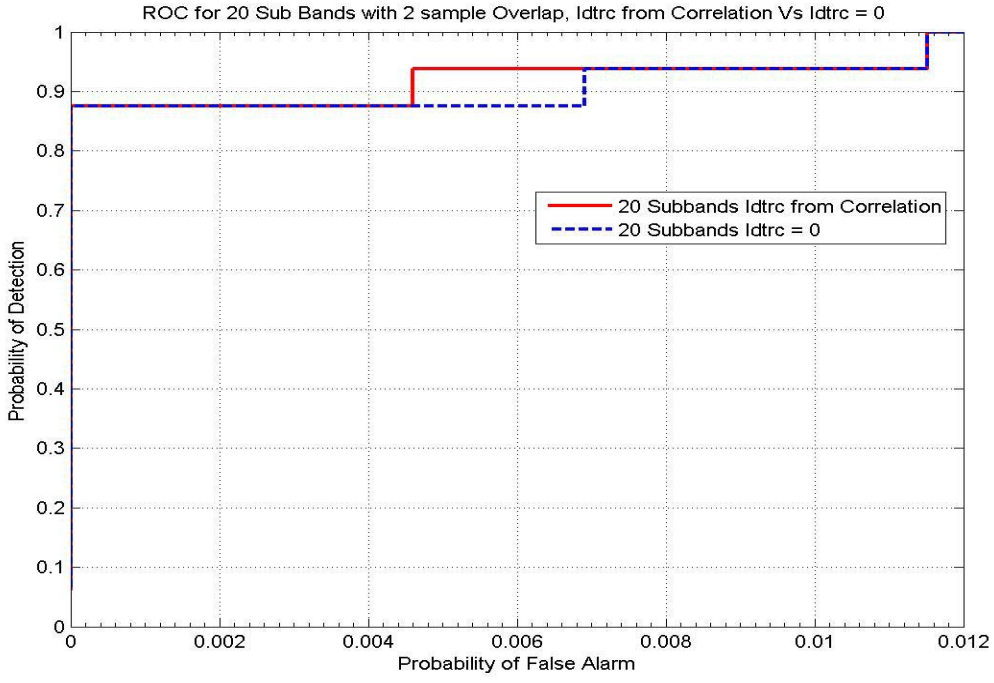


**Figure 35(b): Dataset 4 ROC for 20 Subbands with Idtrc from Correlation and Idtrc = 0 for 2 sample overlap in subbands**

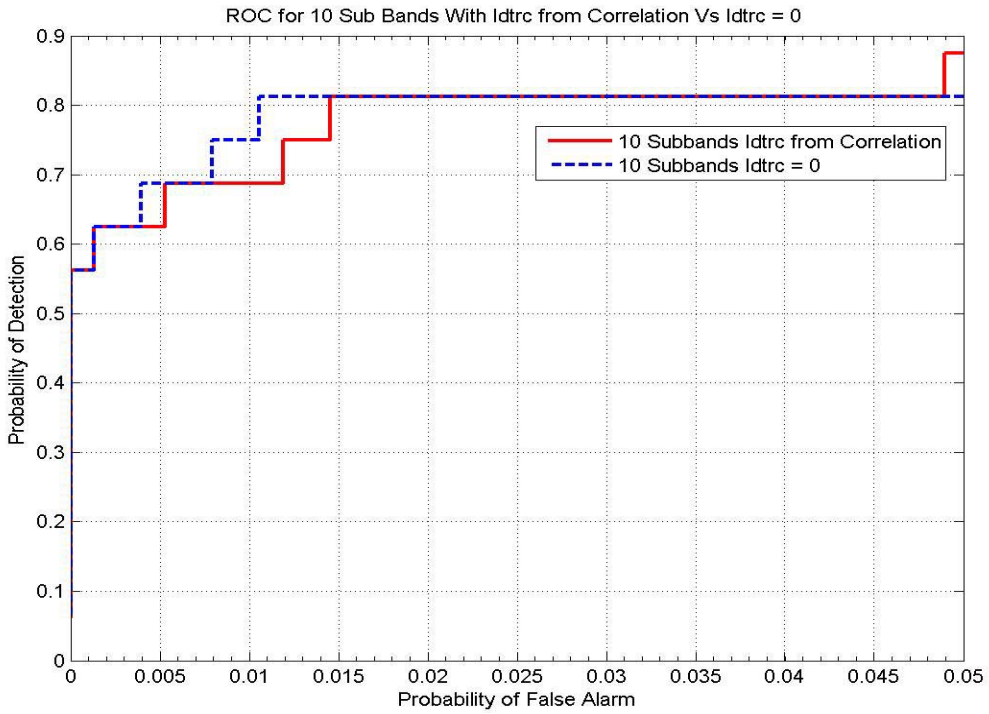


**Figure 36(a): Dataset 5 ROC for 10 Subbands with Idtrc from Correlation and Idtrc = 0**

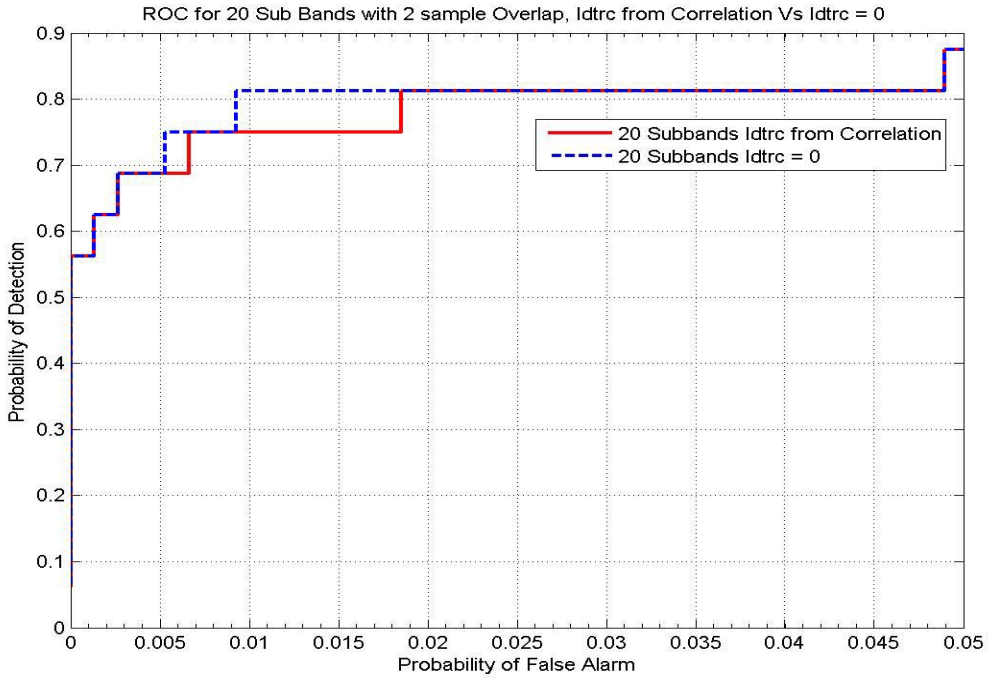


**Figure 36(b): Dataset 5 ROC for 20 Subbands with Idtrc from Correlation and Idtrc = 0 for 2 sample overlap in subbands**

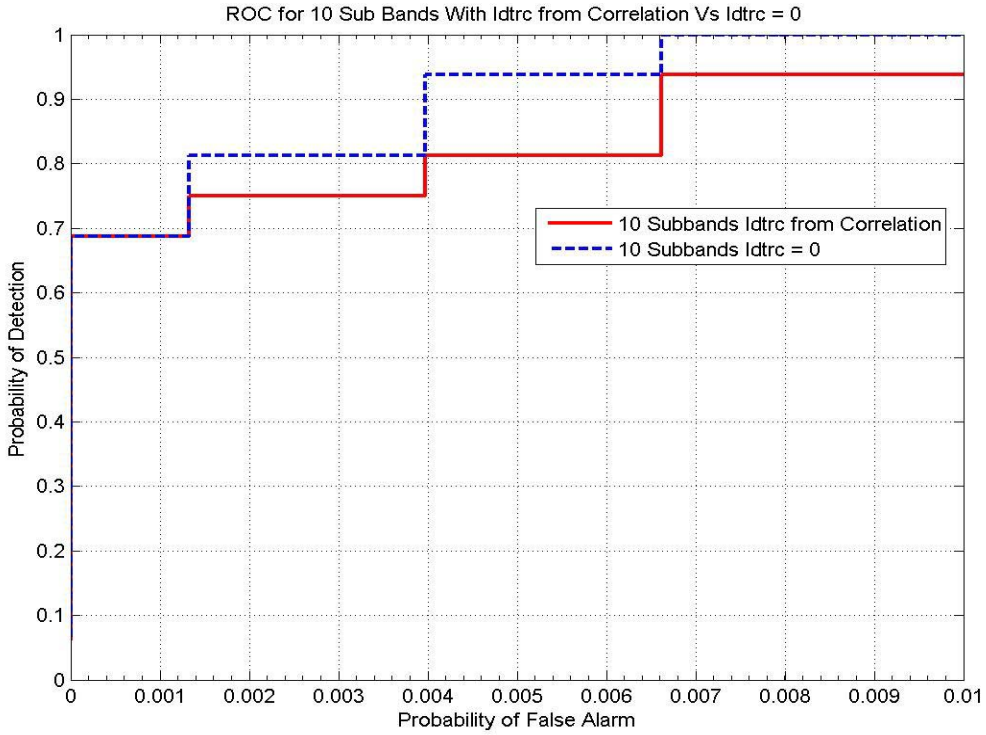


**Figure 37(a): Dataset 6 ROC for 10 Subbands with Idtrc from Correlation and Idtrc = 0**

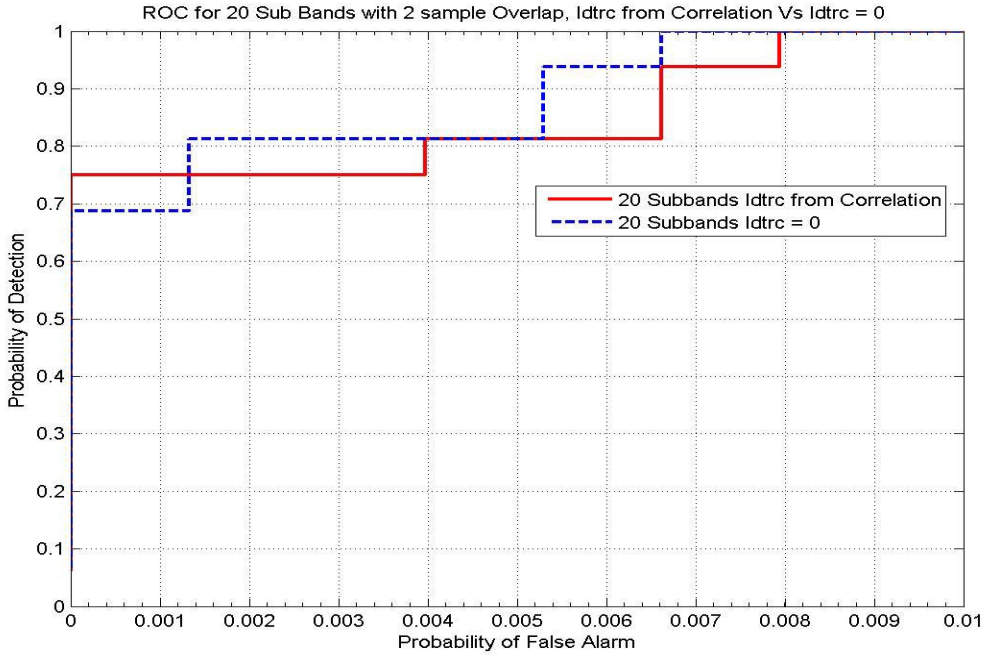


**Figure 37(b): Dataset 6 ROC for 20 Subbands with Idtrc from Correlation and Idtrc = 0 for 2 sample overlap in subbands**

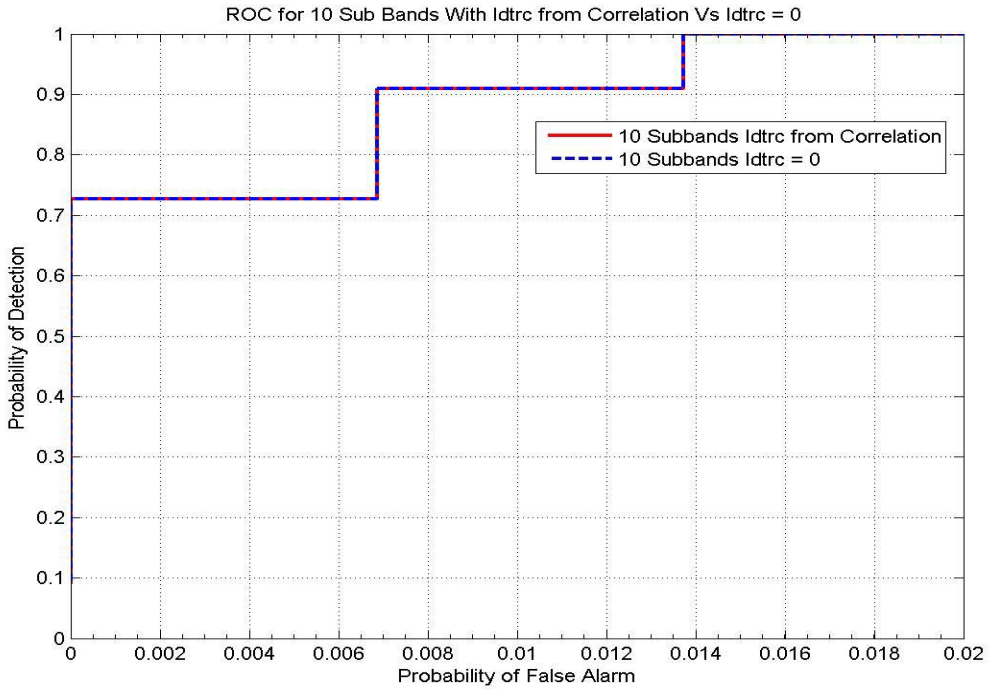


**Figure 38(a): Dataset 7 ROC for 10 Subbands with Idtrc from Correlation and Idtrc = 0**

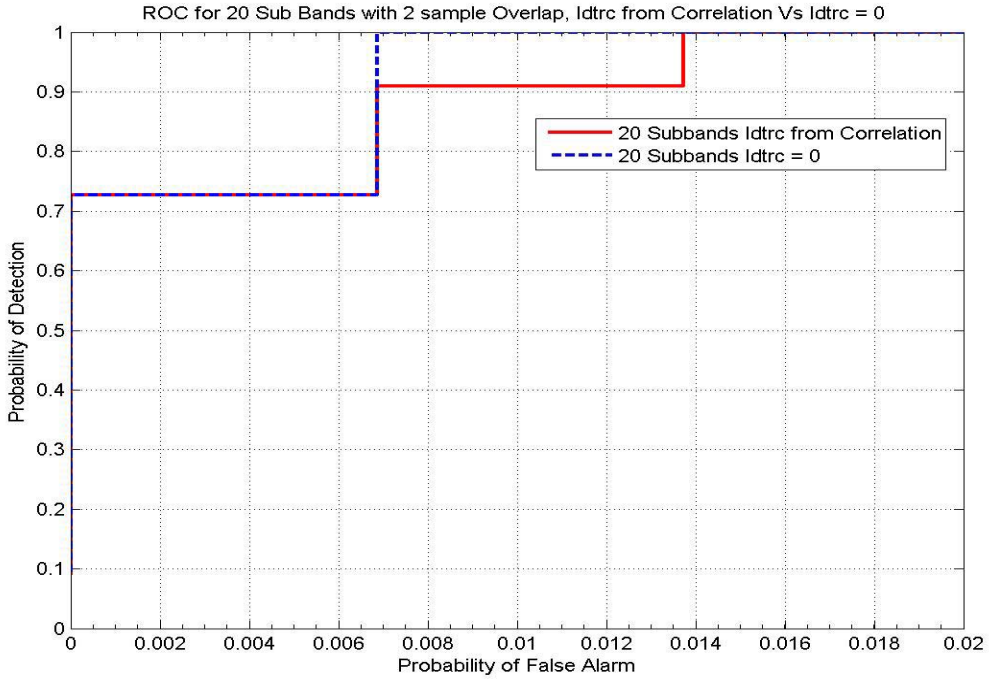


**Figure 38(b): Dataset 7 ROC for 20 Subbands with Idtrc from Correlation and Idtrc = 0 for 2 sample overlap in subbands**

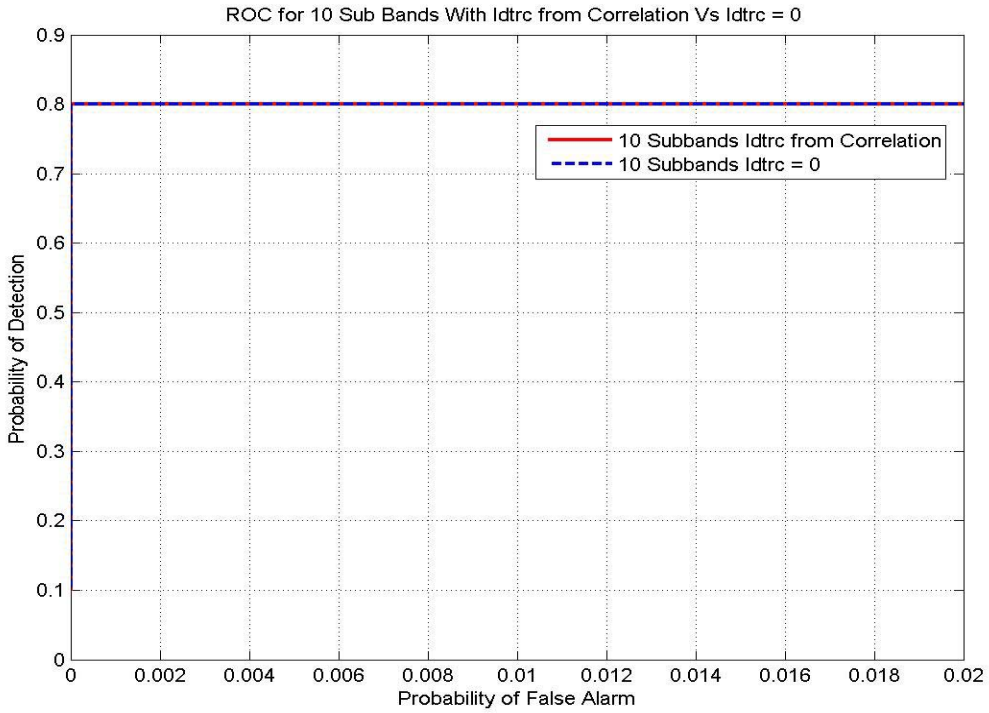


**Figure 39(a): Dataset 8 ROC for 10 Subbands with Idtrc from Correlation and Idtrc = 0**

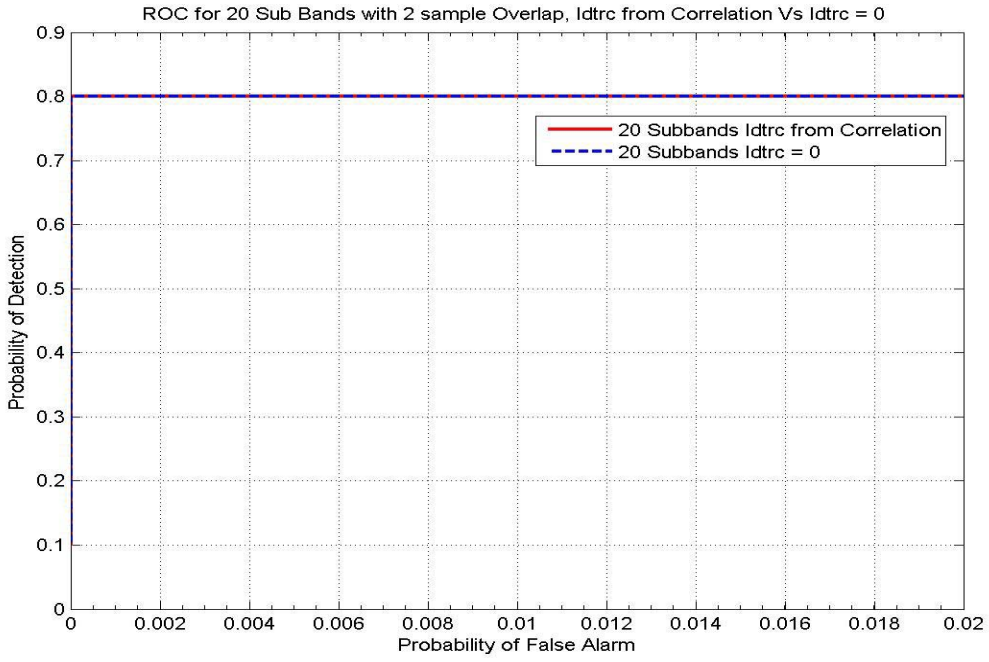


**Figure 39(b): Dataset 8 ROC for 20 Subbands with Idtrc from Correlation and Idtrc = 0 for 2 sample overlap in subbands**

## 4.11 ROC Characteristics with Clutter Dataset

To further evaluate the effectiveness of the technique, another dataset which is collected from a clutter site, is used along with the mine data. Using CTMS software, ROC characteristics are obtained for various test lanes and the data from the clutter lane is merged with them to obtain the ROC. Figures 40 to 43 show the ROC characteristics for 4 datasets 5 to 8.

It can be seen from the figures , that the 20 Subbands cases is still better than the 10 subbands, even when clutter data is included to obtain ROC characteristics. It can also be seen that with the inclusion of clutter data, the Probability of Detection decreased, from what we have without the clutter dataset, for a given probability of false alarm. For the case, without clutter data, for 10 subbands case, the Pd reached its maximum at a Pfa of 0.05, where as for the case with clutter dataset, the Pd reaches its maximum at a Pfa of 0.06. ROC characteristics for other datasets are shown in the following figures.

Similarly, ROC curves are generated with all the datasets together including clutter dataset. The ROC obtained is compared with the ROC obtained from all lanes together, without including clutter lane. It can be seen from the figures 44-45, that including the clutter data, has reduced the probability of detection for a given false alarm, as required. Figure 44 shows the ROC characteristics for 10 subbands with all datasets together, with and without including clutter Dataset and Figure 45 shows the ROC characteristics for 20 subbands.

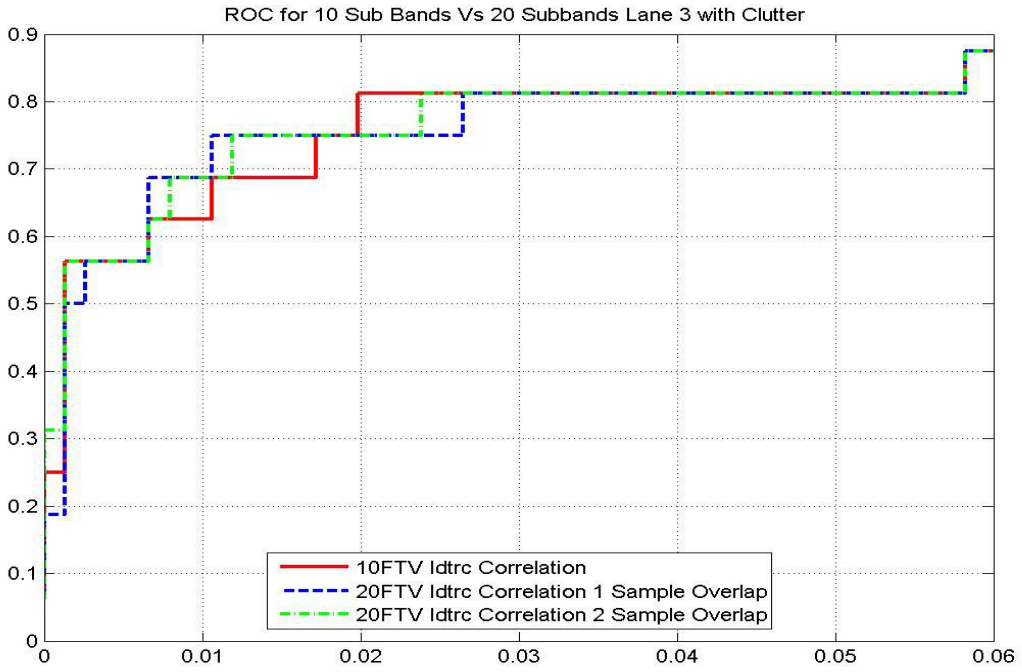


**Figure 40: ROC Characteristic for Dataset 5 with Clutter Dataset**

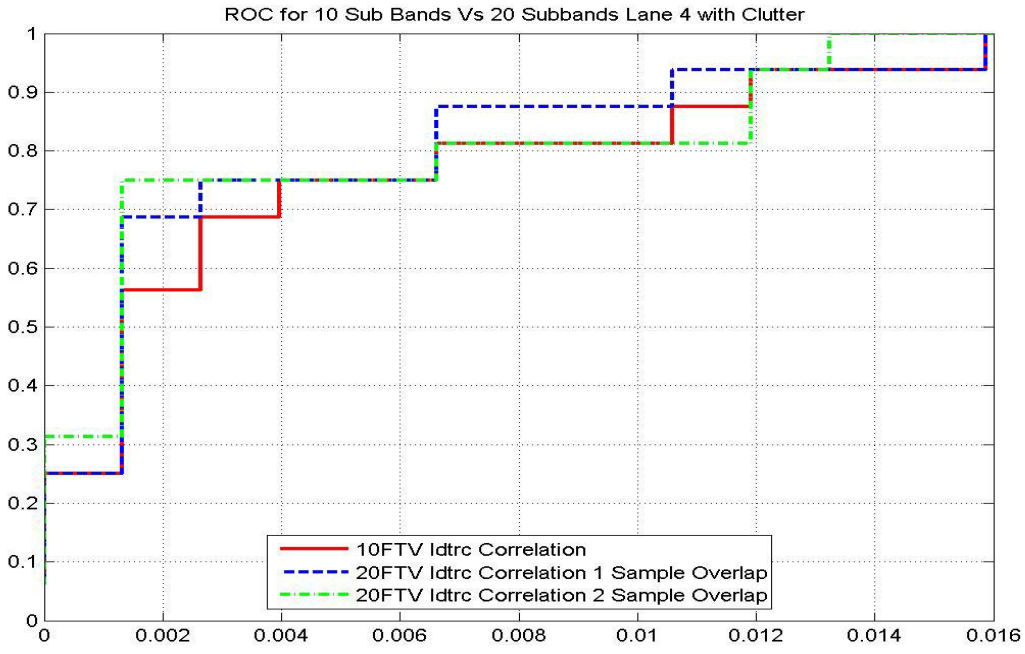


**Figure 41: ROC Characteristic for Dataset 6 with Clutter Dataset**

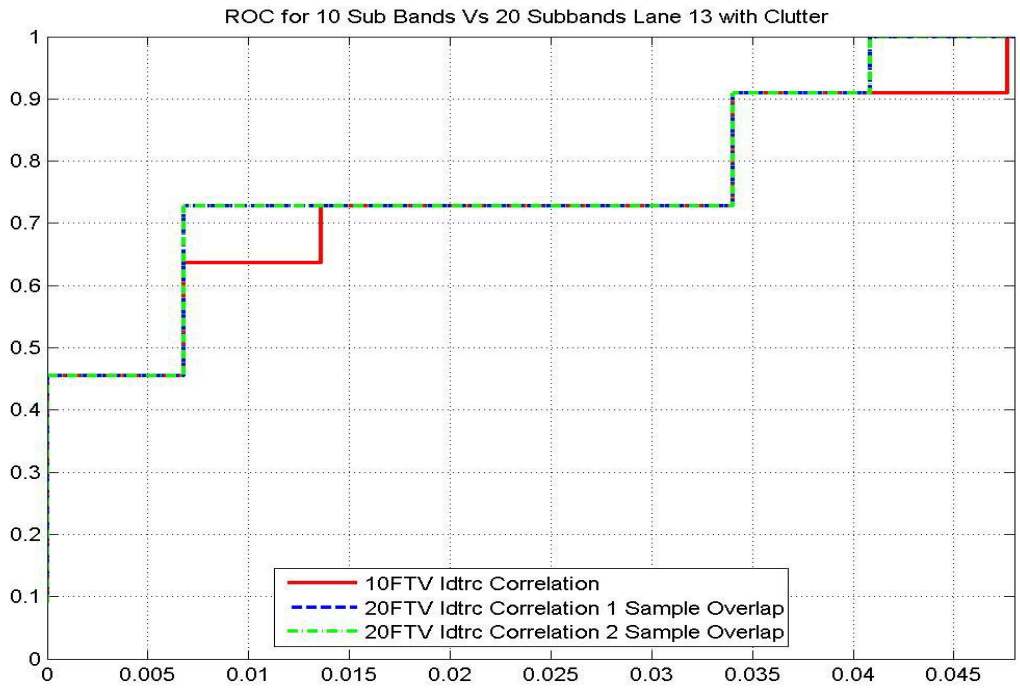


**Figure 42: ROC Characteristic for Dataset 7 with Clutter Dataset**

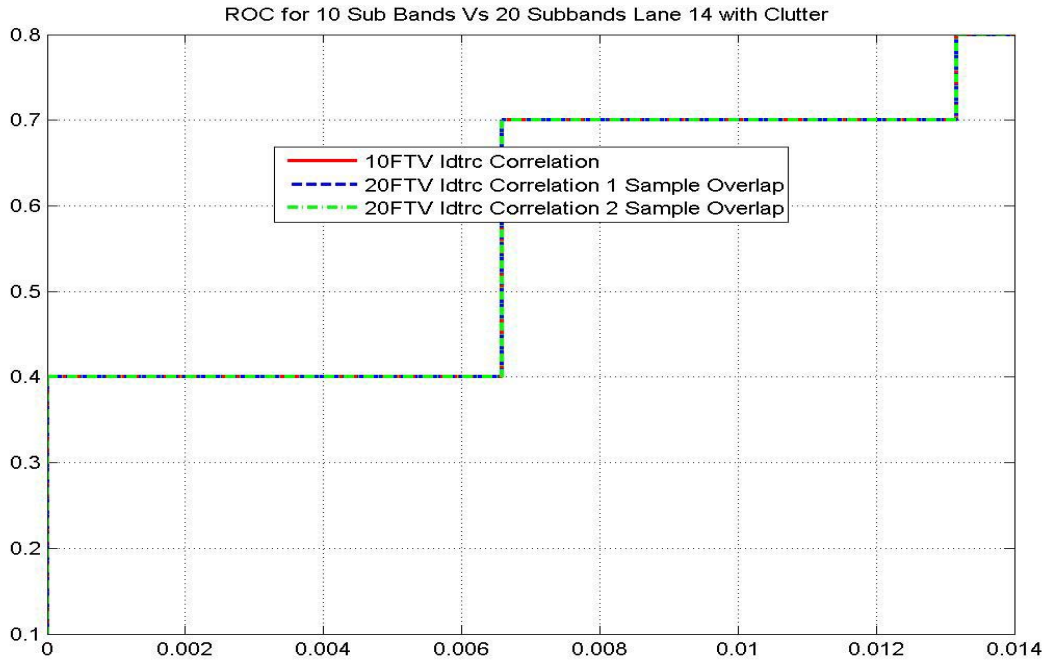


**Figure 43: ROC Characteristic for Dataset 8 with Clutter Dataset**

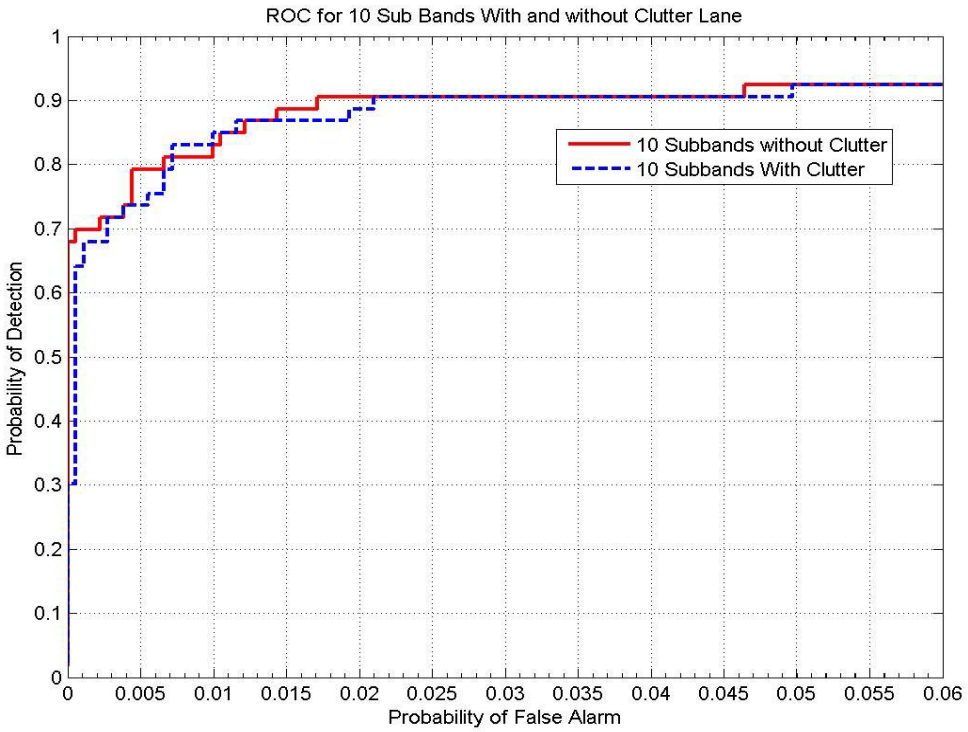


**Figure 44: ROC Characteristics for 10 Subbands with all Datasets together, with and without clutter Lane**

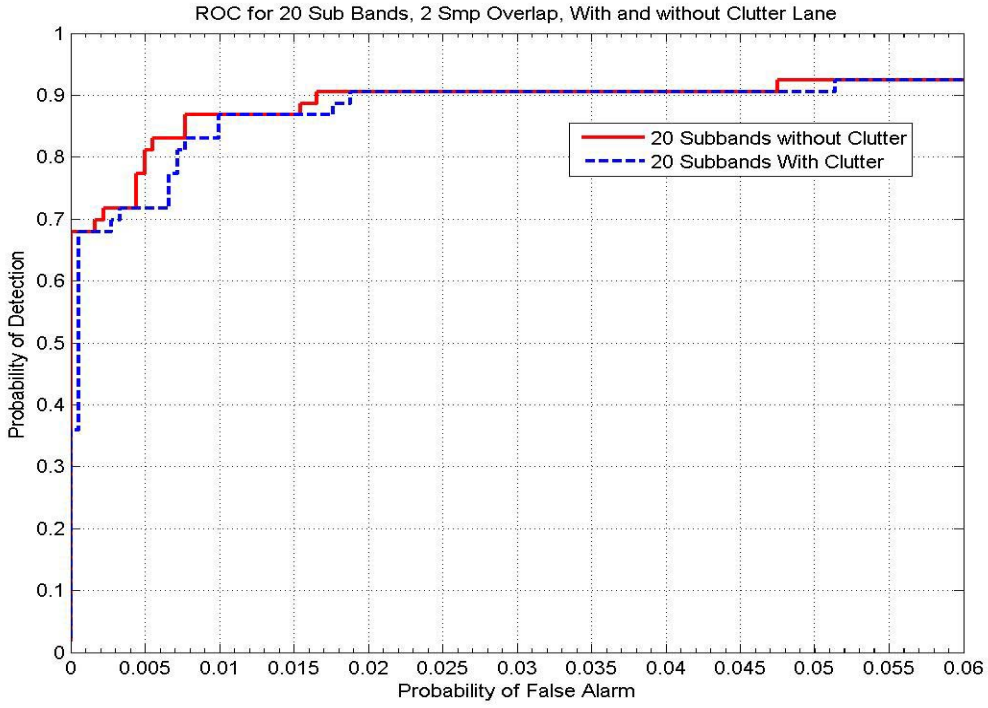


**Figure 45: ROC Characteristics for 20 Subbands, 2 Sample Overlap with all Datasets together, with and without clutter Lane**

## 4.12 Conclusions

The frequency domain features from ground penetrating radar showed some improvement in the probability of detection of weak mines and decreased the false alarm, when the number of subbands is increased to 20. The ROC curves generated using 8 different datasets collected from 8 different test sites, showed that increase in the number of subbands improved the performance of the original algorithm for more than half of the datasets.

# Chapter 5

# SIGNAL PROCESSING TECHNIQUE FOR DEPTH ESTIMATION

## 5.1 Introduction

The fact that the probability of detection of a landmine showed some improvement using feature based techniques motivated our research to further investigate the dependency of the detection technique on the depth of the mine. Different landmines are buried at different depths under the ground. The estimation of the depth of a landmine before further processing in the frequency domain could effect the performance of the frequency domain technique used later. For landmines with low metal content, it becomes hard to estimate the depth with the influence of clutter present around the mine. As the impulse GPR signals propagate through the soil, they will be significantly attenuated. Thus responses from deeply buried large anomalies will have less energy compared to very small, but shallow mines. This discrepancy will result in high false alarms when deeply buried targets need to be detected. The presence of a clutter and potential targets would also hinder the performance of depth processing techniques. Hence, estimating the depth of a landmine is one of the factors that could influence the probability of detection of a landmine with decrease in false alarm rate. After the estimation of the depth, only a few depth bins around the mine signature could be used further, which would also decrease

the complexity of the algorithm. This is the fact that motivated this research to investigate the signal processing technique for depth estimation.

## 5.2 Depth Estimation Routine

The depth estimation technique investigated in this research uses the depth domain data to estimate the depth before converting the data into the frequency domain for subband processing as discussed in Chapter 4. The following are the steps involved in the depth estimation routine.

### 5.2.1 Pre-Processing

The data in depth domain is pre-processed to remove ground level before applying depth estimation routine. The ground level is estimated to be around 100 depth bins in this case. Therefore, depth bins above 125 bins are taken out in this case. After pre processing, the data in the first 25 depth bins is made zero, assuming there are nonzero values only below the next 25 depth bins.

### 5.2.2 Windowing and Normalization

The depth domain data below the first 125 bins is passed through a tukey window to smooth the data. The NIITEK GPR data is collected using 24 antennas and therefore for each channel the background mean is removed and the resultant data is normalized for further processing.

### 5.2.3 Depth Estimation

For the channel with Constant False Alarm Rate (CFAR), the center 3 scans are used to estimate the depth of the mine. The sum of the center 3 scans is computed and the location of maximum and minimum values along depth is used to estimate the depth of the mine using correlation. Figure 46 shows the depth domain data for Maximum CFAR channel in the first subplot and the sum of center 3 scans in the second subplot.

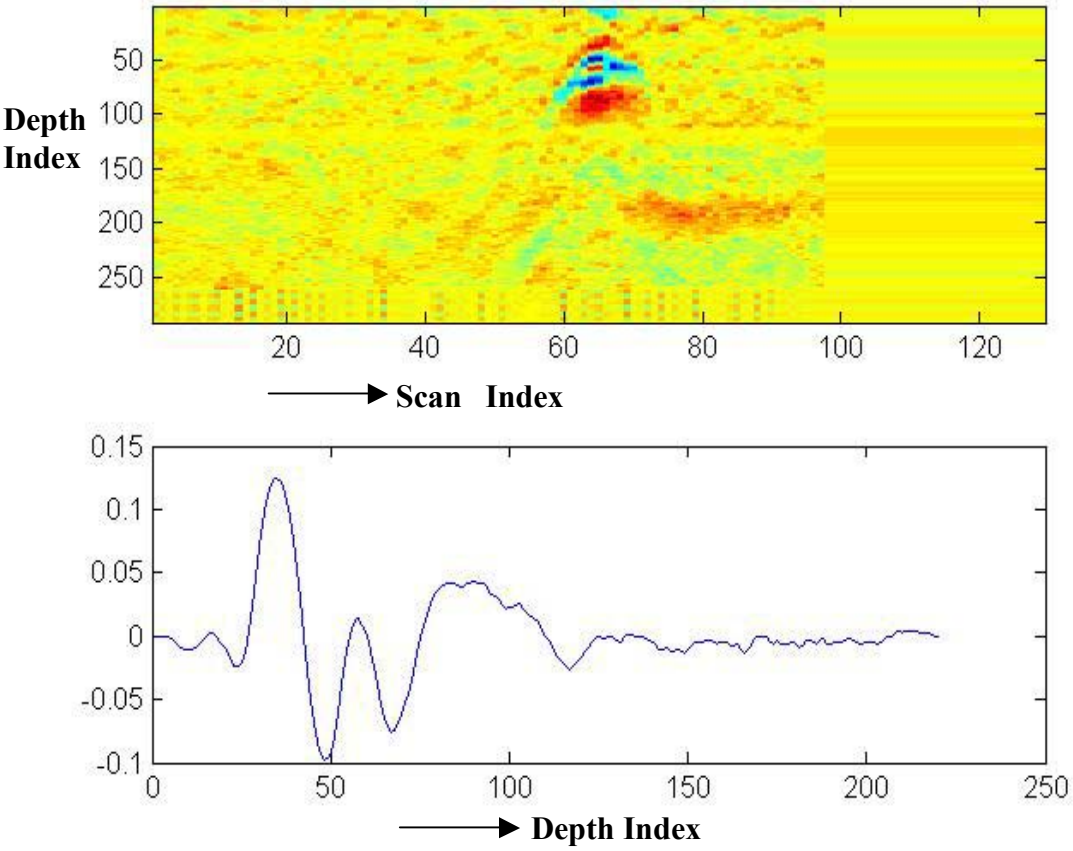


**Figure 46: Depth Domain Data for a plastic, anti-tank mine, Maximum CFAR channel 6 depth 2 mine**

To perform correlation, the 40 depth bins below and above the maximum location of the averaged scans are used and the other bins are not used. A matching score is obtained by cross correlating the 2 dimensional images obtained from data in the cross-track and

down-track along all the depth bins. Similarly a matching score is obtained with the minimum of the sum of center 3 scans. If the matching score obtained by taking the maximum index is 90% of the score obtained by taking the minimum, then the minimum index is estimated to be the depth of the mine. Otherwise, Maximum index is decided as the depth, and the score corresponding to this depth is taken as the confidence value.

The depth estimate obtained from the estimation routine is then used to decide the number of depth bins to be used to convert to frequency domain for subband processing. If the depth estimate value obtained is less (which corresponds to a mine near the surface), the depth domain data starting from below the ground level is used and 64 depth bins at the end are removed. If the depth estimate is high enough, a few depth bins below the ground level are removed, and the depth bins starting from a few bins below the ground level are used for further processing. Thus depth estimation routine before frequency subband processing, reduces the number of depth bins as well as removes the data which does not contain any information in it.

## 5.3 ROC Characteristics with Depth Estimation Routine

The ROC curves generated without using the depth estimation routine in chapter 4 are compared with the ROC curves using the depth estimation routine, to investigate the performance improvement with depth processing. Figures 47-54 show the ROC characteristics with and without depth estimation routine using 10 subbands. The parameter Idtrc stands for a spectral sharpness measure, as explained in Chapter 4 and FTV stands for feature vectors obtained for each subband. The Idtrc obtained from correlation is used for the study in this chapter. It can be seen from the figures that the

depth estimation routine improved the performance of original frequency domain technique with increase in the Probability of detection, except for data sets 4 and 6. For datasets 3 and 7, the technique showed an improvement of 15% in the probability of detection for a fixed False Alarm Rate. For Datasets 1, 2 and 5, the ROC showed a little improvement from the ROC characteristics with the original algorithm. For dataset 8, the probability of detection remained the same. From these conclusions, it can be said that the depth estimation routine is worth further investigation.

Tables 3(a) and 3(b) show the False Alarm Rates at probability of detection of 80%, 90% and 95% respectively, with depth estimation and without depth estimation. From the tables, it can be seen that at 95% probability of detection, the false alarm rate is reduced for all datasets except for dataset 6. But, at 90% probability of detection, the false alarm rate is increased for all datasets, and this resulted in worse ROC characteristics with depth estimation routine for the datasets at 90% probability of detection. But, the False alarm rates at 80% probability of detection show some improvement with depth estimation routine compared to the false alarm rate without depth estimation routine. Therefore, for datasets 3 and 6, which showed some degradation in performance with depth estimation routine at 90% probability of detection, are still better at 80% probability of detection.

| | Dataset 1 | | Dataset 2 | | Dataset 3 | | Dataset 4 | |
|---|---|---|---|---|---|---|---|---|
| | (i) | (ii) | (i) | (ii) | (i) | (ii) | (i) | (ii) |
| FAR at 80%Pd | 0.001336 | 0.001336 | 0.001336 | 0.002672 | 0.001323 | 0.003969 | 0.002157 | 0.000000 |
| FAR at 90%Pd | 0.001336 | 0.001336 | 0.008017 | 0.008017 | 0.007939 | 0.005292 | 0.007551 | 0.003453 |
| FAR at 95%Pd | 0.002672 | 0.004008 | 0.020042 | 0.028058 | 0.007939 | 0.005292 | 0.008630 | 0.010359 |

**Table 3(a): 10 subbands with and without depth estimation routine for Datasets 1 to 4**

**i. 10 Subbands with Depth Estimation routine**

**ii. 10 Subbands without Depth Estimation routine**

| | Dataset 5 | | Dataset 6 | | Dataset 7 | | Dataset 8 | |
|---|---|---|---|---|---|---|---|---|
| | (i) | (ii) | (i) | (ii) | (i) | (ii) | (i) | (ii) |
| FAR at 80% Pd | 0.00793 | 0.0145 | 0.003969 | 0.003969 | 0.0000 | 0.006868 | 0.00000 | 0.0070 |
| FAR at 90% Pd | NA | NA | 0.011908 | 0.006616 | 0.006868 | 0.013736 | NA | NA |
| FAR at 95% Pd | NA | NA | 0.027786 | 0.010585 | 0.013736 | 0.013736 | NA | NA |

**Table 3(b): 10 subbands with and without depth estimation routine for Datasets 5 to 8**

**i. 10 Subbands with Depth Estimation routine**

**ii. 10 Subbands without Depth Estimation routine**

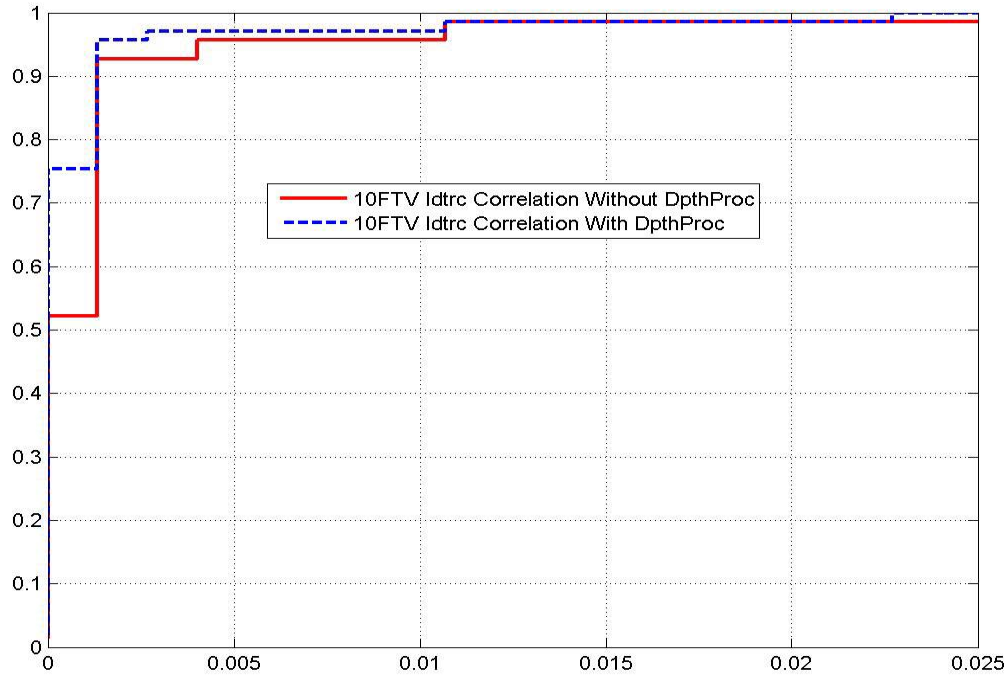


**Figure 47: ROC Characteristics for Dataset 1 with and without Depth Estimation**

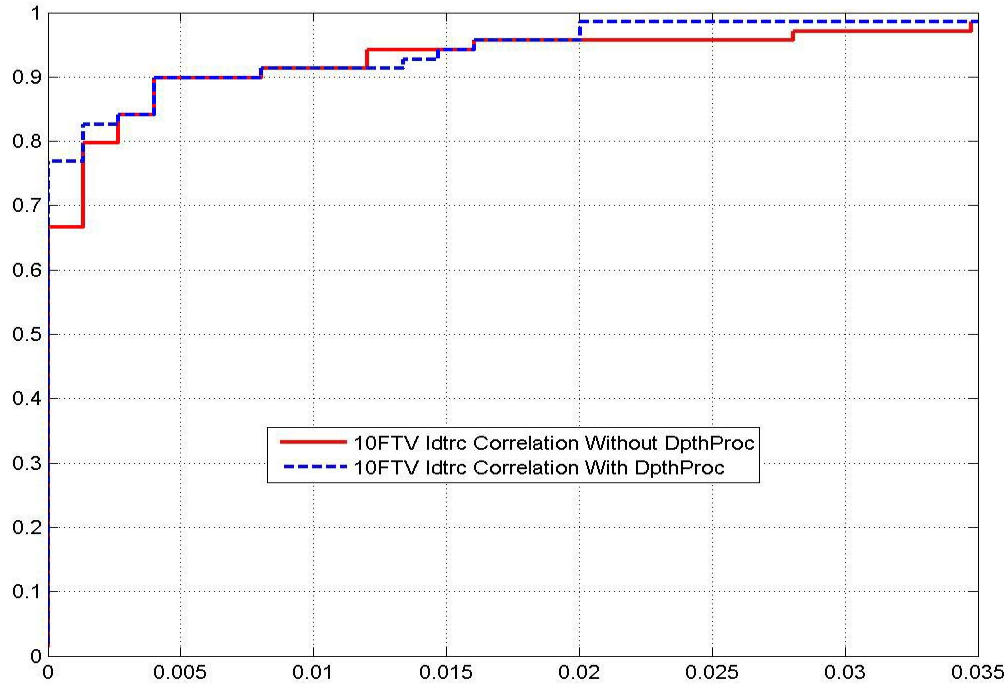


**Figure 48: ROC Characteristics for Dataset 2 with and without Depth Estimation**

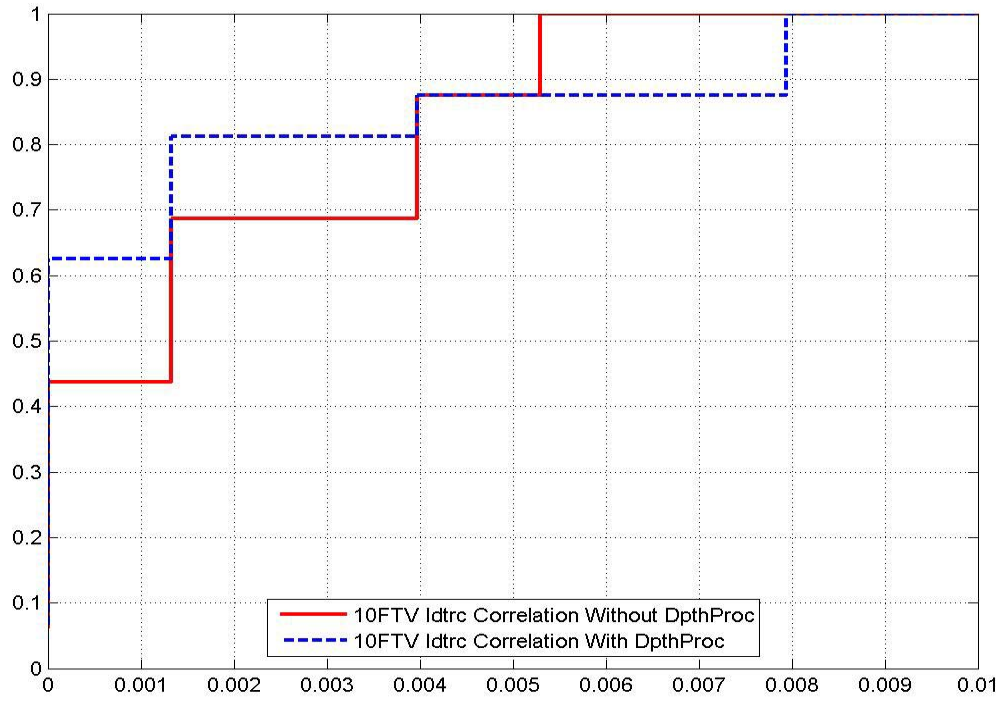


**Figure 49: ROC Characteristics for Dataset 3 with and without Depth Estimation**

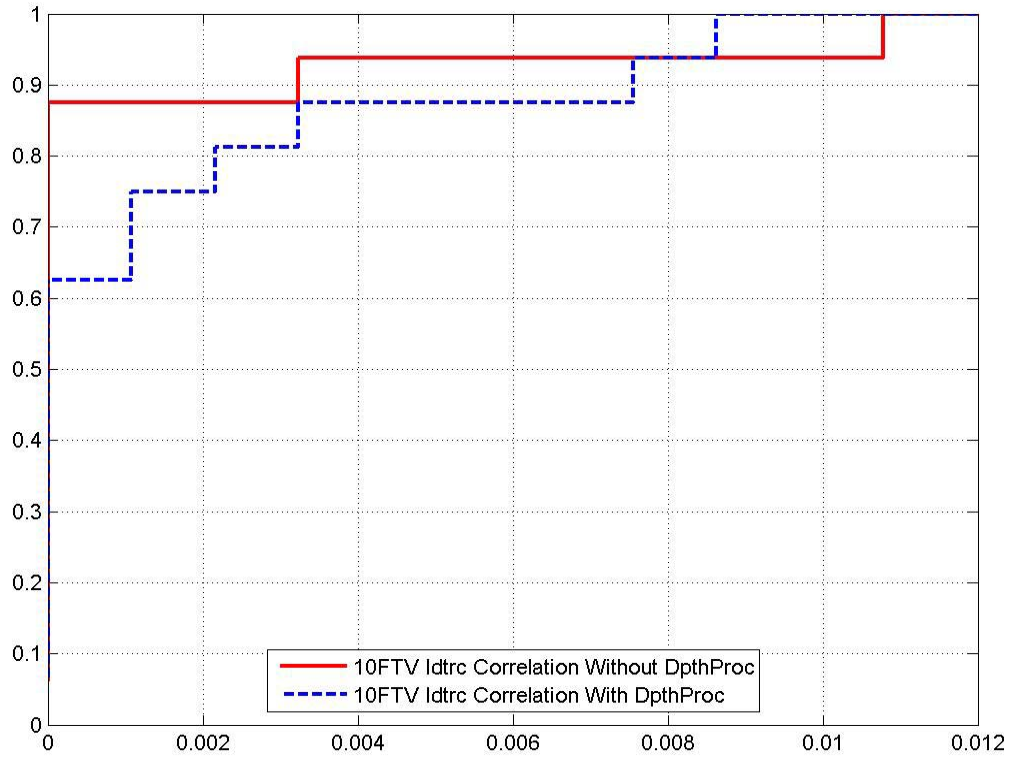


**Figure 50: ROC Characteristics for Dataset 4 with and without Depth Estimation**

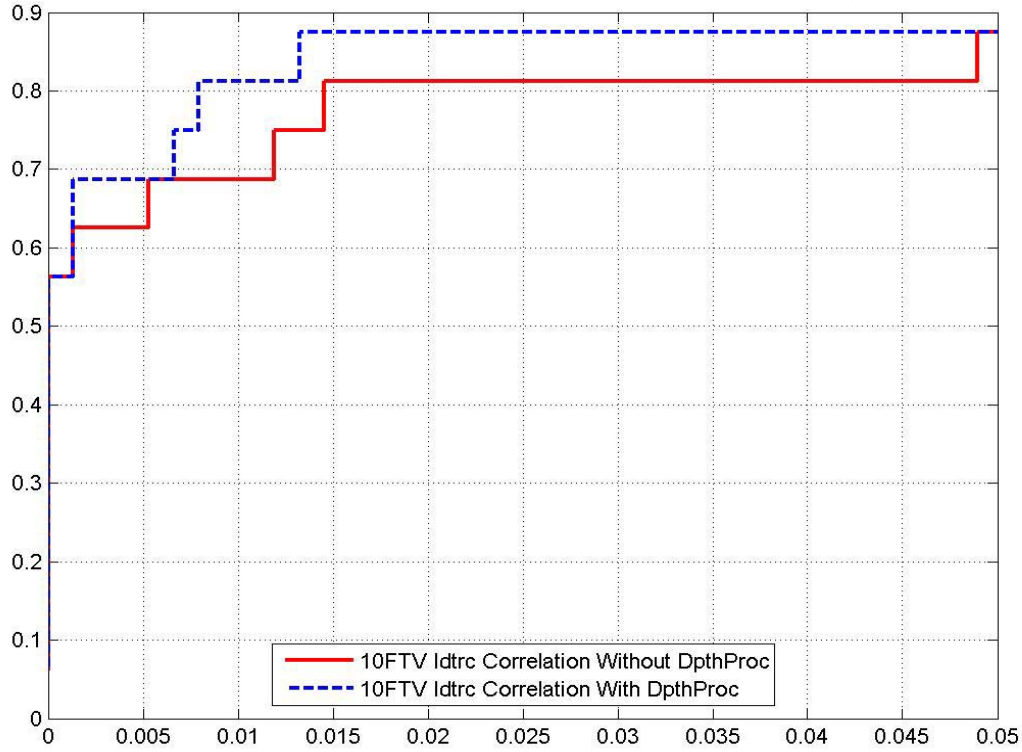


**Figure 51: ROC Characteristics for Dataset 5 with and without Depth Estimation**

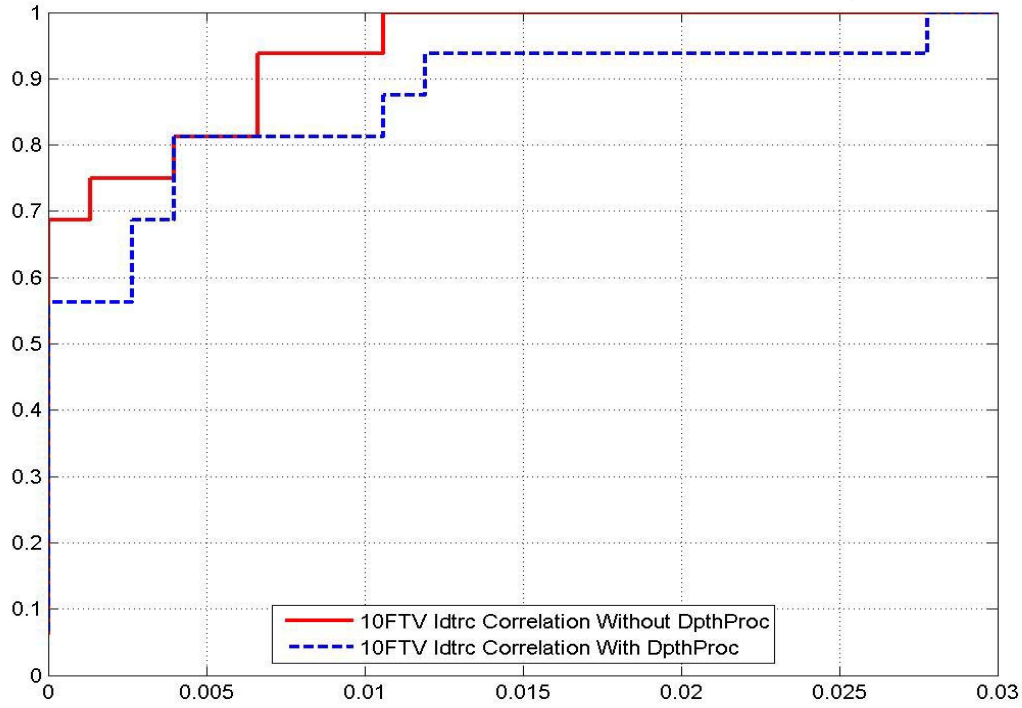


**Figure 52: ROC Characteristics for Dataset 6 with and without Depth Estimation**

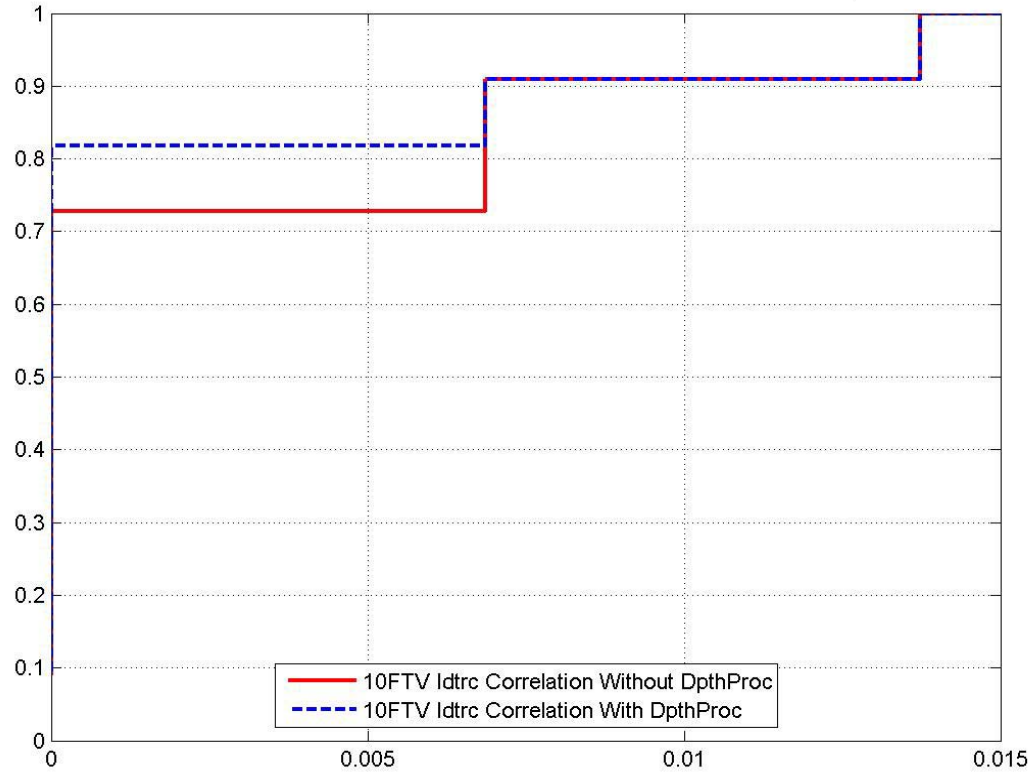


**Figure 53: ROC Characteristics for Dataset 7 with and without Depth Estimation**

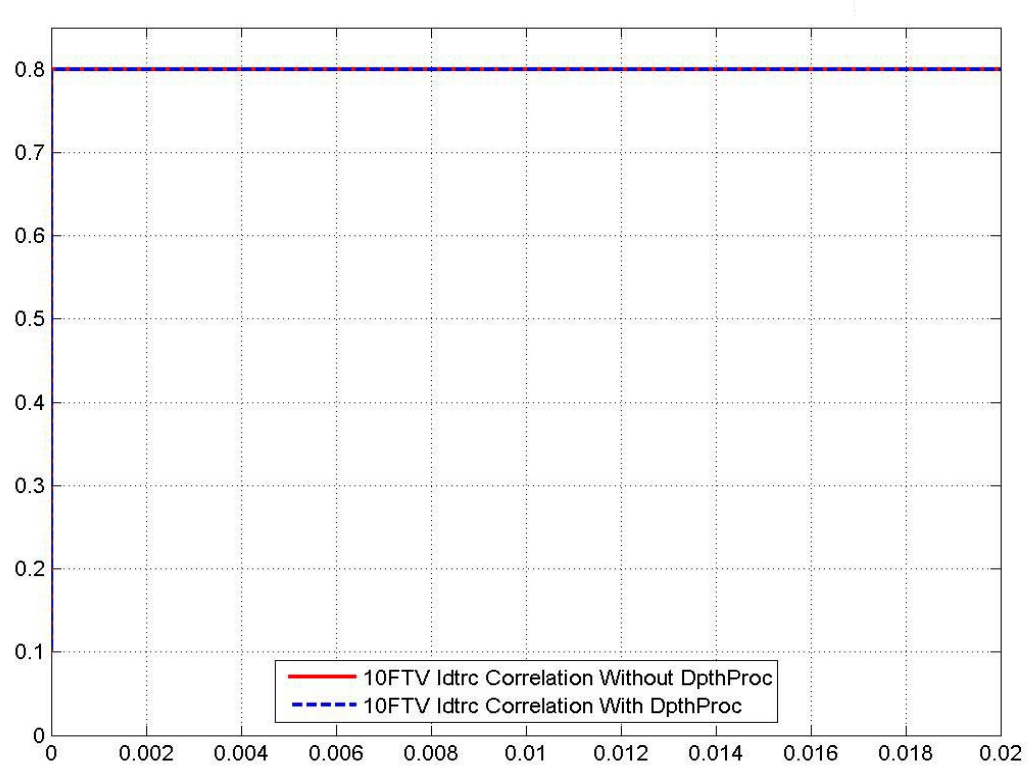


**Figure 54: ROC Characteristics for Dataset 8 with and without Depth Estimation**

## 5.4 ROC Characteristics with Depth Estimation Routine for 20 Subbands

Figures 55-62 show the ROC characteristics with depth estimation for the case of 20 subbands. The figures compare the ROC characteristics obtained by using 20 subbands with 1 sample overlap and 2 sample overlap, with the ROC obtained from 10 subbands. Except for datasets 4 and 7 (Figure 58 and Figure 61), 20 subbands with 2 sample overlap shows better improvement in ROC over the case with 20 subbands with 1 sample overlap between the bands. Therefore, 2 sample overlap is only investigated in further analysis in this chapter. From the figures below, it is evident that using 20 subbands in frequency domain processing, once again proved to be useful in improving the probability of detection of landmines

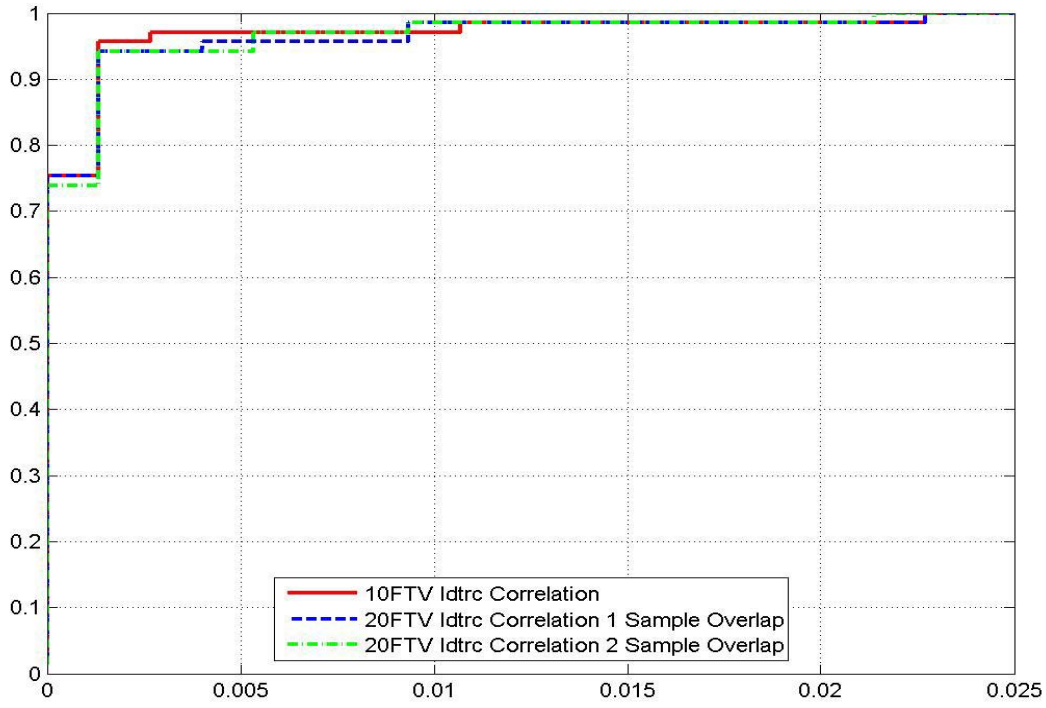


**Figure 55: ROC Characteristics 10 Vs 20 Subbands with Depth Estimation for Dataset 1**

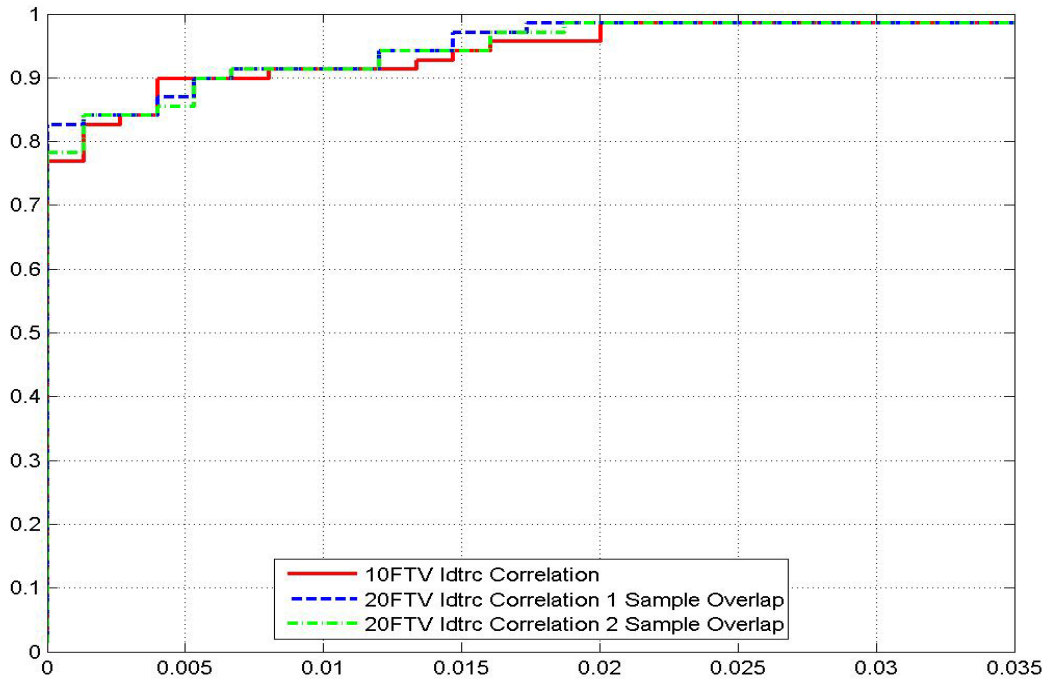


**Figure 56: ROC Characteristics 10 Vs 20 Subbands with Depth Estimation for Dataset 2**

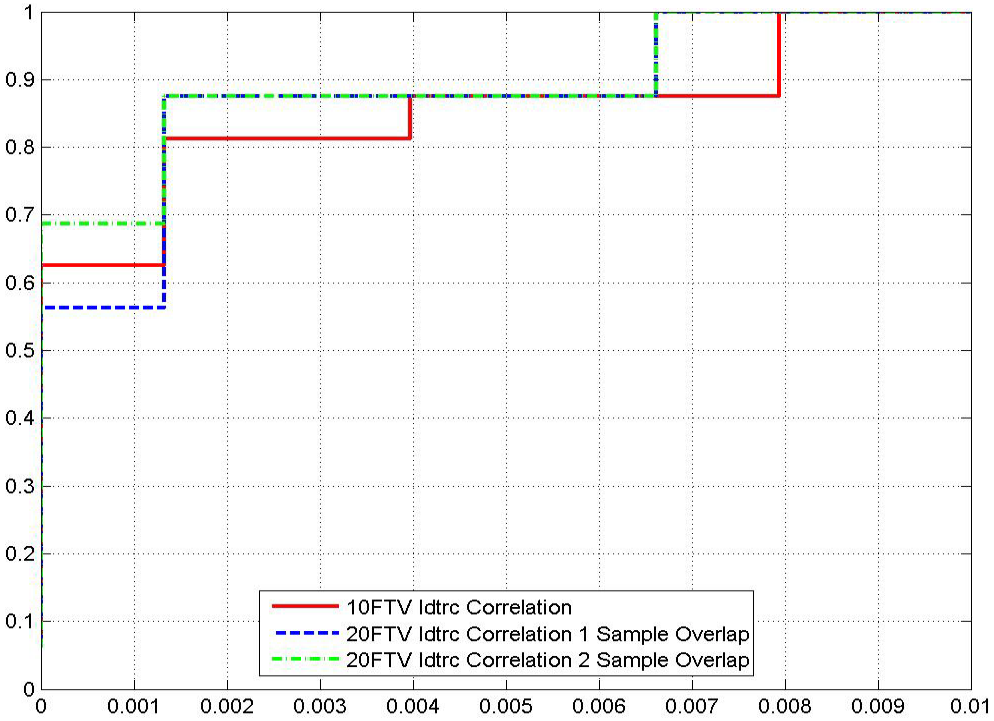


**Figure 57: ROC Characteristics 10 Vs 20 Subbands with Depth Estimation for Dataset 3**

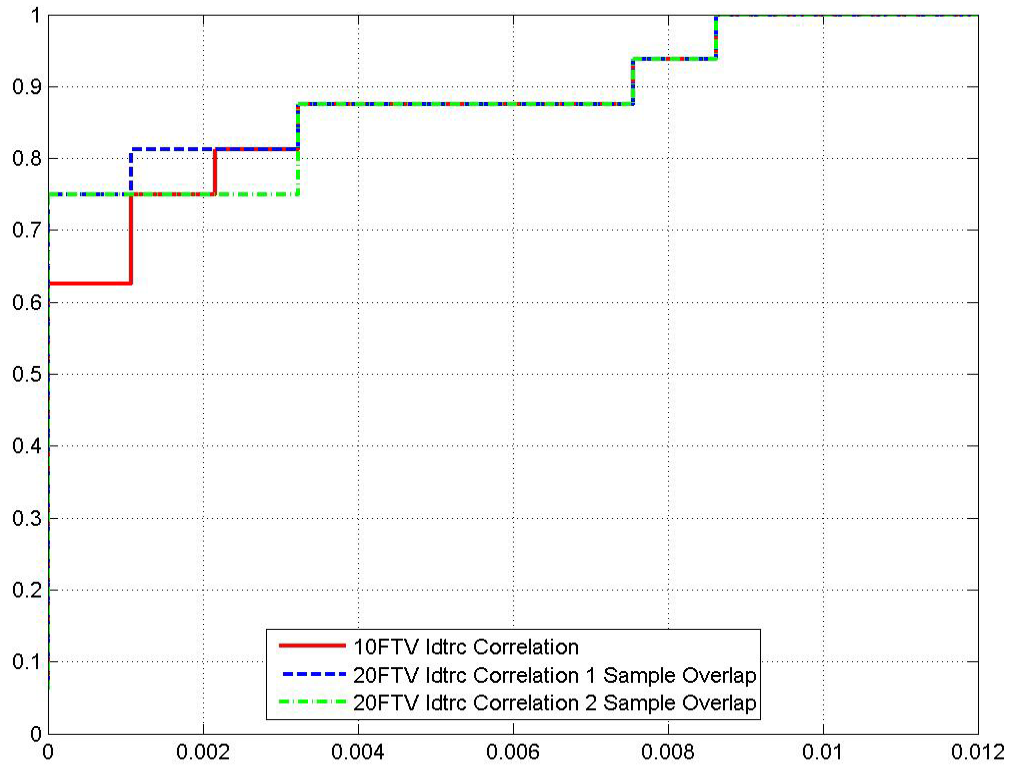


**Figure 58: ROC Characteristics 10 Vs 20 Subbands with Depth Estimation for Dataset 4**

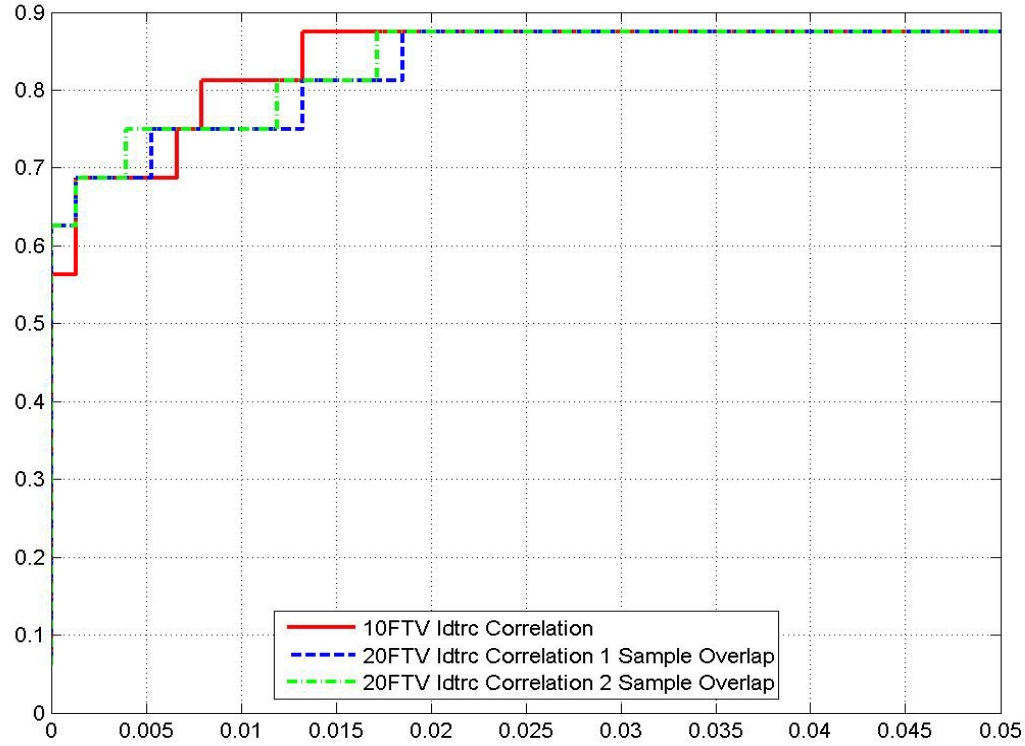


**Figure 59: ROC Characteristics 10 Vs 20 Subbands with Depth Estimation for Dataset 5**

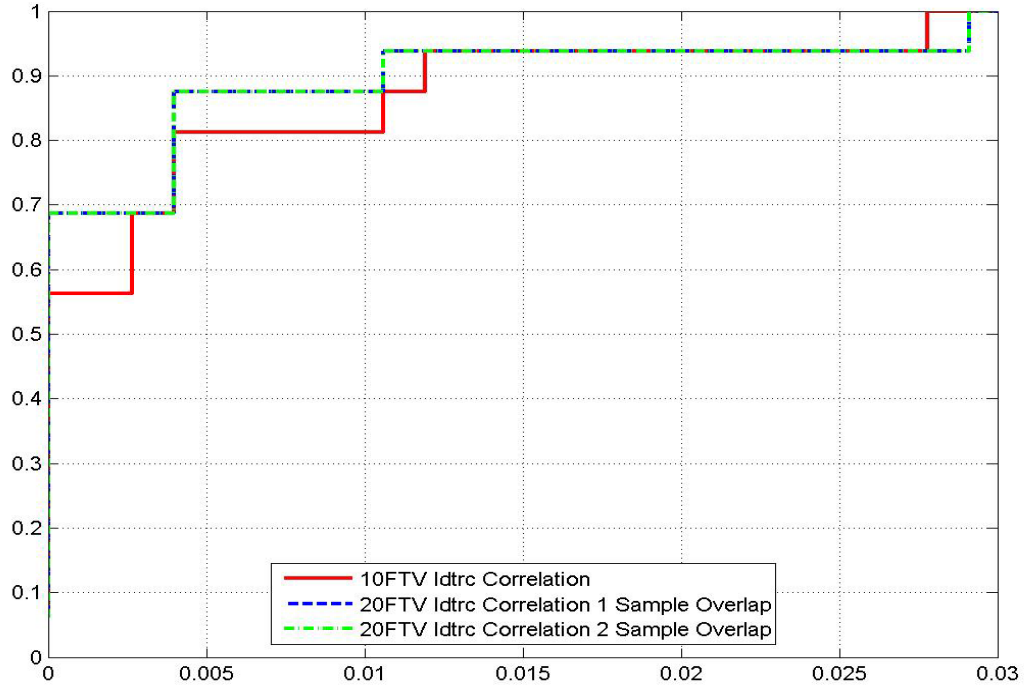


**Figure 60: ROC Characteristics 10 Vs 20 Subbands with Depth Estimation for Dataset 6**

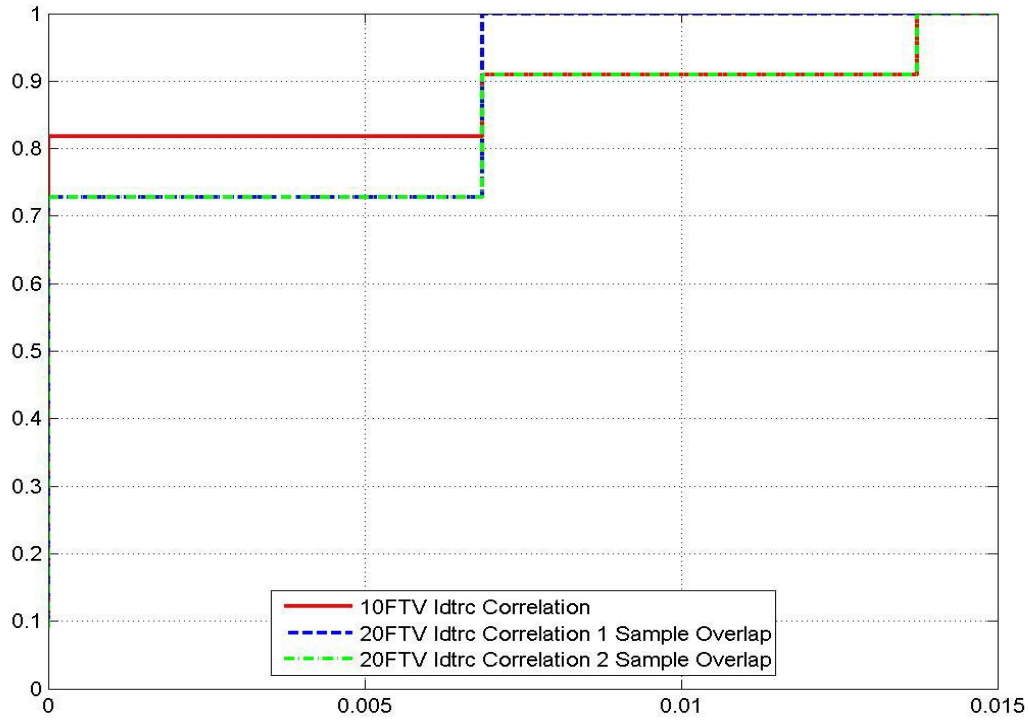


**Figure 61: ROC Characteristics 10 Vs 20 Subbands with Depth Estimation for Dataset 7**

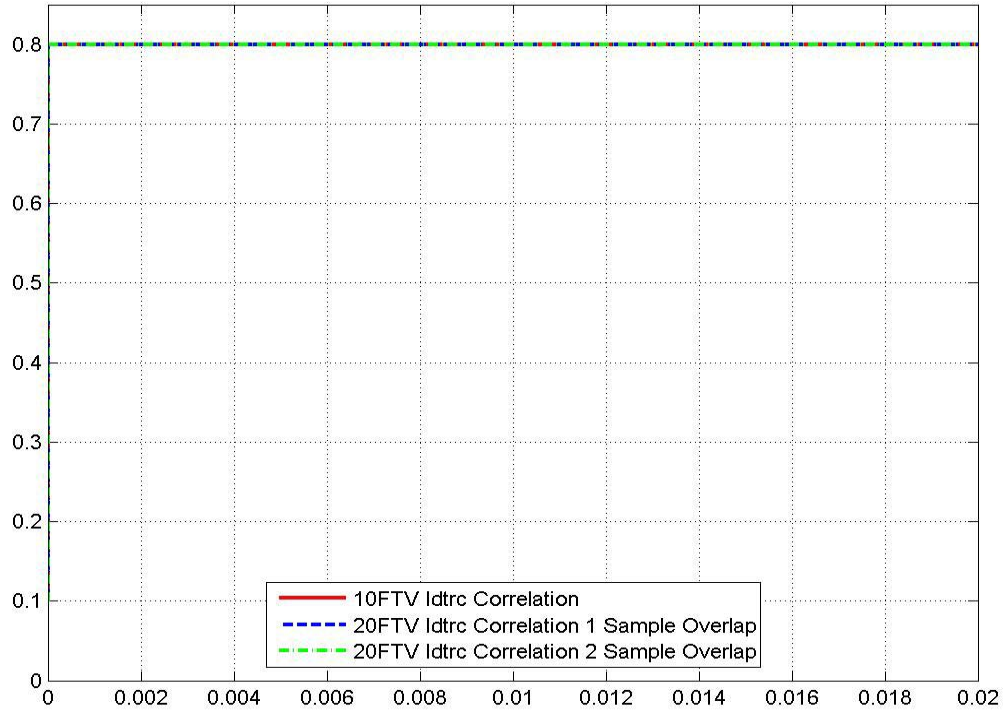


**Figure 62: ROC Characteristics 10 Vs 20 Subbands with Depth Estimation for Dataset 8**

Tables 4(a) and 4(b) give the false alarm rate at 90% probability of detection and 95% probability of detection respectively. The letters NA represents that the probability of detection does not reach 90% and 95% for those datasets. At 90% probability of detection, for dataset 2, it can be seen that the false alarm rate reduced from 0.008 to 0.006. Similarly for all the other datasets, the false alarm rate reduced by 25%. But, at a probability of detection of 95%, for datasets 1 and 6, the false alarm rate is increased by 10 %, which shows some degradation in performance at higher probabilities.

| | Dataset 1 | | Dataset 2 | | Dataset 3 | | Dataset 4 | |
|---|---|---|---|---|---|---|---|---|
| | 10 Subbands | 20 subbands | 10 subbands | 20 subbands | 10 subbands | 20 subbands | 10 subbands | 20 subbands |
| FAR at 90% Pd | 0.001336 | 0.001336 | 0.008017 | 0.006681 | 0.007939 | 0.006616 | 0.007551 | 0.006472 |
| FAR at 95% Pd | 0.002672 | 0.005344 | 0.020042 | 0.016033 | 0.007939 | 0.006616 | 0.008630 | 0.008630 |

**Table 4(a): False Alarm Rate at 90 % and 95 % probability of detection for 10 vs. 20 Subbands with depth Estimation for datasets 1 to 4**

| | Dataset 5 | | Dataset 6 | | Dataset 7 | | Dataset 8 | |
|---|---|---|---|---|---|---|---|---|
| | 10 Subbands | 20 subbands | 10 subbands | 20 subbands | 10 subbands | 20 subbands | 10 subbands | 20 subbands |
| FAR at 90% Pd | NA | NA | 0.011908 | 0.010585 | 0.006868 | 0.006868 | NA | NA |
| FAR at 95% Pd | NA | NA | 0.027786 | 0.029109 | 0.013736 | 0.013736 | NA | NA |

**Table 4(b): False Alarm Rate at 90 % and 95 % probability of detection for 10 vs. 20 Subbands with depth Estimation for datasets 5 to 8**

## 5.5 Modified Algorithm for Depth Estimation

In the original depth Estimation routine, the sum of center 3 scans is used to obtain the location of maxima and minima. In some cases where the three scans are not aligned with respect to each other, there might be a shift in the depth bins which results in estimating wrong depths of the mines. To overcome this difficulty, the data in the scans adjacent to the centre scan, are aligned with respect to the center scan, along the depth. This algorithm is implemented on the data before normalization. To find the shift along the depth, the scans adjacent to the center scans are cross correlated with the center scan and the lag where the cross correlation value is maximum is taken as the shift along the depth. Since the shift can be less than one depth bin sample, the up sampled data is used to find the shift and then, the data is down sampled after shifting with the corresponding lag value. The steps in the algorithm are as follows

1) Upsample the 3 scans on either sides of the center scan
2) Find the shift in the scans adjacent to center scan on either sides, and shift by corresponding value.
3) Perform steps 1 and 2 for Center -3 to Center +3 Scans
4) Average the aligned data
5) Downsample the data back to the original size
6) Sum all the 7 Scans and find the maximum and minimum of the sum
7) Decide between the maximum and minimum using steps involved in the original algorithm

To further increase the performance of the algorithm, and to avoid any discrepancy in deciding between the maxima and minima, four cases described below were considered

Case 1: All the depth bins below the ground were taken

Case 2: Data from 30 depth bins below the ground were taken

Case 3: Data from 40 depth bins below the ground were taken

Case 4: Data from 50 depth bins below the ground were taken

The depth corresponding to the maximum of the correlation values obtained from the four cases above is taken as the estimated depth.

## 5.6 Comparison of Depth Estimates Using Original and Modified Algorithm with Depth from the structure

Figures 63-70 show the depth estimates obtained with the original algorithm and the modified algorithm for 8 different datasets. They also show the depth from the original data for comparison. The upper sub plot in each figure shows the depth from the structure and the lower subplot compares the depth obtained from the original and modified algorithm. It can be seen from the figures that depth obtained from the algorithms show a similar pattern as the depths from the original structure. But with the depth Estimation routine, in some cases the mines that are far below the surface (depth 6) are under estimated and the mines that are just below the surface (depth 1 or 2) are overestimated. The modified algorithm works well in estimating the depth in the order of the original depth from the structure. But there are still some cases where the depth Estimation routine fails. Looking at the overall performance, it is evident that the modified depth Estimation algorithm improved the estimates compared to the original algorithm for nearly 6 out of 8 data sets.

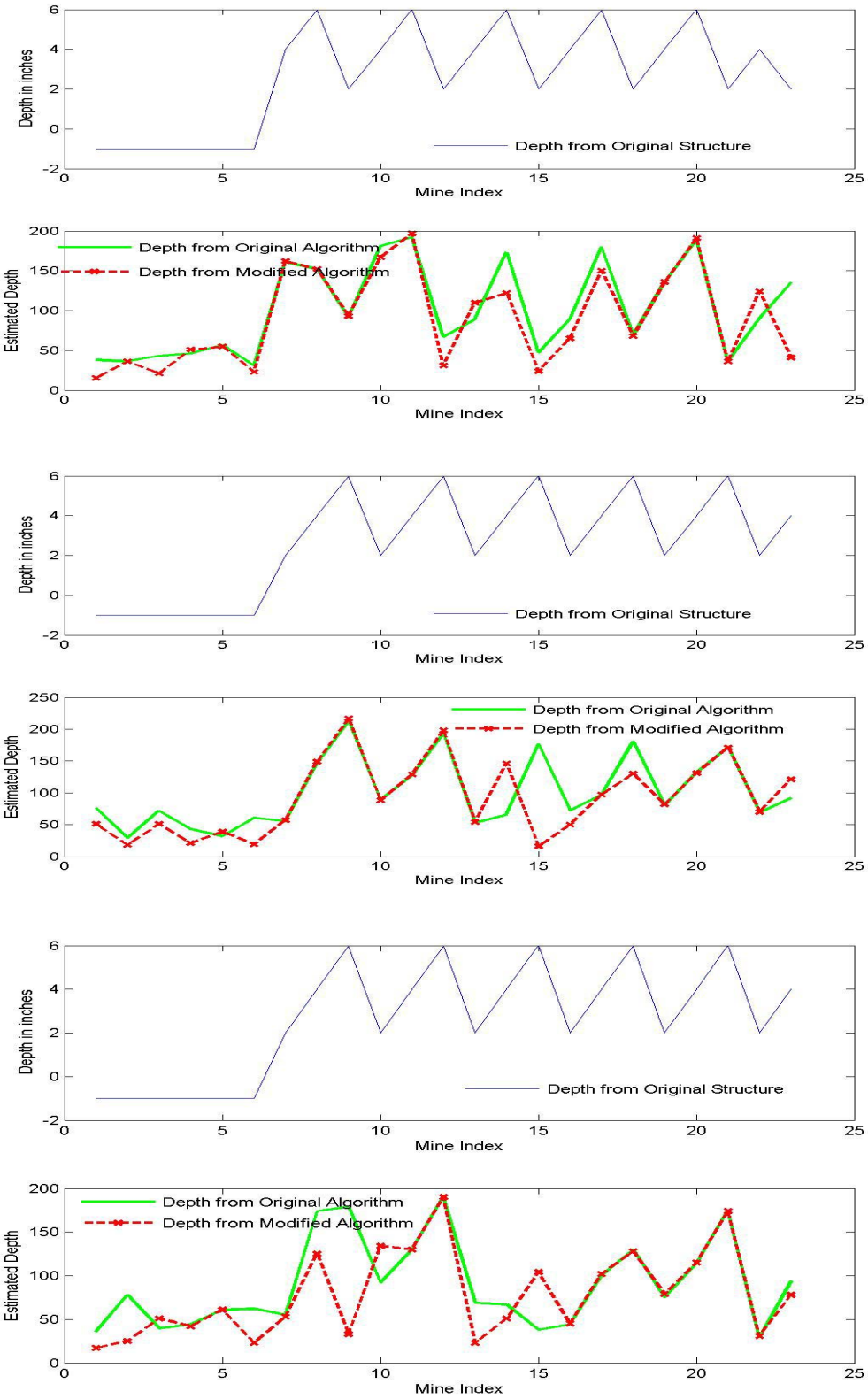


**Figure 63: Depth Estimates from Original Vs Modified algorithm and original structure for Dataset 1**

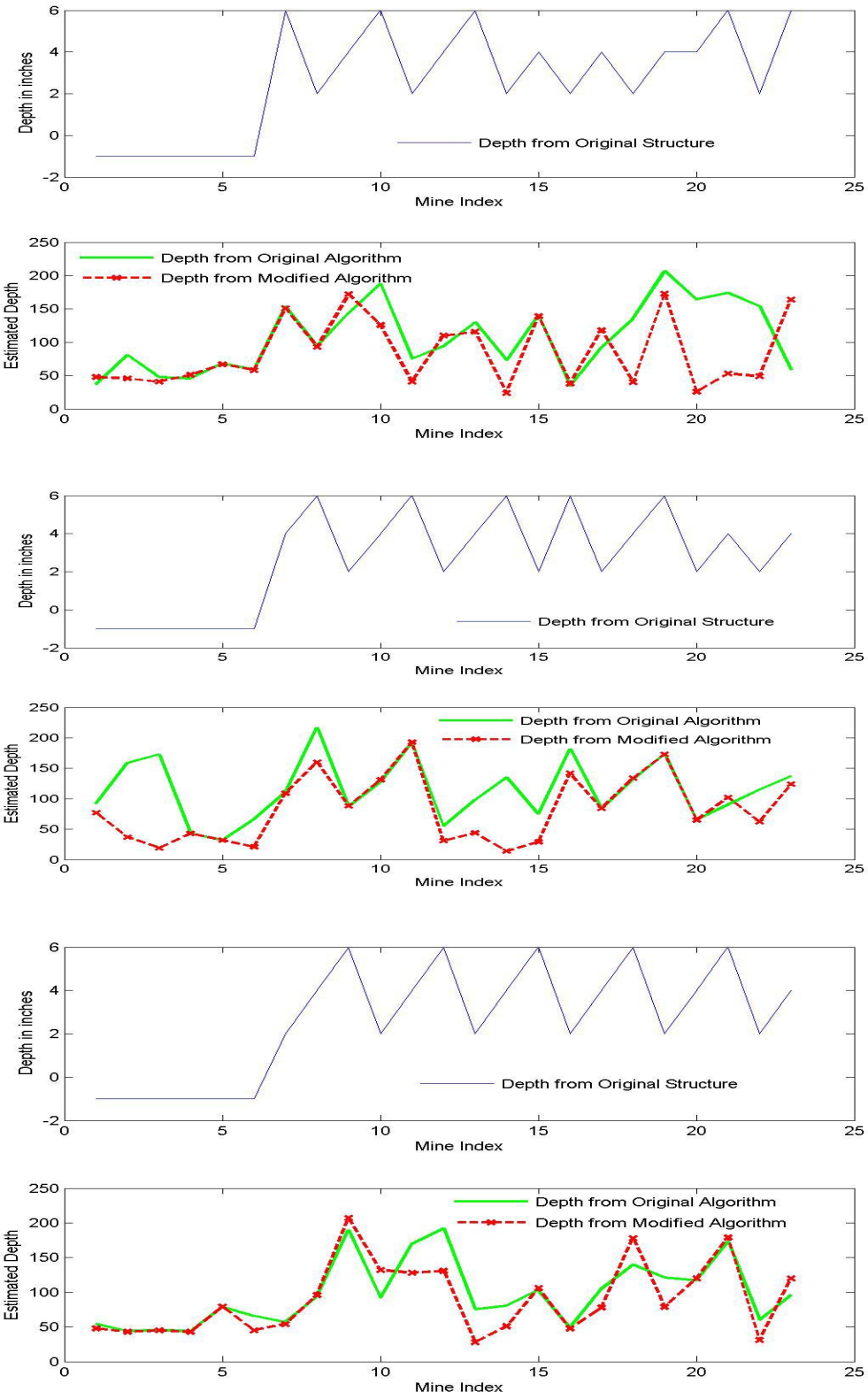


**Figure 64: Depth Estimates from Original Vs Modified algorithm with original structure for Dataset 2**

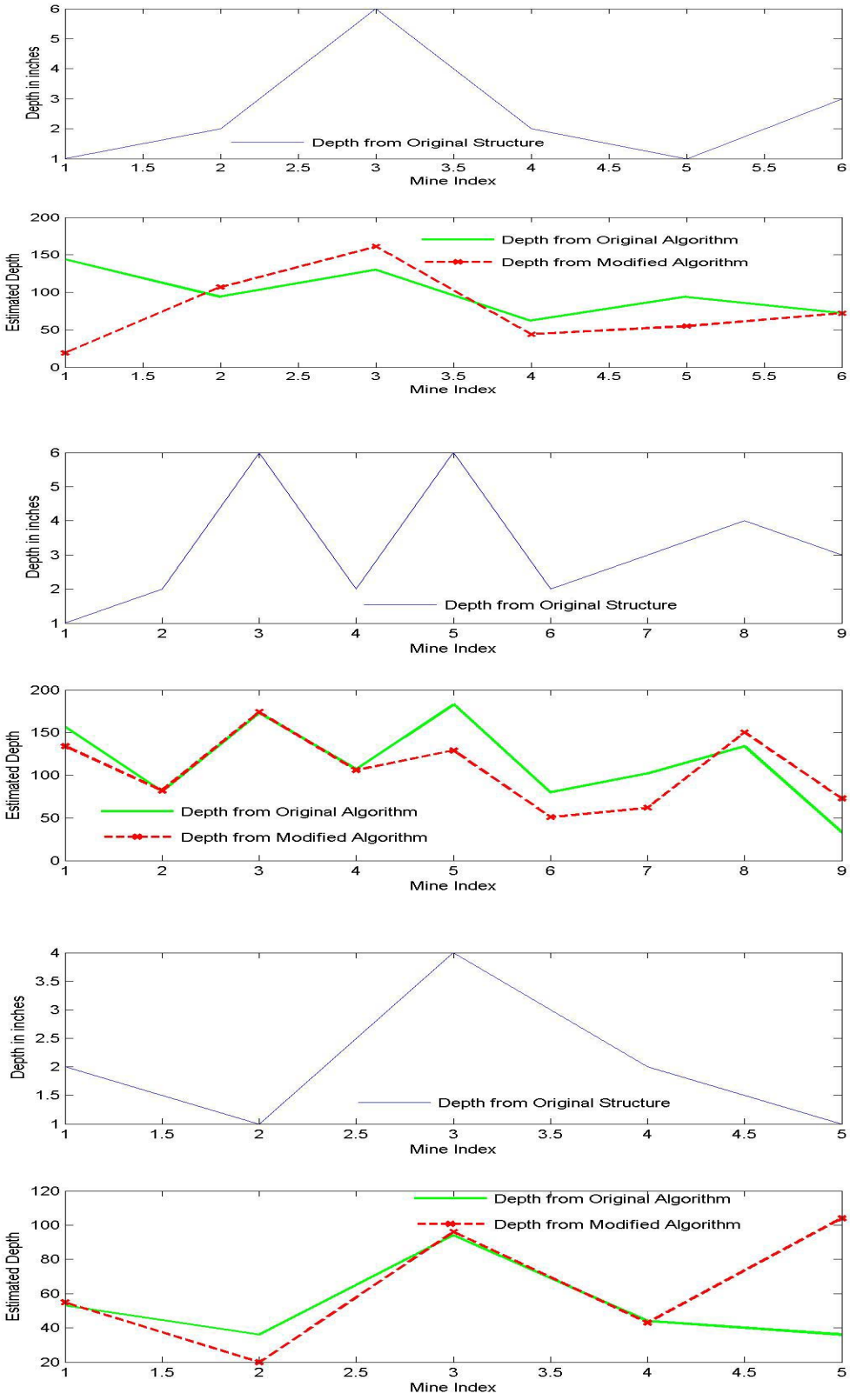


**Figure 65: Depth Estimates from Original Vs Modified algorithm with original structure for Dataset 3**

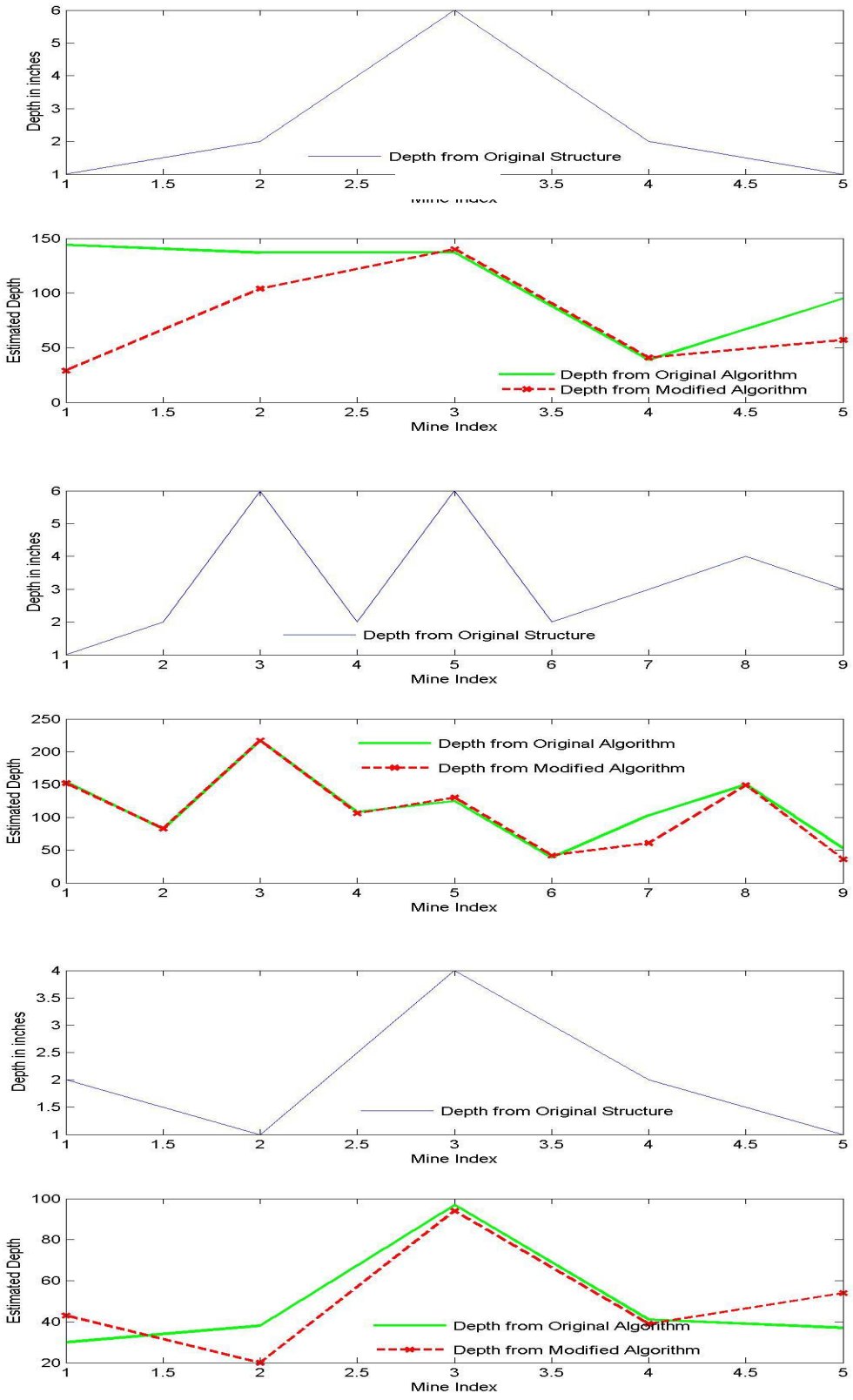


**Figure 66: Depth Estimates from Original Vs Modified algorithm with original structure for Dataset 4**

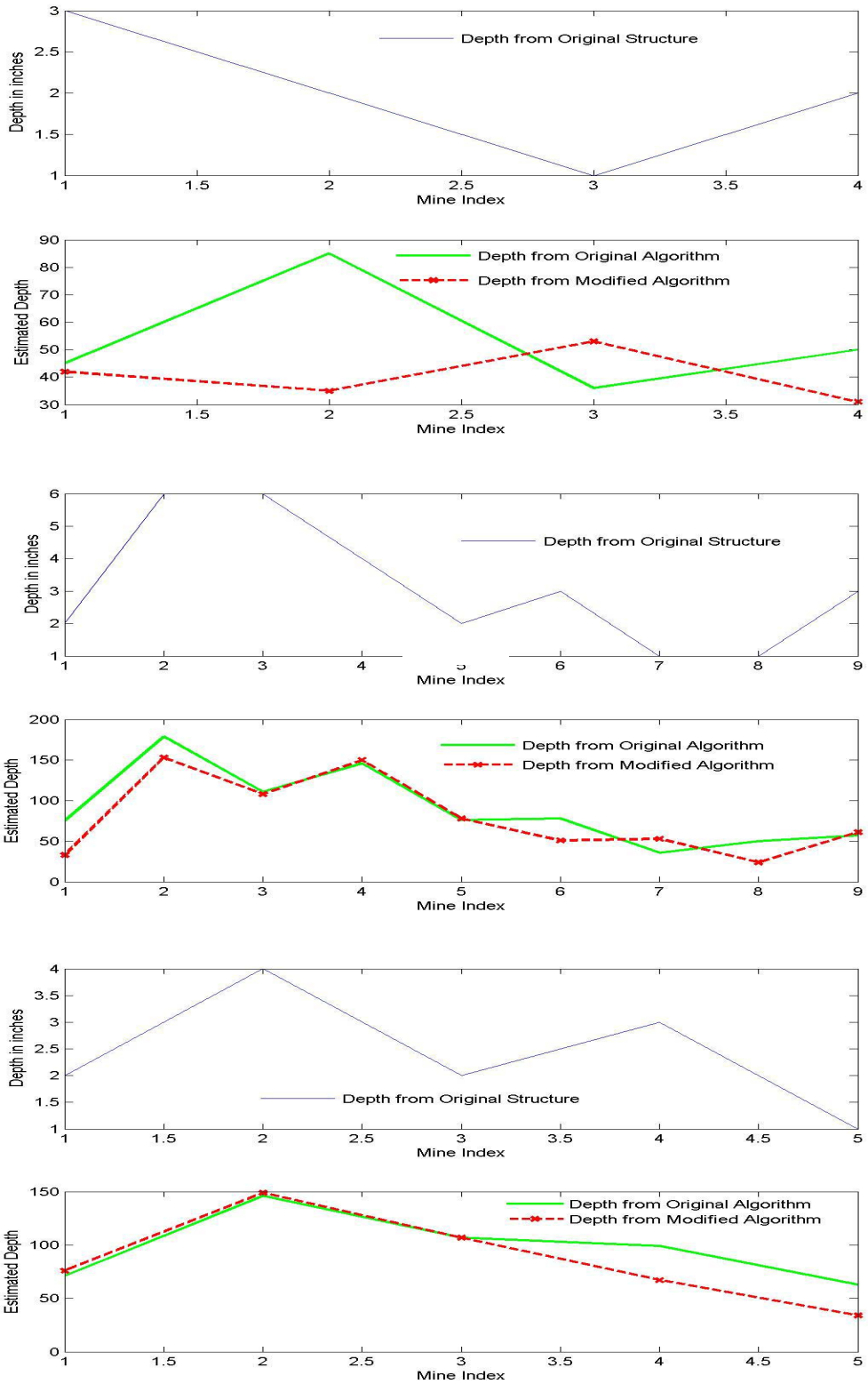


**Figure 67: Depth Estimates from Original Vs Modified algorithm with original structure for Dataset 5**

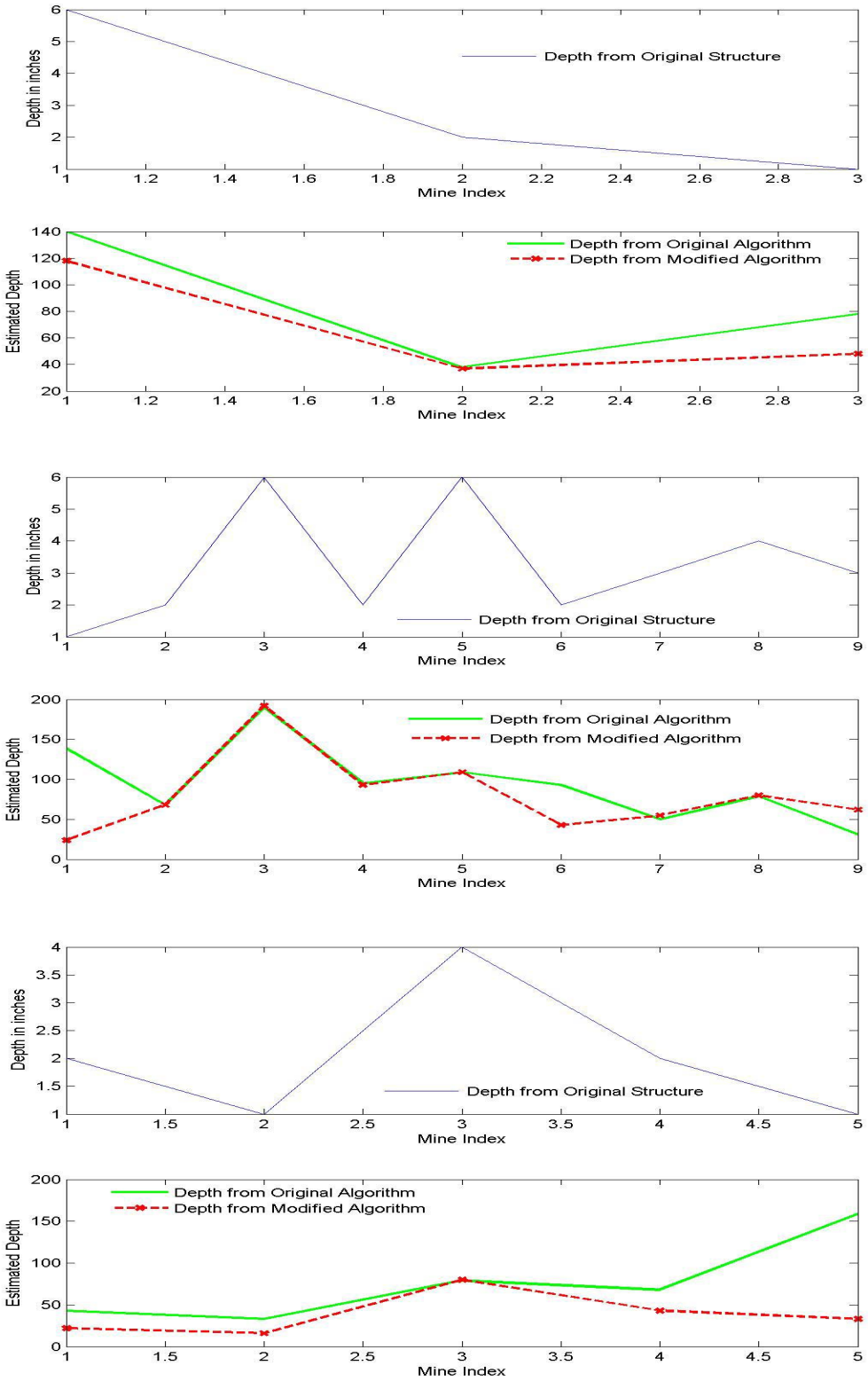


**Figure 68: Depth Estimates from Original Vs Modified algorithm with original structure for Dataset 6**

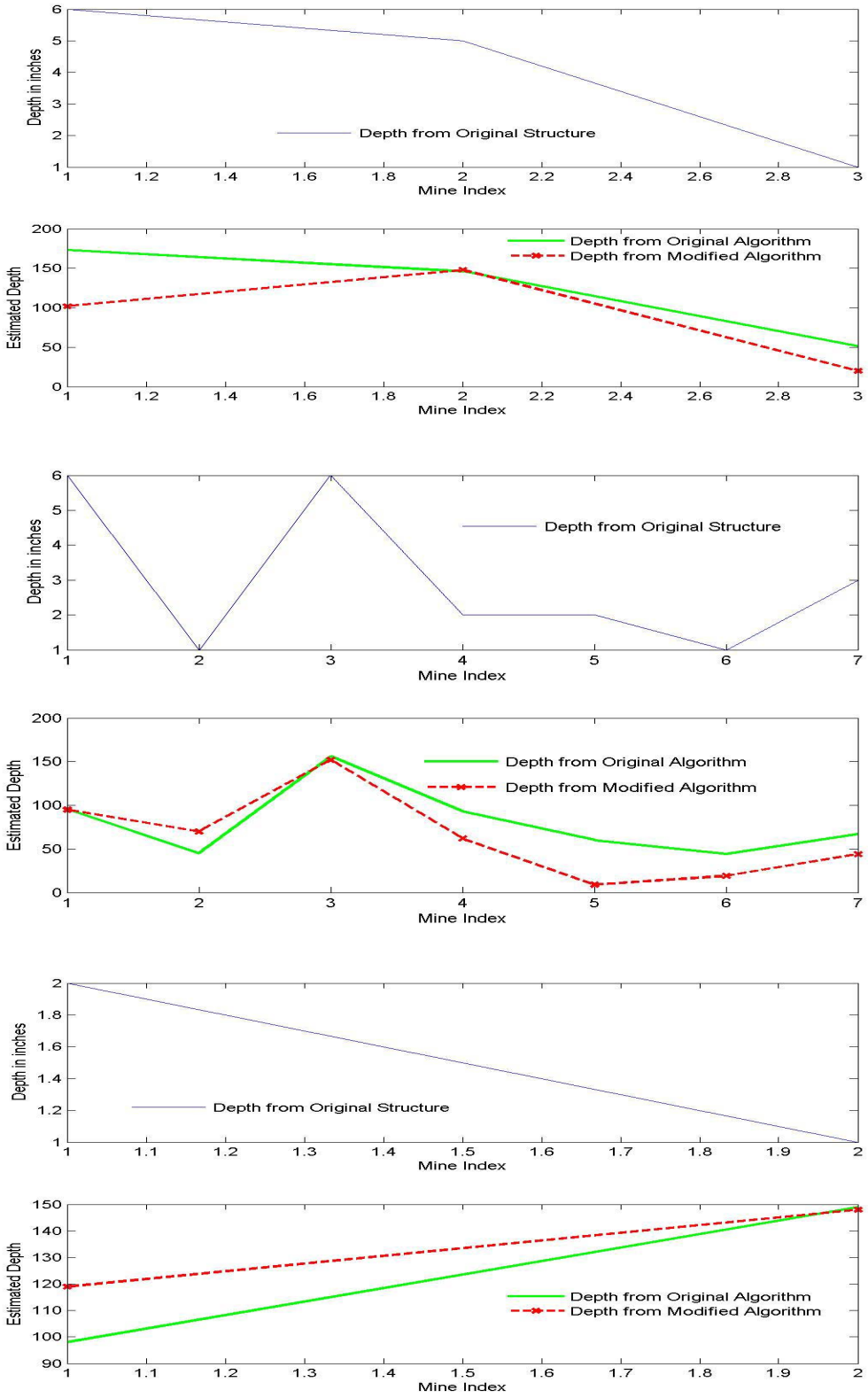


**Figure 69: Depth Estimates from Original Vs Modified algorithm with original structure for Dataset 7**

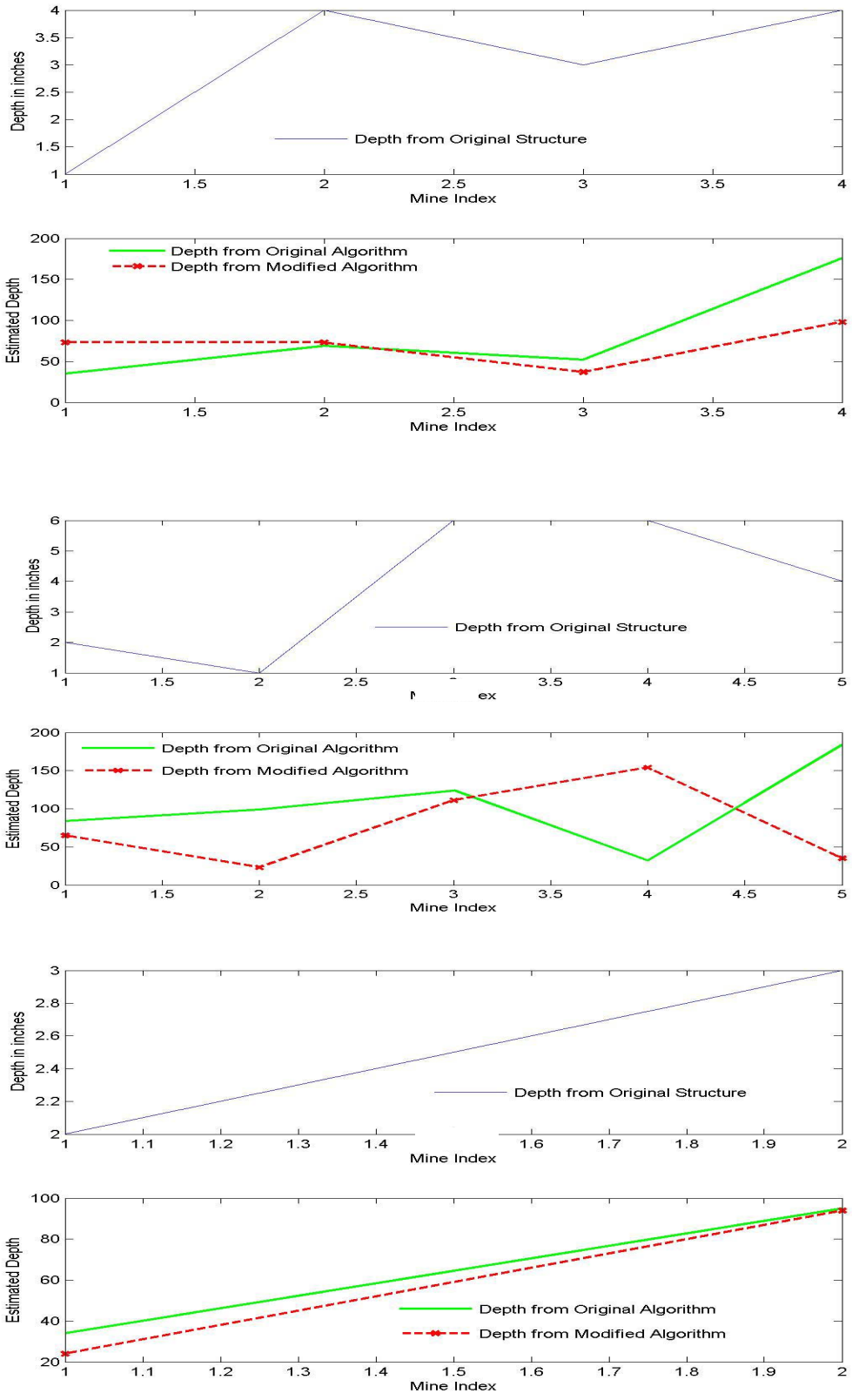


**Figure 70: Depth Estimates from Original Vs Modified algorithm with original structure for Dataset 8**

## 5.7 ROC Comparison Using Depth Estimation with Original and Modified algorithm

The ROC characteristics were studied using the original and modified algorithm to evaluate the performance of the modified depth Estimation routine. Part (a) of each figure from figure 71-78 , shows the ROC characteristics obtained by using the frequency domain technique explained in chapter 4 with Original and modified Algorithm for depth Estimation. Part (b) shows the ROC characteristics for 20 subbands, using original and modified algorithm for depth Estimation. Datasets 2, 3, 4 and 6 showed some improvement with the modified technique. The probability of detection increased by 15% for these datasets. For datasets 1 and 5, the original technique seemed to be a little better and for datasets 7 and 8, both the techniques give the same ROC characteristics.

Tables 5(a) and 5(b) show the False Alarm Rates at probability of detection of 90% and 95% respectively, with the Original depth Estimation routine and modified routine for all the 8 datasets. From the tables, it is evident that except for dataset 1, the false alarm rates at Pd of 90% and 95% are reduced for all datasets with the use of modified Depth Estimation routine. Thus, the modified routine improved the ROC characteristics as well.

| | Dataset 1 | | Dataset 2 | | Dataset 3 | | Dataset 4 | |
|---|---|---|---|---|---|---|---|---|
| | (i) | (ii) | (i) | (ii) | (i) | (ii) | (i) | (ii) |
| FAR at 90% Pd | 0.001336 | 0.001634 | 0.008017 | 0.003268 | 0.007939 | 0.006616 | 0.007551 | 0.005393 |
| FAR at 95% Pd | 0.002672 | 0.003268 | 0.020042 | 0.009805 | 0.007939 | 0.006616 | 0.008630 | 0.007551 |

**Table 5(a): False Alarm Rate at 90% and 95% Probability of detection for 10 subbands with Original and Modified depth Estimation for Datasets 1 to 4**

**i. Original Depth Estimation**

**ii. Modified Depth Estimation**

| | Dataset 5 | | Dataset 6 | | Dataset 7 | | Dataset 8 | |
|---|---|---|---|---|---|---|---|---|
| | (i) | (ii) | (i) | (ii) | (i) | (ii) | (i) | (ii) |
| FAR at 90% Pd | NA | NA | 0.011908 | 0.005292 | 0.006868 | 0.006868 | NA | NA |
| FAR at 95% Pd | NA | NA | 0.027786 | 0.009262 | 0.013736 | 0.013736 | NA | NA |

**Table 5(b): False Alarm Rate at 90% and 95% Probability of detection for 10 subbands with Original and Modified depth Estimation for Datasets 5 to 8**

**i. Original Depth Estimation**

**ii. Modified Depth Estimation**

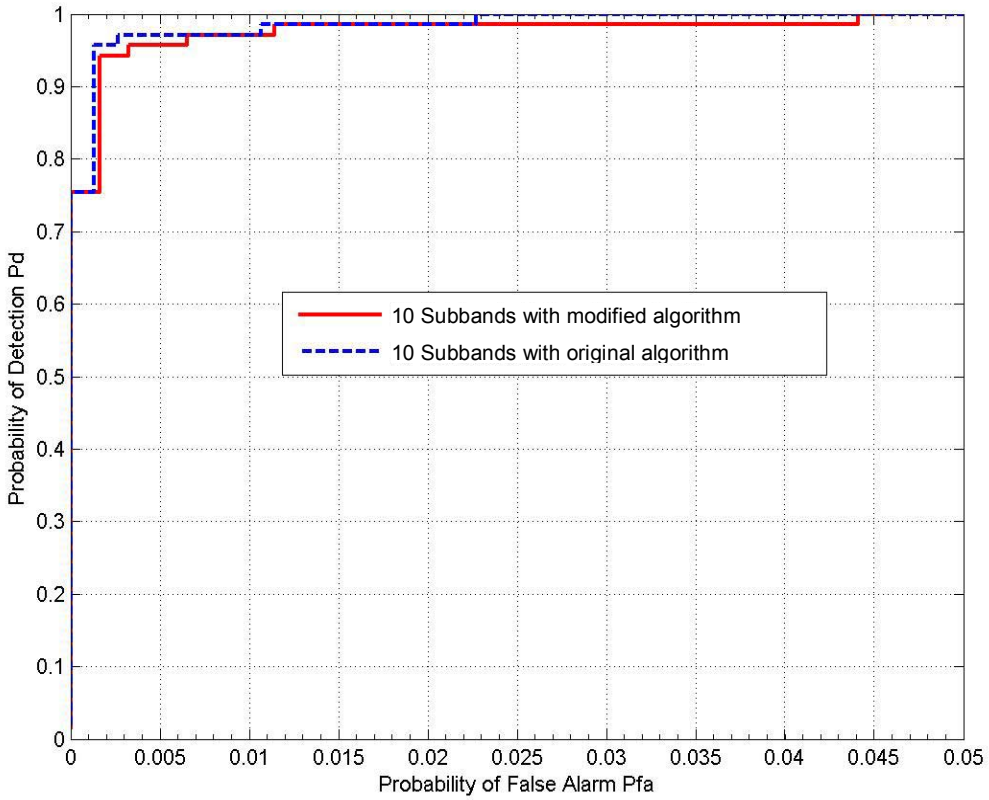


**Figure 71(a): ROC for 10 Subbands with Modified Vs Original Algorithm for Dataset 1**

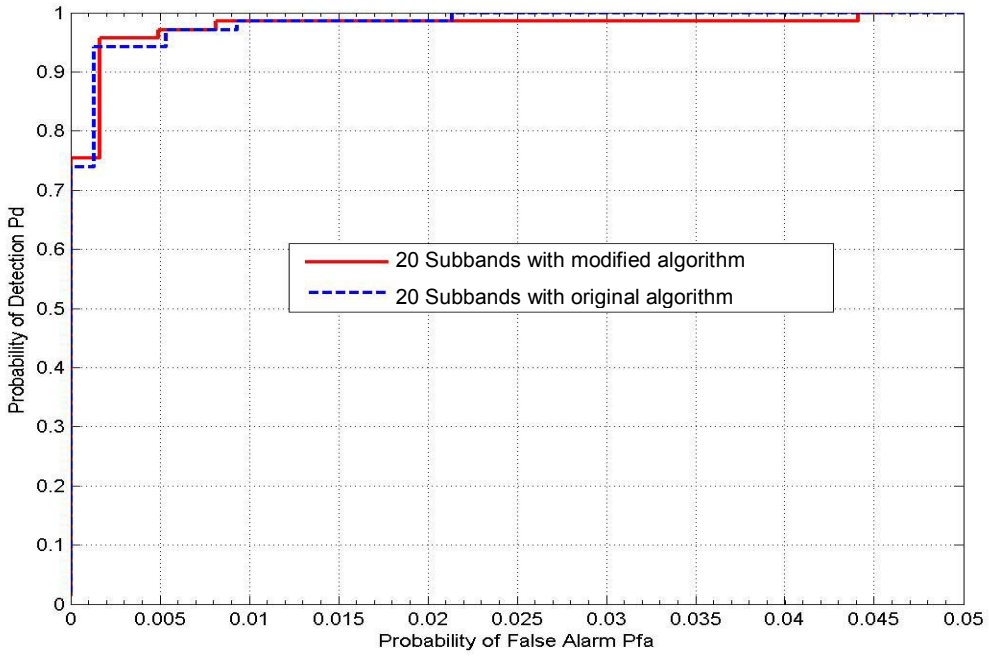


**Figure 71(b): ROC for 20 Subbands with Modified Vs Original Algorithm for Dataset 1**

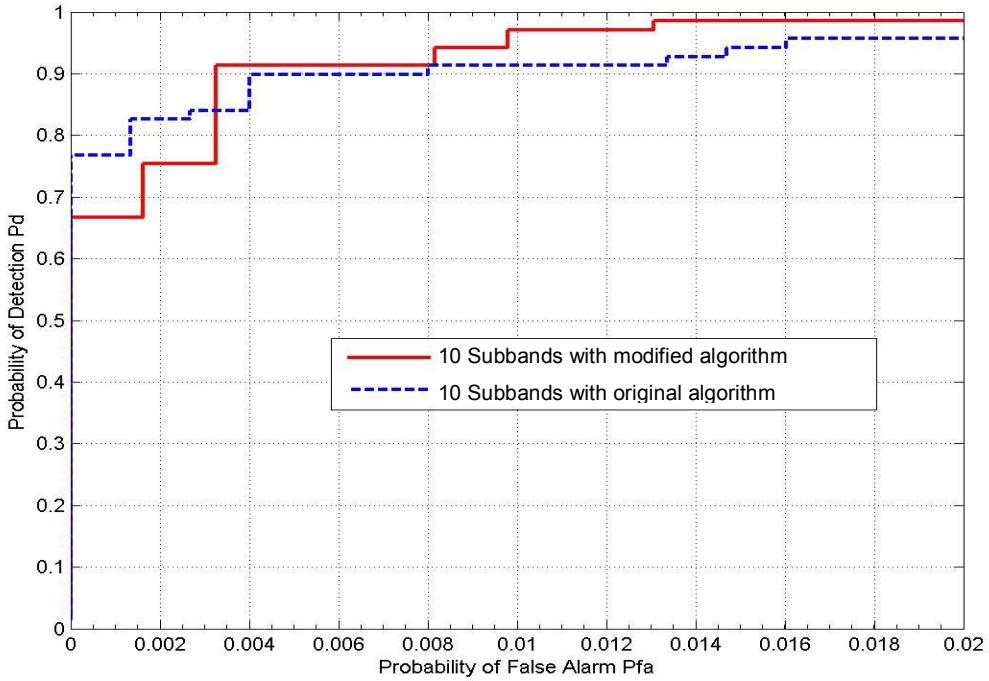


**Figure 72(a): ROC for 10 Subbands with Modified Vs Original Algorithm for Dataset 2**

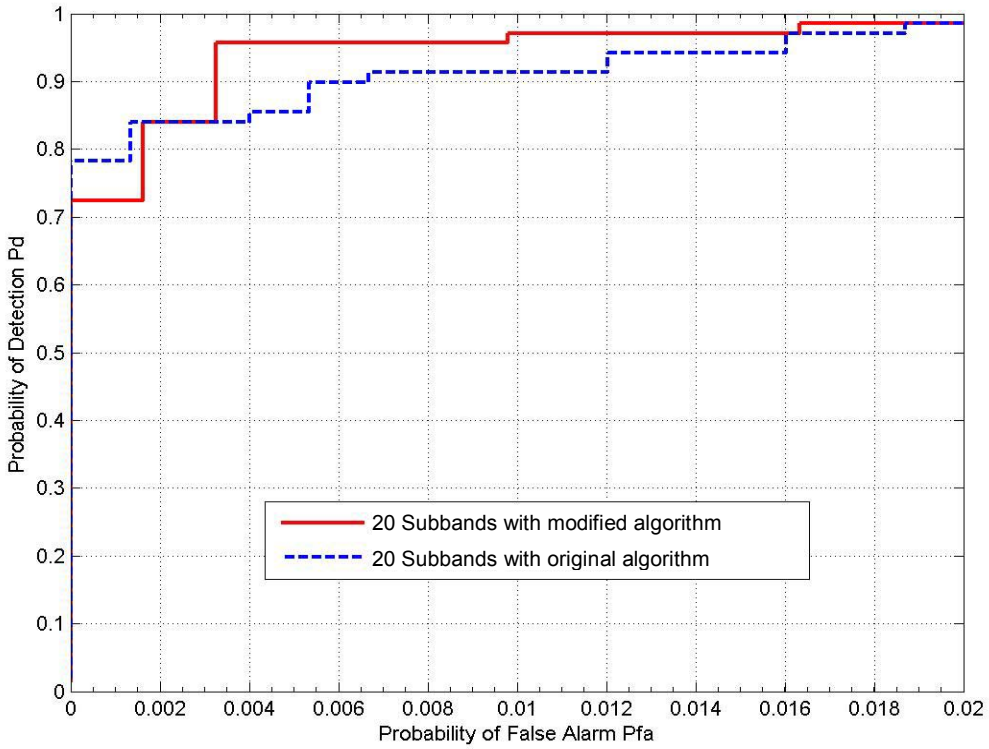


**Figure 72(b): ROC for 20 Subbands with Modified Vs Original Algorithm for Dataset 2**

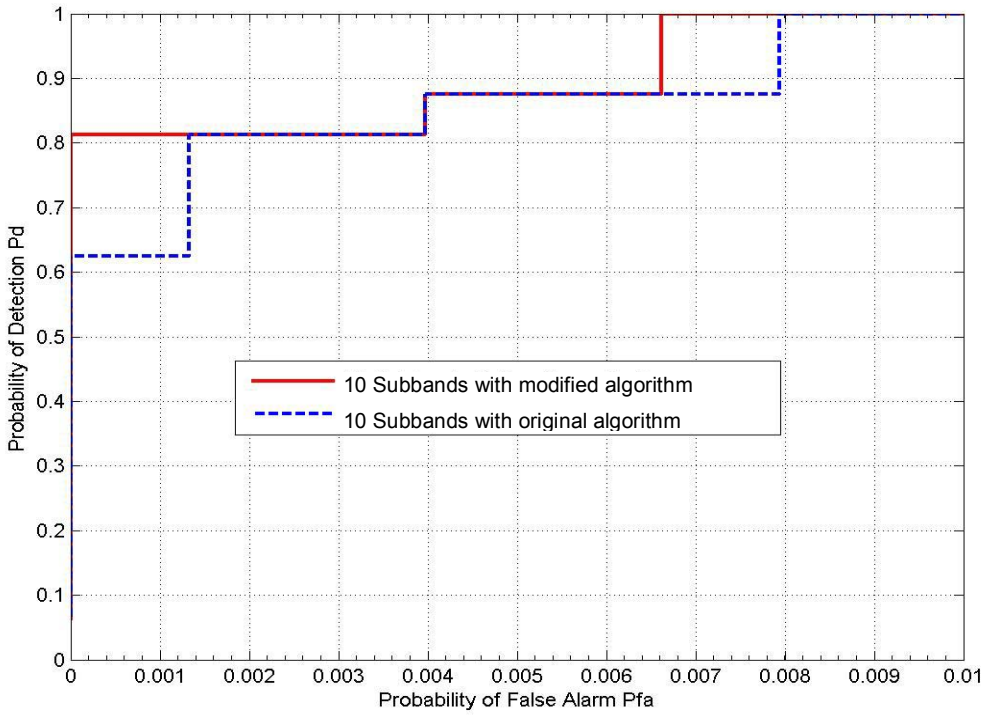


**Figure 73(a): ROC for 10 Subbands with Modified Vs Original Algorithm for Dataset 3**

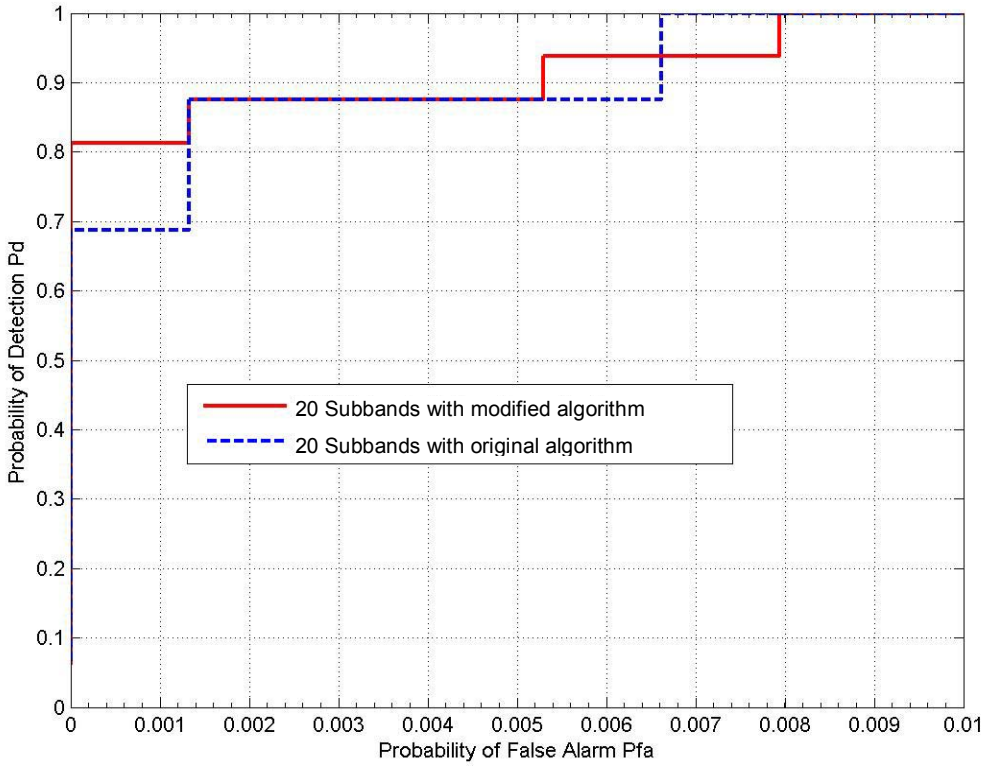


**Figure 73(b): ROC for 20 Subbands with Modified Vs Original Algorithm for Dataset 3**

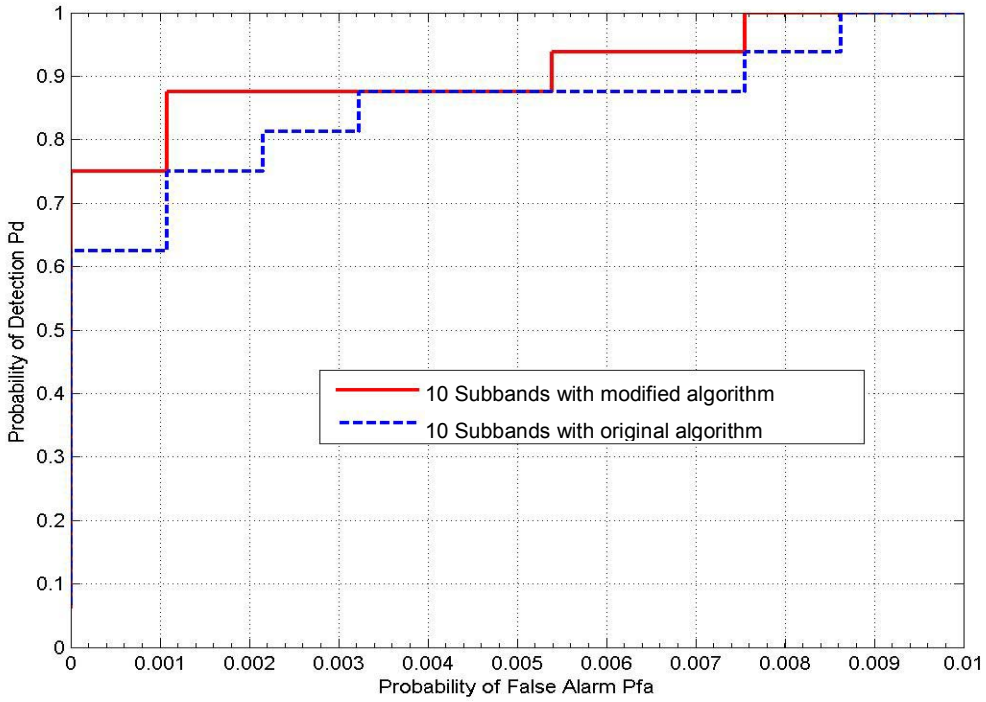


**Figure 74(a): ROC for 10 Subbands with Modified Vs Original Algorithm for Dataset 4**

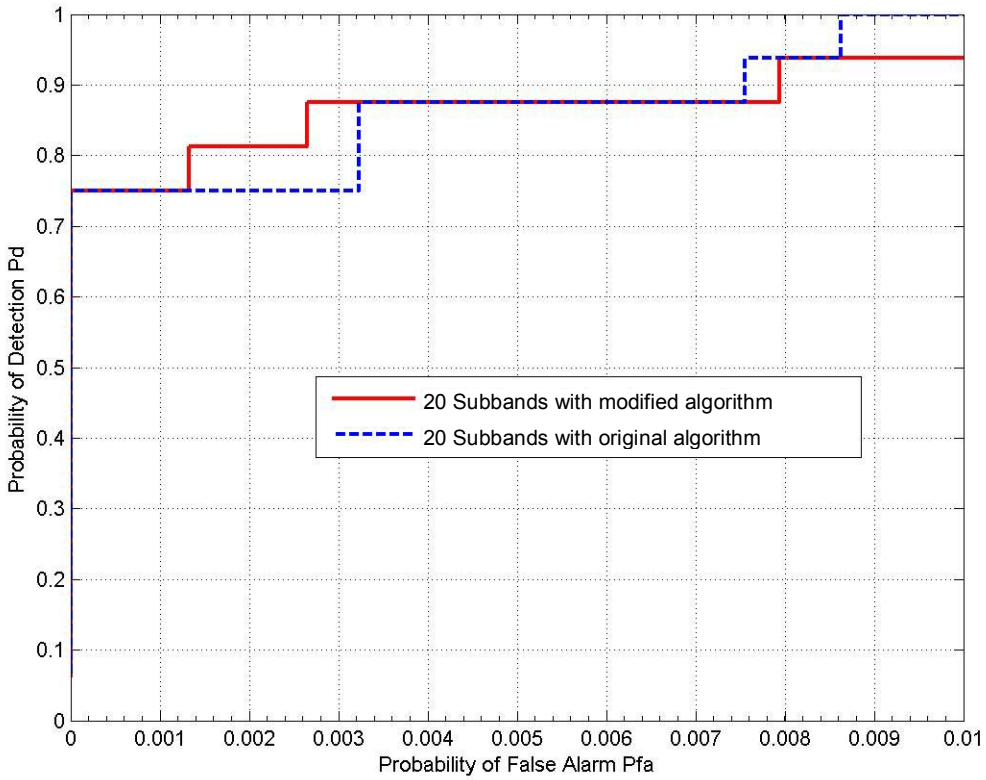


**Figure 74(b): ROC for 20 Subbands with Modified Vs Original Algorithm for Dataset 4**

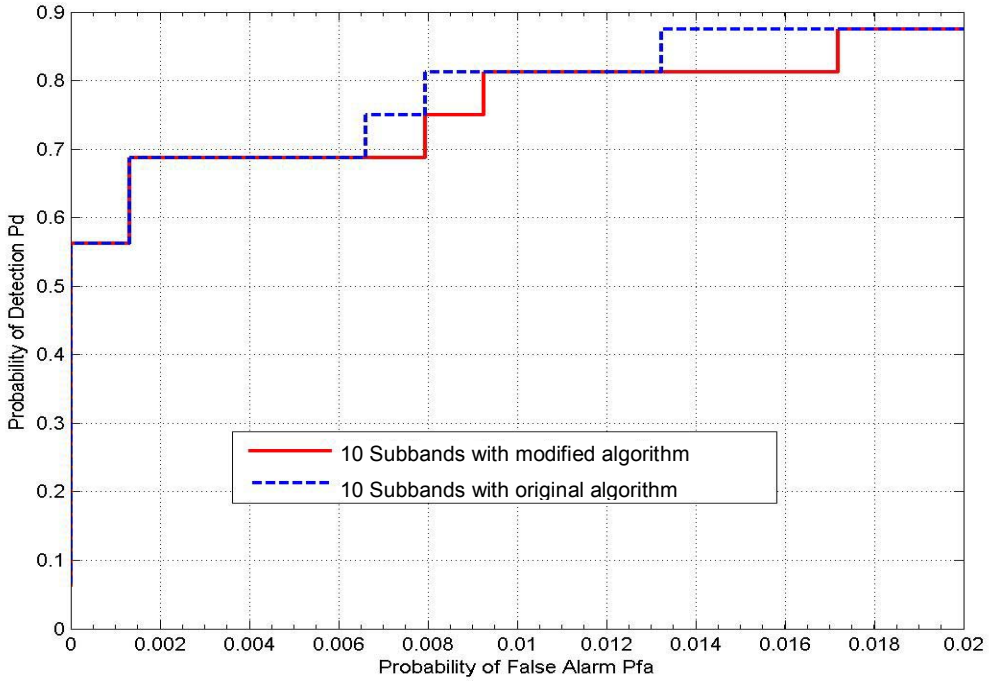


**Figure 75(a): ROC for 20 Subbands with Modified Vs Original Algorithm for Dataset 5**

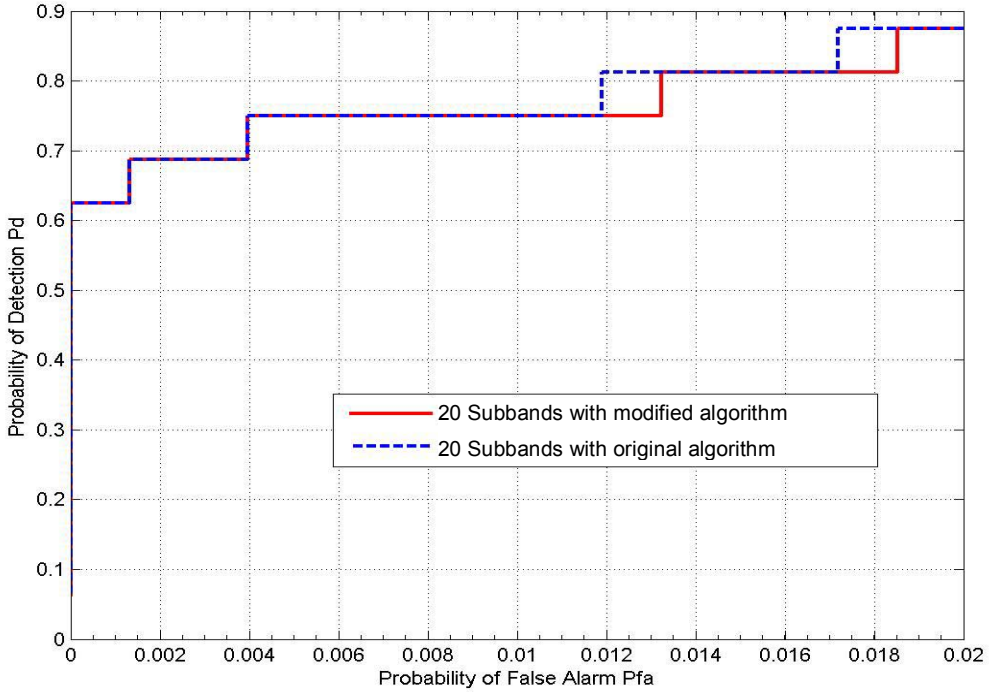


**Figure 75(b): ROC for 20 Subbands with Modified Vs Original Algorithm for Dataset 5**

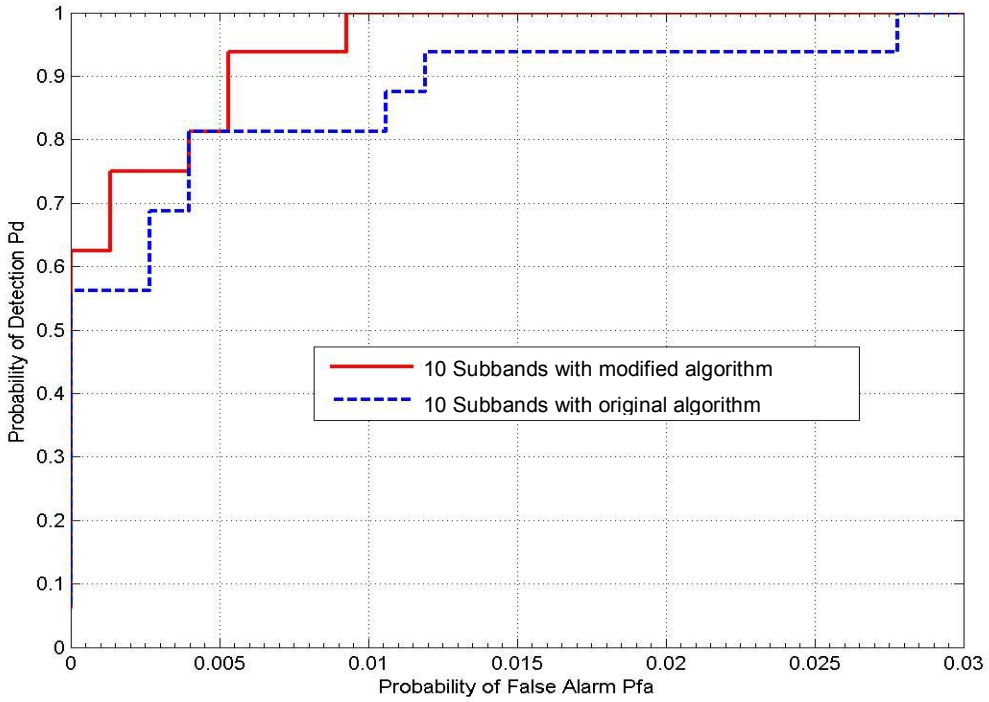


**Figure 76(a): ROC for 10 Subbands with Modified Vs Original Algorithm for Dataset 6**

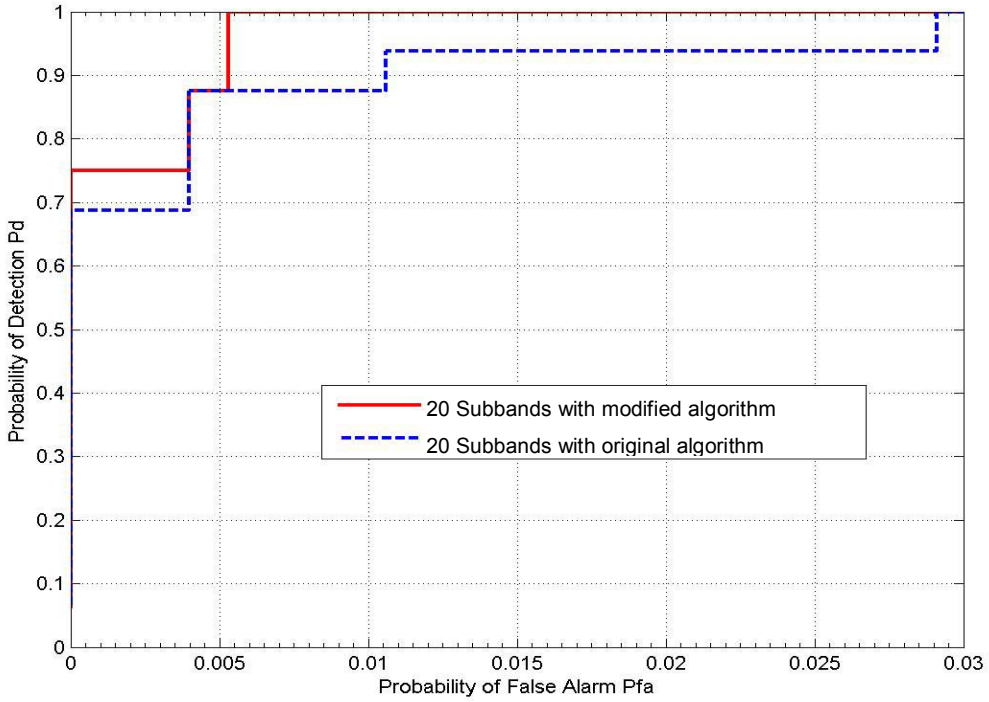


**Figure 76(b): ROC for 20 Subbands with Modified Vs Original Algorithm for Dataset 6**

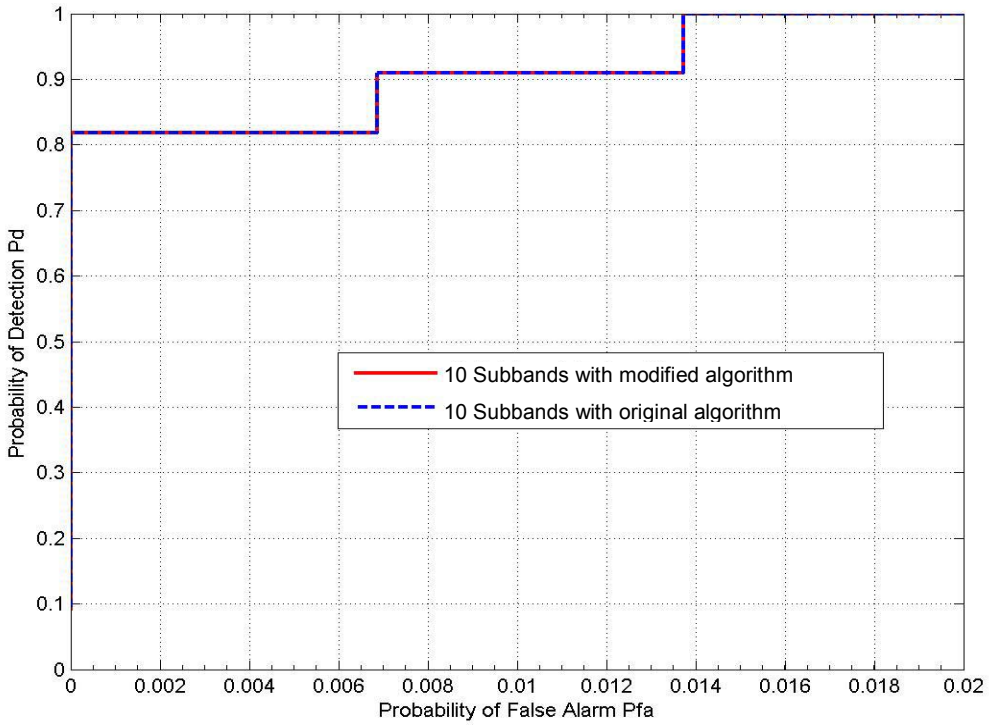


**Figure 77(a): ROC for 10 Subbands with Modified Vs Original Algorithm for Dataset 7**

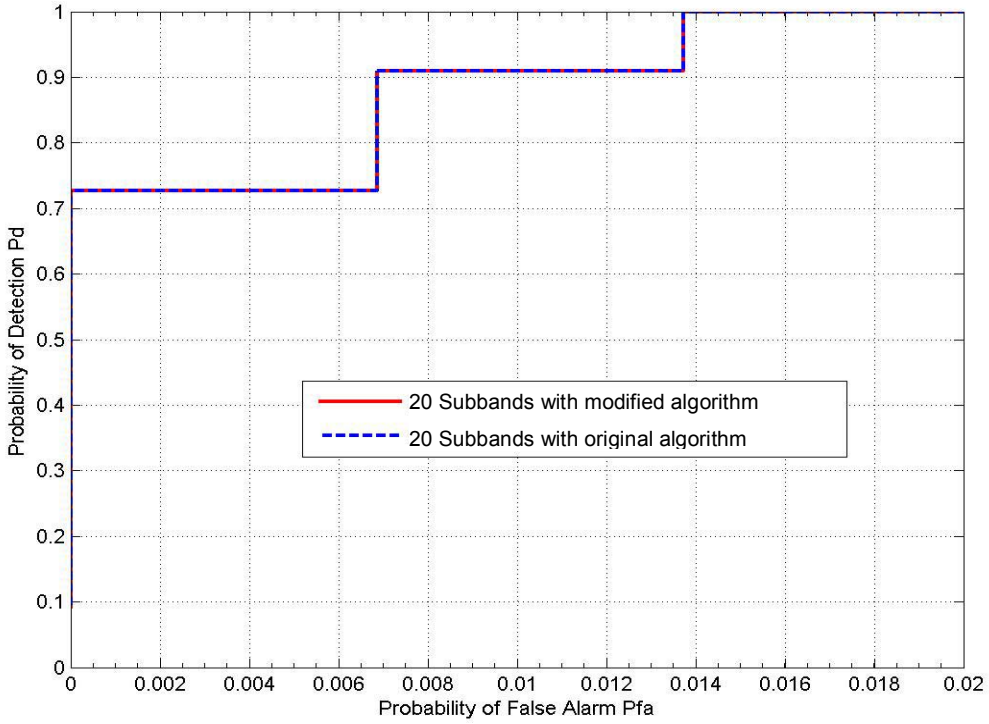


**Figure 77(b): ROC for 20 Subbands with Modified Vs Original Algorithm for Dataset 7**

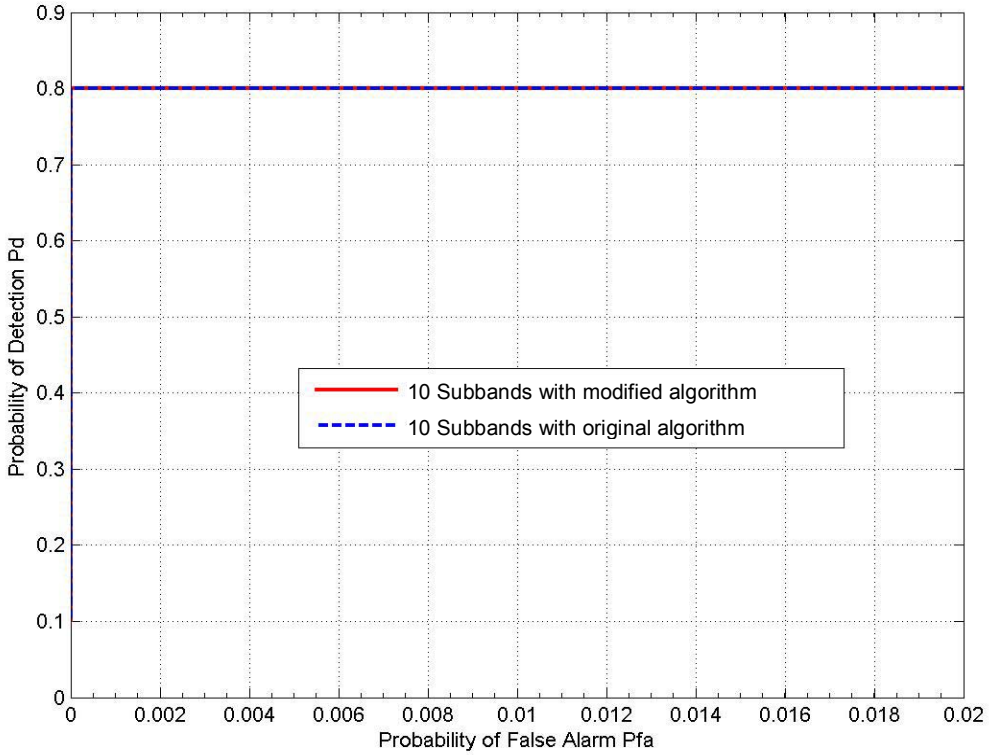


**Figure 78(a): ROC for 10 Subbands with Modified Vs Original Algorithm for Dataset 8**

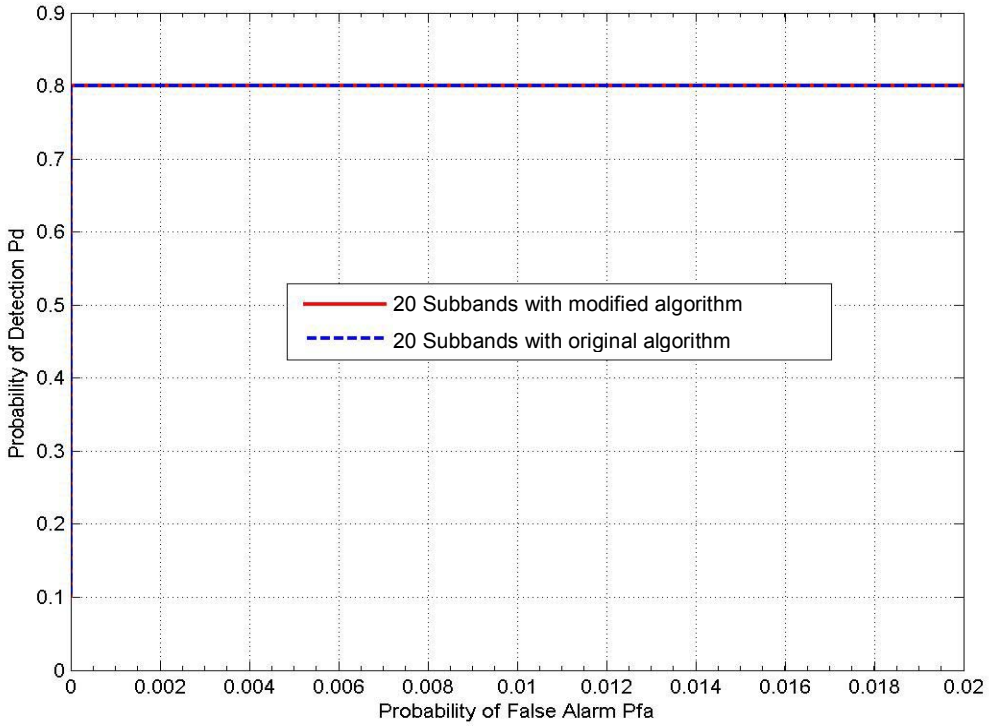


**Figure 78(b): ROC for 20 Subbands with Modified Vs Original Algorithm for Dataset 8**

## 5.8 ROC Characteristics for 10 Vs 20 Subbands with Modified Depth Estimation

The ROC characteristics obtained by using the Modified depth Estimation routine are verified for improvement in the 20 subbands case compared to 10 subbands, and as expected, it is found that the algorithm improved the probability of detection in 20 subbands case, compared to 10 subbands. It can be seem from the figures 79-86 that 20 subbands improved the ROC for all datasets except datasets 4 and 7. In fact, the improvement is more with the modified algorithm compared to the original algorithm.

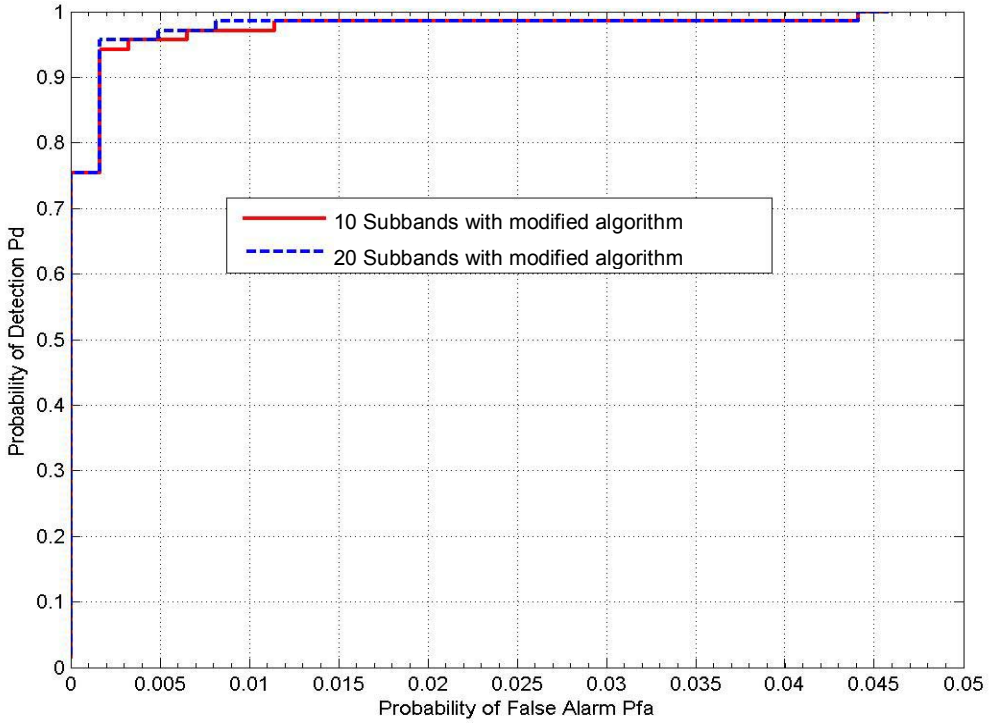


**Figure 79: ROC 10 Vs 20 Subbands with Modified Depth Estimation for Dataset 1**

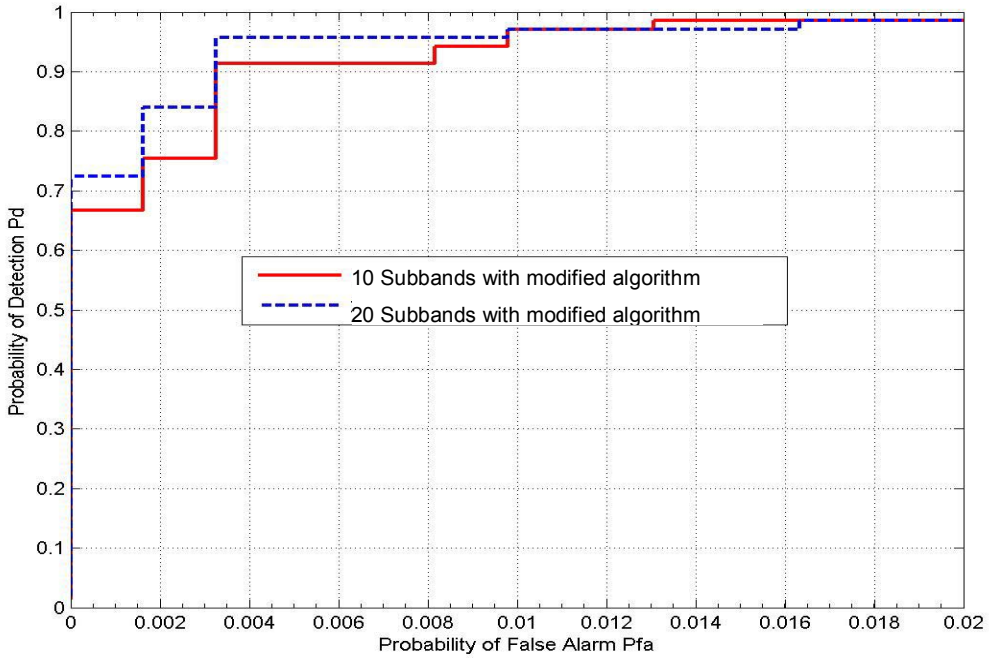


**Figure 80: ROC 10 Vs 20 Subbands with Modified Depth Estimation for Dataset 2**

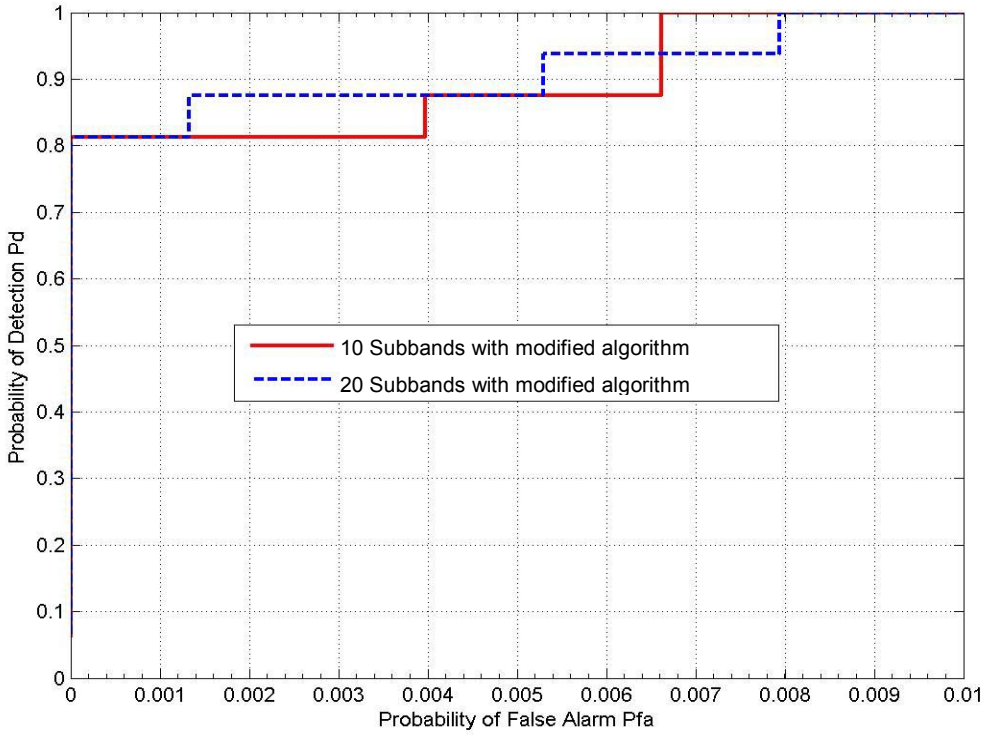


**Figure 81: ROC 10 Vs 20 Subbands with Modified Depth Estimation for Dataset 3**

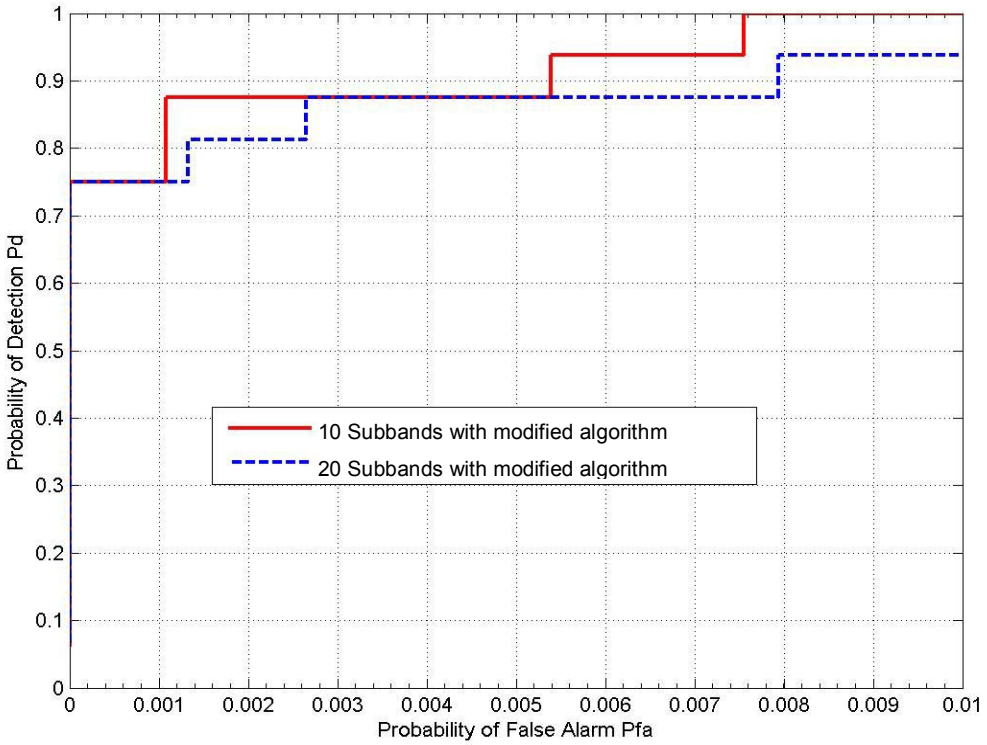


**Figure 82: ROC 10 Vs 20 Subbands with Modified Depth Estimation for Dataset 4**

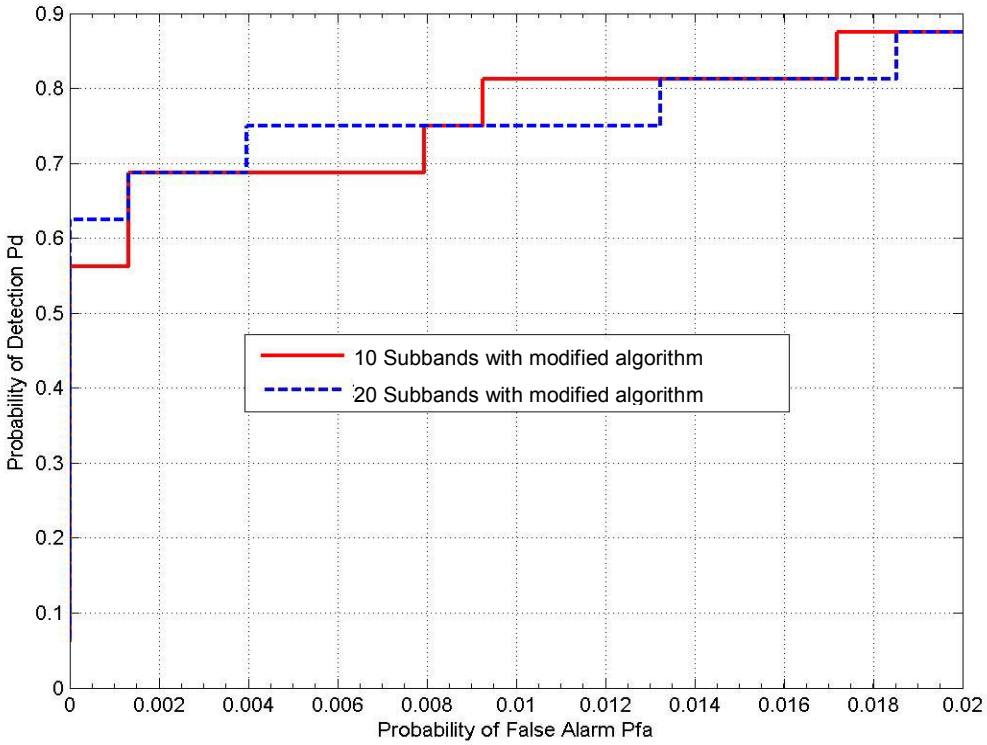


**Figure 83: ROC 10 Vs 20 Subbands with Modified Depth Estimation for Dataset 5**

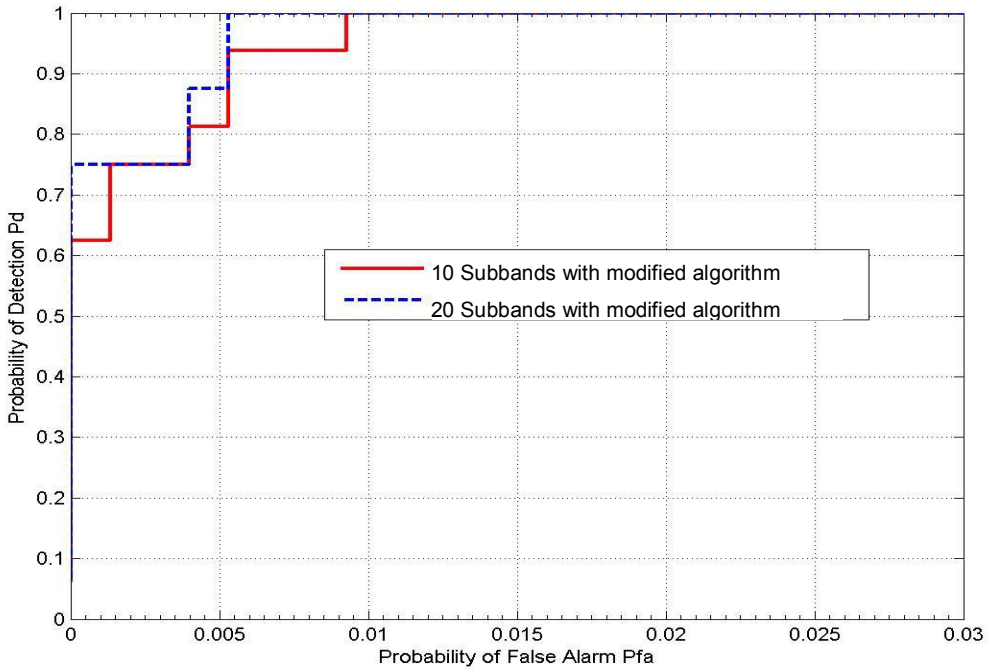


**Figure 84: ROC 10 Vs 20 Subbands with Modified Depth Estimation for Dataset 6**

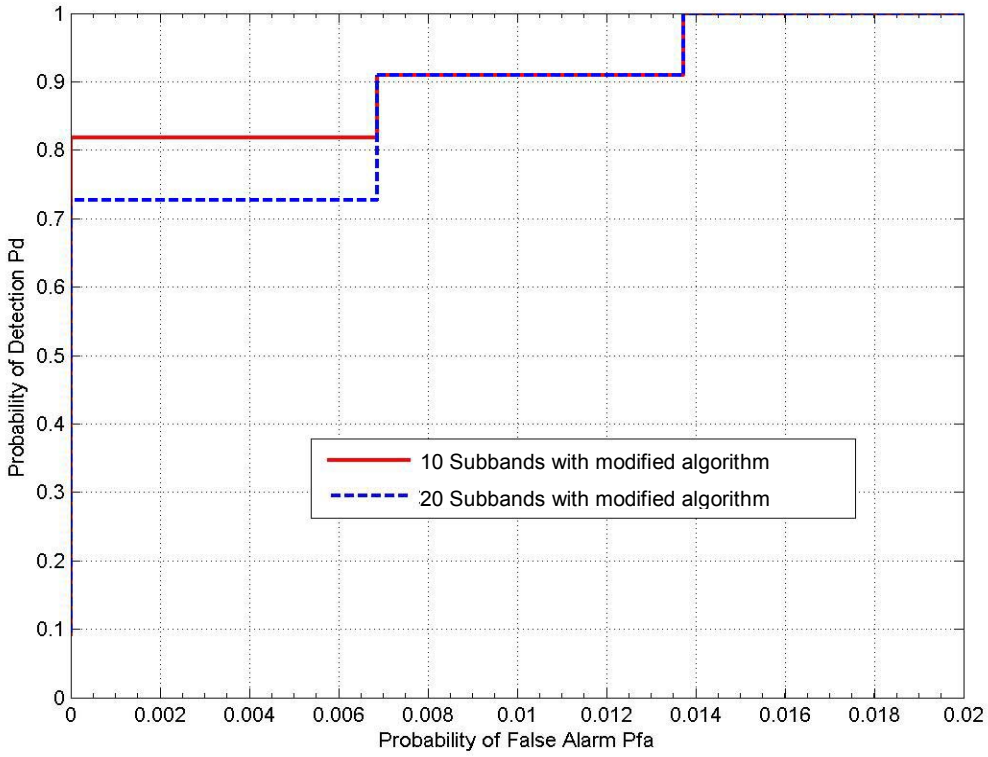


**Figure 85: ROC 10 Vs 20 Subbands with Modified Depth Estimation for Dataset 7**

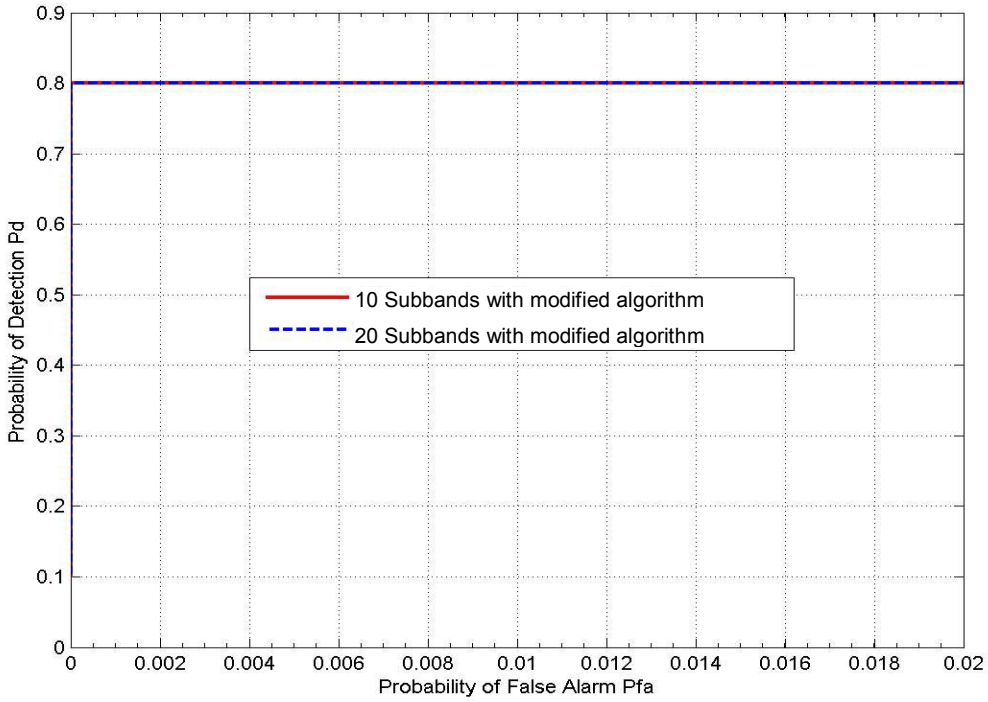


**Figure 86: ROC 10 Vs 20 Subbands with Modified Depth Estimation for Dataset 8**

## 5.9 Conclusions

Depth Estimation before frequency domain processing proved to be an important factor in improving the probability of detection of the landmines. The techniques proposed in this chapter improved the probability of detection of landmines for most of the datasets that were tested. Thus, further research on depth Estimation routine should be done to increase the probability of detection.

# Chapter 6

# CONCLUSIONS AND FUTURE WORK

## 6.1 Conclusions

We presented two techniques for improving the probability of detection of landmines and decreasing the false alarm rate. The first technique, Dynamic Template Matching technique, proposed by Dr. Ho, extracts the templates from the first few sweeps in the GPR data, and uses these templates to find the confidence value using correlation. The technique and its modifications studied in this research showed some improvement in the probability of detection of mines, while reducing the probability of false alarms. The algorithm is found to be effective to extract low metal content mines, especially anti-tank mines. Also, the effect of using real and complex data is studied.

The second technique developed, operates in the frequency domain, where the data in the depth domain is converted to the frequency domain to study the spectral features and their effect on the detection of landmines. The original algorithm proposed by Dr. Ho is further investigated by increasing the number of sub bands from 10 to 20. This increase in the number of sub bands showed 10% increase in the probability of detection of landmines. Eight different datasets collected from various test sites are used to evaluate the performance of the frequency domain technique, and the results were improved in more than half of the datasets, which is a good margin to decide the effectiveness of frequency domain technique. Thus, the frequency domain technique proved to be useful in the detection of plastic mines.

To further improve the probability of detection, the effect of estimating the depth of the mine before converting to frequency domain, is also investigated as a final part of this research. With the inclusion of depth estimation routine, the results improved by 15% for some of the datasets. Thus, the technique proved to be useful in improving the probability of detection of landmines.

## 6.2 Future Work

Future work should focus on improving the frequency domain technique to further improve the detection of plastic landmines. Though the spectral features were studied in this research, the effect of the size and shape of the mine on the spectral peaks still needs to be investigated. Also, though this research gave some good results using the depth estimation routine, the algorithm still fails in some cases to determine the depth of objects buried under the ground. Thus, the depth processing routine needs further investigation, to determine the depth of the objects buried far below the ground.

# References


[1] Esam M.A. Hussein and Edward J. Waller, "Landmine Detection: The Problem and the Challenge", Applied Radiation and Isotopes, Volume 53, pp. 557-563, 2000

[2] K. C. Ho and Paul D. Gader, "A Linear Prediction Land Mine Detection Algorithm for Hand-Held Ground Penetrating Radar" *IEEE Transactions on Geoscience And Remote Sensing,* Vol. 40, No. 6, June 2002

[3] P. D. Gader, B. N. Nelson, H. Frigui, G. Vaillette, and J. M. Keller, "Fuzzy logic detection of land mines with ground penetrating radar," *Signal Processing, Spec. Issue Fuzzy Logic Signal Processing (Invited Paper)*, vol. 80, no. 6, pp. 1069-1084, June 2000.

[4] P. D. Gader, B. N. Nelson, A. Koksal Hocaoglu, S. Auephanwiriyakul, and M. A. Khabou, "Neural versus heuristic development of Choquet fuzzy integral fusion algorithms for land mine detection," in *NeuroFuzzy Pattern Recognition*, H. Bunke and A. Kandel, Eds, Singapore: World Scientific, 2000.

[5] P.D. Gader and M. Mystkowski, " Application of Hidden Markov Model to detecting land mines with ground penetrating radar," in Proc. SPIE'99 Conf., Orlando,FL, 1999

[6] P. D. Gader, M. Mystkowski, and Y. Zhao, "Application of Hidden Markov Model to Landmine detection using ground penetrating radar," *IEEE Trans. Geosci. Remote Sensing,* vol. 39, pp. 1231-1244, June 2001.

[7] K. C. Ho and P. D. Gader, "Fusion of statistical deviance and HMM GPR algorithms For the mine hunter/killer system," in *Proc. SPIE'01 Conf.,* Orlando, FL, 2001.

[8] P. D. Gader, M. Mystkowski, and Y. Zhao, "Adaptive Hidden Markov Models for Extended land mine detection," in *Proc. SPIE'01 Conf.,* Orlando, FL, 2001.

[9] H. Brunzell, "Clutter reduction and object detection in surface penetrating radar", in *Proc. Radar'97* Conf., 1997 pp. 688-691.

[10]Dynatilaka, A. H. and B. A. Baertlein, "A Subspace Decomposition Technique to Improve GPR Imaging of Anti-personnel Mines," *Proc. of SPIE, AeroSense 2000: Detectection and Remediation Technologies for Mines and Minelike Targets,* Vol. 4038, 1008-1018, 2000.

[11]L. van Kempen and H. Sahli, "Signal Processing Techniques for Clutter parameters Estimation And Clutter Removal in GPR data for Landmine Detection", *Statistical Signal Processing,* Aug 2001, pp. 158-161.

[12]L. van Kempen, H Sahli and J. Brooks and J. Cornelis, " New Results on Clutter Reduction and Parameter Estimation for Landmine Detection using GPR", GPR

2000, *Eighth International Conference on Ground Penetrating Radar,* Gold Coast, Australia, May 23-25, 2000", pp 872-879

[13]Carevic, D., "Wavelet-based Method for Detection of Shallowly Buried Objects from GPR data," *Proc. Of Information Decision and Control,* 201-206, 1991

[14]Brian, Karlsen, Helge B.D. Sorensen, Jand Larsen and Kaj B. Jalobsen, "Independent Component Analysis for Clutter Reduction in Ground Penetrating Radar Data," *Proc. Of SPIE, Detection and Remediation Technologies for Mines and Minelike Targets,* Vol. 4742, 378-389, 2002.

[15] R. W. Deming, "Automatic buried mine detection using the Maximum Likelihood Adaptive Neural System (MLANS)," in P*roc. 1998 IEEE ISIC/CIRA/ISAS Joint Conf.*, Gaithersburg, MD, Sept. 1998, pp. 428-433.

[16] C. M. Rappaport and D. M. Reidy, "Focused array radar for real time imaging and Detection," in *Proc. SPIE'96 Conf.*, Orlando, FL, 1996.

[17] M. D. Patz and M. A. Belkerdid, "Evaluation of a model-based inversion algorithm for GPR signal processing correlation for target classification," in *Proc. SPIE'98 Conf.*, Orlando, FL, 1998.

[18] T. R. Witten, "Present state of the art in ground-penetrating radars for mine Detection," in *Proc. SPIE'98 Conf.*, Orlando, FL, 1998.

[19] S.M. Shrestha and I Arai, "High resolution image reconstruction by GPR using MUSIC and SAR processing method for landmine detection", *Geoscience and Remote sensing Symposium*, Volume 4, pp. 2921-2923, 2003.

[20] UWBGPR measurement at the Royal Military Academy, Belgium on May 31, 1999

[21] X. Xu, E.L. Miller, G.D. Sower, and T. Broach, "Detection of buried mines from GPR array measurement: a statistical approach", International Geoscience and Remote Sensing Symposium (IGARSS), Honolulu, HI, July 2000

[22] S. Yu, R.K. Mehra, and T.R. Witten, "Automatic mine detection based on ground penetrating radar," in SPIE Conf. Detection and Remediation Technologies for Mines and MineLike Targets , Orlando, FL,1999, pp.961-972

[23] K. C. Ho and P. D. Gader, "Correlation based landmine detection using GPR," in *Proc. SPIE '00 Conf.*, Orlando, FL, 2000.

[24] Quan Zhu and Leslie M. Collins, "Application of Feature Extraction Methods for Landmine Detection Using the Wichmann/Niitek Ground-Penetrating Radar," IEEE Transactions on Geoscience and Remote Sensing, VOL. 43 NO. 1, January 2005

[25] K. C. Ho, Leslie M. Collins, Lisa G. Huettel and Paul D. Gader, "Discrimination Mode Processing for EMI and GPR Sensors for Hand-Held LandMine Detection," IEEE Transactions on Geoscience and Remote Sensing, VOL. 42 NO. 1, January 2004

[26] K. C. Ho, P. D. Gader, J. Devaney, " Locate Mode Processing for Hand-Held Land Mine Detection," Proceedings of SPIE, Detection and Remediation Technologies for Mine and Mine like Targets IV , Orlando, FL

[27 _____, "An improved correlation based detector for a hand-held landmine detector," in Proc. SPIE Conf. Detection and Remediation Technologies for Mines and Minelike Targets , Orlando, FL, April 2001, pp. 483-493

[28] K. C. Ho, Paul D. Gader, "Dynamic Template-Matching-Based Processing for HandHeld LandMine Detector," Proc. SPIE, Detection and Remediation Technologies for Mines and Minelike Targets, Volume 5089, pp. 1261-1270 (2003)

[29] John McFee, Vic Aitken, Robert Chesney, Yogadhish Das, Kevin Russell, "A Multisensor, Vehicle-Mounted, Teleoperated Mine Detector with Data Fusion"

[30] Y. Das, K. Russell, N.Kircanski and A.A.Goldenberg, "An articulated robotic scanner for mine detection- a novel approach to vehicle mounted systems

[31] K.C.Ho, P.D. Gader, J.N. Wilson, "Improving landmine detection using frequency domain features from ground penetrating radar," Geoscience and Remote Sensing Symposium, 2004, IGARSS '04, Proceedings, 2004 IEEE International

[32] L. M. Collins, P. Torrione, V. Munshi, C. S. Throckmorton, Q. Zhu, F. Clodfelter and S. Frasier, "Algorithms for landmine detection using NIITEK ground penetrating radar," in Proc. SPIE Detection and Remediation Technologies for Mines and Minelike Targets VII, Orlando, Apr. 2002, pp. 709 – 718.

[33] P. Torrione, L. Collins, F. Clodfelter, S. Frasier, I. Starnes, "Application of the LMS algorithm to anomaly detection using the Wichmann/Niitek ground penetrating radar," in Proc. SPIE Detection and Remediation 0-7803-8742-2/04/$20.00 (C) 2004 IEEE 1619 Technologies for Mines and Minelike Targets VIII, Orlando, Apr. 2003, pp. 1127 – 1136.

[34] P. D. Gader, M. Mystkowski and Y. Zhao, "Landmine detection with ground penetrating radar using hidden markov model," IEEE Trans. Geoscience Remote Sensing, vol. 39, pp. 1237-1244, June 2001.

[35] P. D. Gader, R. Grandhi, W. Lee, J. Wilson and K. C. Ho, "Feature analysis for the NIITEK ground-penetrating radar using order-weighted averaging operators for landmine detection," in Proc. SPIE Detection and Remediation Technologies for Mines and Minelike Targets IX, Orlando, Apr. 2004.